UNIVERSITY OF GENOVA

PHD PROGRAM IN BIOENGINEERING AND ROBOTICS

‘Development of discoidal polymeric nanoconstructs for the treatment of cancer disease’

Candidate: Alessia Felici

Thesis submitted for the degree of *Doctor of Philosophy* (33° cycle)

March 2021

Prof. Paolo Decuzzi — Supervisor

Thesis Jury:

Prof. Stefano Salmaso, Università di Padova — External examiner

Prof. Nunzio DeNora, Università di Bari — External examiner

Dibris

Department of Informatics, Bioengineering, Robotics and Systems Engineering

Declaration

I hereby declare that except where specific reference is made to the work of others, the contents of this dissertation are original and have not been submitted in whole or in part for consideration for any other degree or qualification in this, or any other university. This dissertation is my own work and contains nothing which is the outcome of work done in collaboration with others, except as specified in the text and Acknowledgements. This dissertation contains fewer than 65,000 words including appendices, bibliography, footnotes, tables and equations and has fewer than 150 figures.

Alessia Felici
March 2021

Acknowledgments

I am extremely grateful to my mentor Prof. Paolo Decuzzi for his constructive criticism and precious suggestions, his mentorship was extremely important during my studies.

I wish to thank all my colleagues and friends for their invaluable relevance.

I am deeply indebted to Anna Lisa and Daniele for their consistent support and guidance during the development of this project, they have been a constant source of inspiration. My debit to them goes beyond this work.

Furthermore, I gratefully acknowledge the assistance of Sayanti, her help has been fundamental to complete this manuscript.

This dissertation is dedicated to my family and my life partner Andrea.

TABLE OF CONTENTS

1 Introduction *8*

1.1 Tumor pathology 8

1.2 Breast cancer 9

1.3 Conventional treatment in breast cancer 13

1.4 Brain cancer 15

1.4.1 Classification of brain cancer subtypes 17

1.4.2 Brain cancer treatment 19

2 Nanomedicine for cancer therapy *20*

2.1 Drug delivery system 20

2.2 Nano carrier aspects for tumor targeting 26

2.3 The EPR effect in Nano medicine development 28

2.4 Targeting the vasculature using Discoidal nanoconstructs 30

3 Chapter 1: Vascular-confined multi-passage Discoidal Nanoconstructs for the low-Dose Docetaxel inhibition of Triple-Negative Breast Cancer growth *32*

3.1 Abstract 32

3.2 Introduction 33

3.3 Experimental 36

3.3.1 Chemicals. 36

3.3.2 Methods 36

3.3.2.1 Fabrication of Discoidal Polymeric Nanoconstructs. 36

3.3.2.2 Physio-chemical characterization. 37

3.3.2.3 Loading and Release studies. 38

3.3.2.4 In vitro cell viability tests. 39

3.3.2.5 Cell Uptake experiments. 40

3.3.2.6 Optical imaging of orthotopic breast cancer. 40

3.3.2.7 Tumor model and therapeutic experiments. 40

3.3.2.8 Statistical Analysis. 41

3.4 Results and discussions 42

3.4.1 'Multi-passage' loaded Discoidal Polymeric Nanoconstructs. 42

3.4.2 Controlled drug release and *in vitro* cytotoxicity. 46

3.4.3 Preclinical imaging and therapeutic performance of DTXL-DPN. 50

3.5 Conclusions 57

4 Chapter 2: modulating the chemical proprieties of Docetaxel for improving the retention within a soft plga matrix *58*

4.1 Abstract 58

4.2 Introduction 59

4.3 Experimental 62

4.3.1 Chemicals 62
4.3.2 Methods 63
4.3.2.1 Synthesis of Discoidal polymeric nanoconstructs 63
4.3.2.2 Loading of Discoidal polymeric nanoconstructs with Drug 63
4.3.2.3 Synthesis of oleic-docetaxel prodrug 64
4.3.2.4 Synthesis of Succinic-docetaxel 64
4.3.2.5 Synthesis of PEG 1k-Docetaxel 65
4.3.2.6 Particles size and shape characterization. 65
4.3.2.7 Chemical characterization 66
4.3.2.8 Loading and Release studies. 66
4.3.2.9 In vitro cell viability tests. 67

4.4 Results and discussion 68
4.4.1 Synthesis of Discoidal polymeric nanoconstructs 68
4.4.2 Characterization of Docetaxel conjugates 70
4.4.3 Loading of Docetaxel prodrug into Discoidal polymeric nanoconstructs 73
4.4.4 Encapsulation and release profile of prodrug loaded in DPNs 75
4.4.5 Cell Viability Studies for the Prodrugs 78

4.5 Conclusion 79

5 Chapter 3: Soft Discoidal polymeric Nanoconstructs delivering PEG-Docetaxel prodrug for the treatment of Glioblastoma multiforme *81*

5.1 Abstract 81

5.2 Introduction 82

5.3 Experimental 84
5.3.1 Chemicals 84
5.3.2 Methods 84
5.3.2.1 Synthesis of Discoidal polymeric nanoconstructs 84
5.3.2.2 Synthesis of PEG 550-Docetaxel 85
5.3.2.1 Particles size and shape characterization. 85
5.3.2.2 Chemical characterization 86
5.3.2.1 Loading and Release studies. 86
5.3.2.2 In vitro cell viability tests. 87
5.3.2.1 Tumor model and therapeutic experiments. 88

5.4 Results and discussion 89
5.4.1 Synthesis and Characterization of Docetaxel conjugates 89
5.4.2 Loading of Docetaxel prodrug into Discoidal polymeric nanoconstructs 93
5.4.3 Pharmacological proprieties of PEG_{550}-DTXL prodrug loaded in DPNs 95
5.4.4 Cell Viability Studies for PEG_{550}-DTXL and preliminary in vivo study 96

5.5 Conclusion 98

6 References *99*

Part I

General

introduction

1 INTRODUCTION

1.1 TUMOR PATHOLOGY

Cancer is the second leading cause of death globally, with an estimation of 10 million deaths in 2020 meaning that 1 in 6 deaths is due to cancer as reported by the World Health Organization (WHO)[1]. Several hypothesis suggest that the development of human tumor start with a single mutation in a normal cell that acquires new biological capability and selective growth propensity over other cells. The proliferation of the mutated cells leads to progressive evolution and sequential selection of sublines that show increasingly abnormal behavior leading to a tumor formation.[2]

Hanahan and Weinberg, in 2000 defined six hallmark of cancer for rationalizing the complex disease. They include sustaining proliferative signaling, evading growth suppressors, resisting cell death, enabling replicative immortality, inducing angiogenesis, activating invasion and metastasis[3]. Typically, most of the numerous genomic mutations are on genes encoding Proteins involved in cellular processes such as DNA replication, DNA repair, cell cycle progression that maintain cellular homeostasis. Therefore, alteration of any of these homeostatic processes could entrain cells to the progressive genomic instability and phenotypic evolution characteristic of carcinogenesis[4]. Usually, the normal tissue architecture and function are controlled by the release of growth-promoting signals that ensure the homeostasis of cell number through the cell growth-and-division cycle. Those signals are transmitted by growth factors that bind cell-surface receptors that proceed to emit signals influencing yet other cell-biological properties, such as cell survival and energy metabolism. The loss of normal guard against genomic mutation and the consequent instability of the genomic information leads to a progressive consolidation of the mutations in the genome of affected cells[3].

1.2 BREAST CANCER

Breast cancer is the most common malignancy in females and the second leading cause of cancer related deaths with an incidence of >1,000,000 cases occurring worldwide annually as reported by the International Agency for Research on Cancer (IARC)[5].

Breast cancer is a heterogeneous disease that exhibits numerous morphological features, different immune-histochemical profiles and unique histopathological subtypes that have specific clinical behavior [6]. By definition, adenocarcinomas are the malignant tumors that originate in mammary epithelial layer and specifically in the inner lining epithelium of the ducts (ductal carcinoma) and lobules that supply the ducts with milk (lobular carcinoma). Based on the grade of proliferation and status of the disease, the tumor could be defined “in situ carcinoma” when limited to the epithelial component of the breast, or “invasive carcinoma” when invade the stroma.[7, 8] Among the complexity of the histological characterization, pathologists have identified some specific architectural and cytological patterns that are defined “histological special types” because they consistently associate with distinctive clinical behavior. They include not more than 25% of all breast cancers, all the other are classified as “invasive ductal carcinomas not otherwise specified” (IDC-NOS) that do not exhibit sufficient characteristic to be inserted in the special type *Table 1* [8-10]. Despite the histopathological analysis provide a knowledge about the histological grade and type of the tumor, they are not enough in deciding the therapy . [11, 12],

Over the past decades, the complexity of the disease has been investigated using molecular technique leading to refining of the molecular characterization based on the gene expression[7]. Specifically, the microarray method reveled the gene expression profile and the molecular features

that underlie some biological proprieties such as metastatic behavior or histological grade that help to identify signatures associated with prognosis and response to therapy[13].

Histological type	Prevalence (%) in WHO (2003)[22]	Prevalence (%) in Rosen (2001)[13]	Prevalence (%) in Rakha[23,45]*
Invasive ductal carcinomas (no special type)	50–80	65–80	56.4
Carcinoma with osteoclast-like giant cells	NR	0.5–1.2	NR
Invasive lobular carcinomas	5–15	5	Overall 8.2 Classic 7.4, alveolar 0.1, solid 0.3, tubulolobular 0.4
Pure tubular carcinoma	<2	<2	4.4
Invasive cribriform carcinoma	0.8–3.5	<4	0.6
Medullary carcinomas	1–7	<5–7	Overall 2.6 Typical 0.3, atypical 2.3
Mucinous carcinoma	2	<2	1.4
Neuroendocrine tumors	2–5	NR	NR
Invasive papillary carcinoma	1–2	1–2	0.4
Invasive micropapillary carcinoma	<2	<2.7	NR
Apocrine carcinoma	<4	<1–4	NR
Metaplastic carcinoma	<1	<5	NR
Lipid-rich carcinoma	<1–6	<1	NR
Secretory carcinoma	<0.15	A few cases	NR
Oncocytic carcinoma	A few cases	NR	NR

***Table 1**: prevalence of histological type of breast cancer [8]*

Currently, clinical practice typically uses a surrogate classification of five subtypes on the basis of histological and molecular characteristics *Figure 1* [14]. The intrinsic molecular classification of Perou and Sorlie, reported in 2000, are based on a 50- gene expression signatures and established four subtypes of breast cancer based on the expression of endocrine receptors (estrogen and progesterone receptor ER) and the aberrant expression of human epithelium growth factor (HER2+)[15].

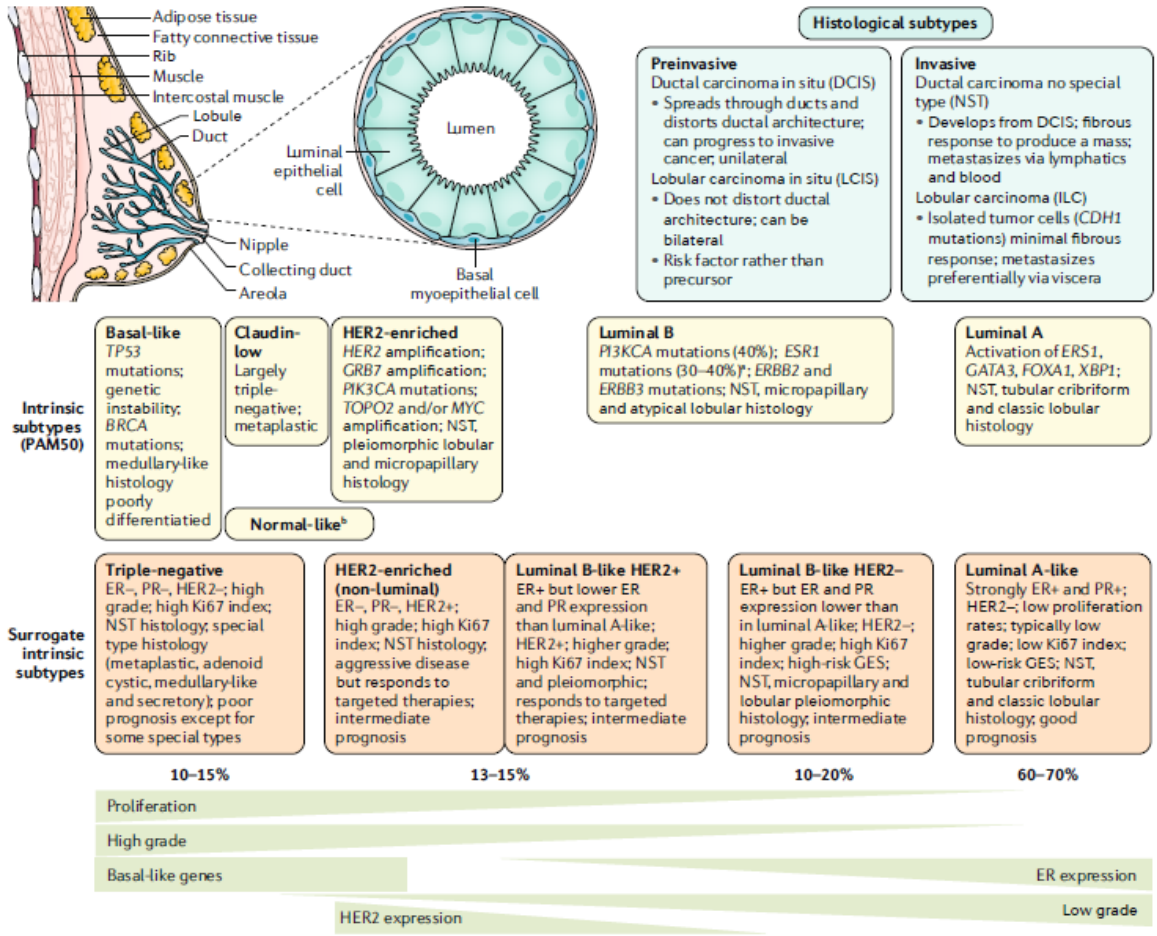

Figure 1.1: Breast cancer. *The histological subtypes described here (top right) are the most frequent subtypes of breast cancer; ductal carcinoma (now referred to as 'no special type' (NST)) and lobular carcinoma are the invasive lesions; their pre-invasive counterparts are ductal carcinoma in situ and lobular carcinoma in situ (or lobular neoplasia), respectively. The surrogate*

intrinsic subtypes are typically used clinically and are based on histology and immunohistochemistry expression of key proteins: estrogen receptor (ER), progesterone receptor (PR), human epidermal growth factor receptor 2 (HER2) and the proliferation marker Ki67. Tumours expressing ER and/or PR are termed 'hormone receptor- positive'; tumours not expressing ER, PR and HER2 are called 'triple- negative'.

The molecular subgroup includes: i) luminal type (expressing the estrogen receptor (ER)); ii) basal- like (include explanation of the characteristic); iii) human epidermal growth factor enriched (overexpressed receptor HER2, without ER expression); normal type. The luminal type incudes roughly the 70% of the invasive breast cancer. Based on the expression of HER2 and proliferation rate it is possible to distinguish between luminal A (HER2-, low grade) and luminal B (HER2+, high grade). Lumina A is the most commonly occurring with a frequency of 30% of all diagnosis, is characterized by the absence of the hormone receptors (HER2-), low pathological grade and proliferation rate consequently showing a good prognosis.

On the contrary, the less frequent type Lumina B showed some overexpression of HER and tend to be higher histological grade than Lumina A, therefore belong to the higher proliferative grade. Although both luminal subtypes are associated with a good prognosis and long-term survival (approximately 80-85% 5-years survival), the luminal B is associated with a significantly worse prognosis compared to the other subtype[16].

The HER2-enriched subtype is characterized by the overexpression of the human epidermal growth factor receptor, HER2. This subtype is usually ER-/PR- /HER2+ and Accounts approximately for 17% of all breast cancers. It is generally associated with poor clinical outcomes and it is also predictive of positive responses to anti HER2 therapy (Trastuzumab).

The “basal-like” subtype, one of the most clinically aggressive subtype, is more commonly negative for all 3 markers ER, PgR and HER2 hence the “triple-negative” phenotypic classification [17].

1.3 CONVENTIONAL TREATMENT IN BREAST CANCER

Breast cancer treatment include Surgery, radiation, chemotherapy and targeting therapy[18]. What guide the treatment choice are numerous factors such as stage of cancer, molecular profile, involvement in lymph nodes and presence of metastases [19].

Early breast cancer, defined when the malignant mass is contained in the breast or if anything has spread to the axillary lymph nodes, is considered curable [20]. Indeed, a combination of local treatment (surgery and radiation) and systemic treatment (chemotherapy and targeting therapy) has made it possible to increase chances for cure in ~ 70-80% of patients [18, 21].

Usually, women with early stage breast cancer without metastasis undergo surgery, if the tumor is deemed operable. Although Surgery (resection) of the primary tumor is the cornerstone of curative breast cancer treatment, in most case a systemic therapy is required before (neoadjuvant) or after (adjuvant) surgery for decreasing the cancer mortality [22]. The treatment before resection aim to reduce the burden size, in this way, it is possible to decrease the invasiveness of the chirurgical practice and perform a breast- conserving surgery [23]. Indeed, it has been reported that in young women < 40 years of age breast conserving surgery plus whole radiation therapy renders equivalent overall survival compared with Mastectomy [24].

The evaluation of the best systemic therapy after surgery depends on specific biomarkers such as ER/PR (that establish the sensitiveness in endocrine therapy), HER2 (predictive marker for anti

HER2 treatment) or Ki67 expression (a value higher than 30% is correlated with high grade of proliferation and is typical of Lumina B tumor) [25].

In the case of Lumina A early breast cancer (ER+/PR+ low proliferation) adjuvant endocrine therapy is standard for at least 5 years after surgery. Typically, Tamoxifen is used, as an ovarian suppressor binding the estrogen receptor alone or associated with GnRH (Gonadotropin releasing hormone) which inhibit estradiol production. In post-menopausal women Tamoxifen is administered with aromatase inhibitor that helps to reduce the rate of recurrence. Several trials demonstrated that in high-risk patients the association improves DFS and overall survival compared with Tamoxifen alone [26-28].

In luminal HER2-negative early breast cancer, the chemotherapy is recommended beyond the endocrine therapy for the individual with high risk of recurrence. In this case, the Standard chemotherapy regimens include anthracycline and taxane given preferentially in sequence with attention to avoid excessive toxicity [29, 30]. Indeed, in patients with high clinical risk an anthracycline–taxane regimen seems to be superior compared with the cyclophosphamide- taxane treatment. For this kind of cytotoxic treatment, it has been demonstrated that Dose-dense administration of chemotherapy (in which the rate of delivery, rather than the overall dose, is increased) significantly improves 10-year breast cancer- related mortality independent of ER status and tumour burden without any detectable adverse effects on non- breast-cancer- related mortality. Adding drugs, such as capecitabine, gemcitabine or bevacizumab, to an anthracycline–taxane chemotherapy does not improve outcomes in early breast cancer [29].

In HER2-positive early breast cancer (that is, luminal like and non- luminal-like HER2-positive early breast cancer), neoadjuvant chemotherapy together with anti- HER2 therapy has become the standard of care. In the neoadjuvant therapy, dual HER2-blockade with trastuzumab and

pertuzumab together with chemotherapy improves rates of pCR and therefore considered standard. Based on data from the adjuvant setting, chemotherapy may consist of either an anthracycline–taxane sequence or a combination of docetaxel and carboplatin together with anti- HER2 therapy (for 1 year) [31-33].

In TNBC, chemotherapy is standard and typically contains an anthracycline and a taxane, although docetaxel and cyclophosphamide are equally effective, in TNBC with limited disease burden and could be used if anthracyclines need to be avoided. Finally, bone modifying agents such as bisphosphonates or the RANK- L antibody denosumab not only improve bone mineral density and decrease treatment related bone loss but may also improve patient outcomes. However, the data on denosumab in early breast cancer are controversial [31, 34, 35].

1.4 BRAIN CANCER

Brain and other central nervous system tumor collectively represent the cancer occurring in the brain and they count more than hundred intrinsic subtype according to the WHO. Firstly, it is possible to distinguish into primary or secondary tumor (metastatic). About 90% of cases are associated to primary tumor and are classified based on the similarity to a neural or glial precursor. Among the primary manifestation, the 30% are malignant and the most common types are: meningioma (37%), gliomas (25%), pituitary tumors (16%) and nerve sheath tumors (8%) as depicted in *Figure 1.2* [36].

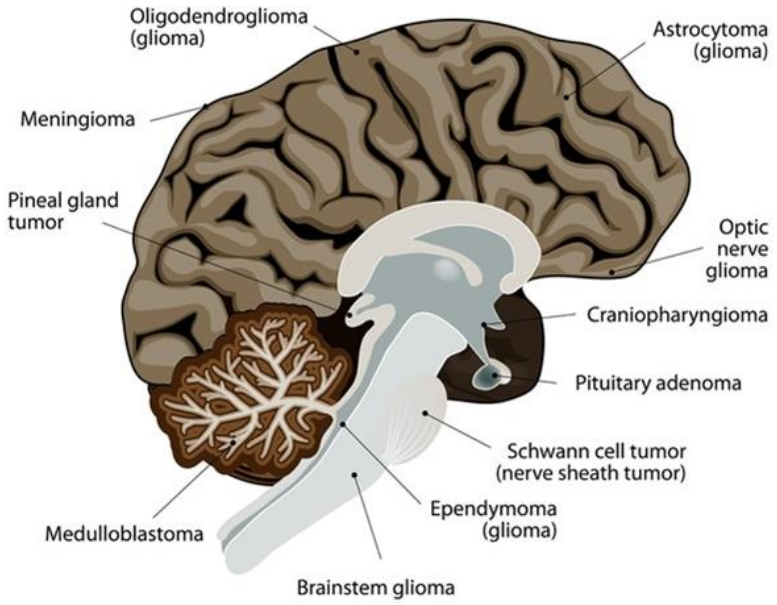

Figure 1.2: Primary brain tumor subtype [36].

Bailey and Cushing for the first time in 1920 classified the tumor of the glioma group referring to "Histological similarity principles" after observations that reveled a direct connection (or similarity) between the different type of glial tumor and a specific CNS cell of origin or its developmental precursor. According to this model, there is a correlation between the morphology of glial tumor and the differentiated stage of glia. For this classification reported in *Figure 1.3* Astrocytoma, for example, is the primary brain tumor composed by cells similar to Astrocytes or oligodedrogliomas is the subtype composed by cells similar to oligodendrocyte. Moreover, in high malignant setting, the tumor cells are similar to less differentiated precursor cells, whereas in less malignant setting they are more similar to neural tissue counterparts. The biological aggressiveness and tumor grade are established based on the extent of Aplasia- defined as the absence of

differentiation- and the presence of important features such as: mitotic activity, necrosis and vascular proliferation[37].

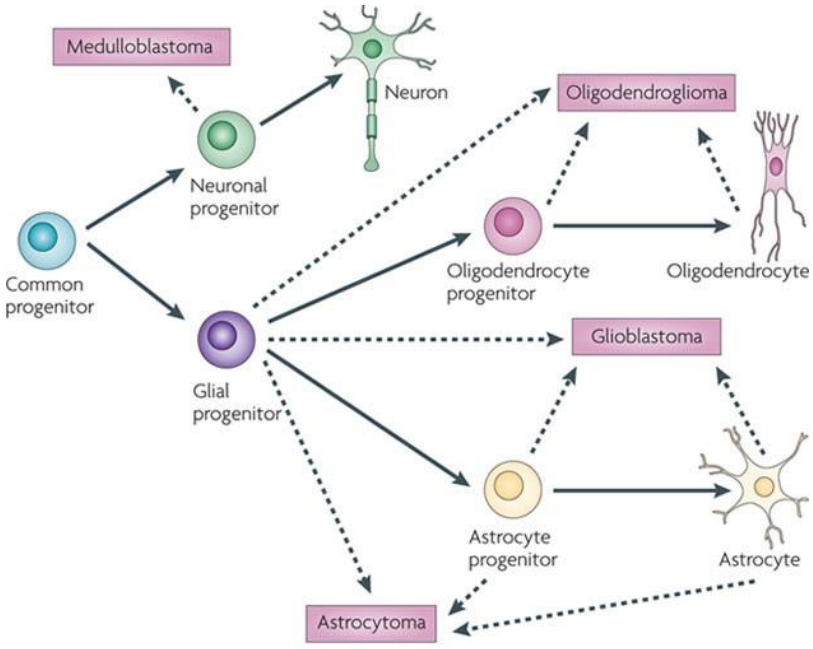

Figure 1.3: *The probable origins of glioma variants and medulloblastoma in the neuroglia lineage tree. Although the precise cells of origin for these cancers remain largely unknown, a selection of likely candidates For each (dashed arrows) is indicated.[38]*

1.4.1 Classification of brain cancer subtypes

The WHO classification for brain cancer introduced in 2016 the genetic component and important molecular markers to define new entities within the histological classification. This integration made the classification more objective and helped the diagnosis and definition of treatment[39].

However, the histology plays an important role for determining the grade of aggressiveness ranging from I to IV where the higher value represent the more aggressive type. Overall, it is

possible to distinguish into three big groups: i) malignances arising from glial cells; ii) arising from non-glial cells (neural cells); iii) metastatic tumor [40, 41].

Medulloblastoma

Medulloblastoma is a malignant tumor with higher incidence in children than adults that show a tendency to metastasize corresponding to WHO malignancy grade IV. Medulloblastoma occur in the posterior fossa. They consist of densely packed tumor cells with round or oval shaped hyperchromatic nuclei with scanty cytoplasm, high mitotic and apoptotic rates. The clinical outcome of patients with medulloblastoma varies according to age, postoperative tumor residuum, and metastatic (M) stage and, based on this, they are stratified into ‘‘standard’’ and ‘‘high’’ risk categories. A combination of chemotherapy and irradiation has allowed a long-term survival in the 85% of the children older than 3 years of age and in 70% of high-risk patients.

Metastatic brain cancer

Brain metastasis usually arise from circulating tumor cells of a primary tumor including lung cancer (40%), breast cancer (17%), and melanoma (11%). Despite the significant advantages using microsurgery and radiosurgery the overall survival is still function of the primary cancer.

Gliomas

Gliomas are most common intracranial cancer in adults accounting for 80% of all malignant brain tumor. Gliomas does not have a specific area of origin in the CNS but surely arise from glial or precursor cells and are classified by WHO between grade I-IV based on malignant behavior. According to this classification, it is possible distinguish astrocyte, oligodendrocyte or both depending on the cells phenotype (grade I-IV). The incidence rate of pathology is confused by the absence of a clear histological definition of glioma subtype that add difficulty in comparing

incidence rate from different sources. The survival rate, significantly change for all histological subtype. The Pylicytic Astrocytoma has the highest 5 years relative survival and glioblastoma the poorest overall survival with only 0.05-4.7% of patients surviving 5 years after prognosis. Overall, the gliomas with oligodendroglial component have increased survival as opposed to those with astrocytic component. The age is considered as a significant parameter for survival expectation after prognosis mostly for glioblastoma.

Glioblastoma grade IV, together with astrocytic tumor (grade II-III) and oligodendroglioma (grade III) are considered the most aggressive.

1.4.2 Brain cancer treatment

Brain cancer is one of the most aggressive tumor considering the high invasiveness, fast progression and inaccessibility for the majority of chemotherapeutic agents leading to poor prognosis and high rate of relapse. Currently, the standard procedures to treat patients with primary brain cancer includes surgery resection followed by radiotherapy and chemotherapeutic treatment with Temozolomide (TMZ). However, the current approved treatment do not provide long-term suppression of the tumor growth and they lack long-term efficacy causing in all patients a development of a recurrent disease. In addition, brain metastasis represent severe complication in the pathology. Conventional treatment involves therapeutic antibodies, cetuximab and trastuzumab which are not able to cross the blood brain barrier (BBB). The BBB is deputed to control the homeostasis of CNS and brain functions by using a neurovascular unit (NUT) thinly regulated by endothelial cells (ECs), pericytes and astrocyte endfeets. However, this peculiar characteristic effectively limit the delivery of systemic therapies into the brain. The BBB included in a tumor microenvironment defined as Blood Tumor Barrier is different from BBB because

disruptions are present due to tumor progression. Indeed, during tumor development the uncontrolled cells proliferation induces the rapid formation of new blood vessels to provide nutrients and oxygen. The effect it is commonly defined as Enhanced Permeability and Retention effect that always characterize the tumor endothelium. In spite of the higher permeability of the BTB, there is an insufficient accumulation of both small and large molecules and this remain as the rate-limiting factor for effective therapy. The neurovascular unit that compose the capillary bed of neuroparenchyma is composed of endothelial cells connected with thin junctions (TJs) surrounded by specialized basal lamina that are in communication with perycites and astrocytes endfeets. All together, they form a specialized system that control cellular and extracellular network, regulating the transport of toxic byproducts and essential molecules, avoiding the passive paracellular diffusion of molecules with a mass higher than 150 Da or slightly more if they are highly hydrophobic compounds.

2 NANOMEDICINE FOR CANCER THERAPY

2.1 DRUG DELIVERY SYSTEM

Over the past years, the translation of Nanotechnology efforts for medical applications and especially for cancer investigation has allowed to appreciate their unique features for drug delivery, diagnosis and imaging intents [42]. Nanotechnology is defined as the science focused on the synthesis, characterization and application of tools and devices within the nanometer scale (around 100 nm or smaller). At the nanoscale, fundamental proprieties of a given material can be precisely controlled by nanotechnology without chemical modification such as optical or magnetic proprieties. Among the numerous application of nanotechnology the use of nano-size particles for

therapeutic and imaging intent has the potential to revolutionize the idea of conventional medicine opening an offshoot of nanotechnology defined as Nanomedicine [43, 44].

Nanomedicine usually involves numerous type of devices including nanoparticles, nanomachines, nanofibers or other nanoscale microconstructs. Materials that showed a particular behavior including Nano shells, iron oxide nanocrystals or quantum dots has been used for diagnostic purposes. For example, gold nano-shells are opticaly tunable nanoparticles composed of a dielectric core of silica covered by a thin gold shell [45]. Indeed, changing the shell thickness and core size they are able to absorb and/or scatter light in a broad range of wavelength including Infrared zone that provide the maximal penetration of light through tissue. Whereas, Iron oxide nanocrystals given the superparamagnetic proprieties are used as contrast agent in magnetic resonance imaging showing high diagnostic accuracy in atherosclerosis, arthritis and cancer detection[46]. Although the potent improvement in imaging and diagnosis, the clinical application is often limited by toxicity, instability and lack of specificity. Therefore, in recent years, biocompatible polymers such as poly (ethylene glycol) (PEG) has been largely used to preserve the metal degradation and allow their blood circulation [47].

The concept of nanomedicine aim to improve the therapeutic index of anticancer drug by modifying their pharmacokinetics and tissue distribution by improving the delivery to the site of action. Current treatment for cancer include the use of chemotherapeutic drugs characterized by high cytotoxicity and no preferential accumulation at target site causing severe toxicity towards patients. Therefore, to provide a more efficient and safe solution it is desirable to develop smart Nano therapy that is able to recognize the tumor environment and selectively release the drugs. In the recent years these Nano-sized delivery systems, are being used for targeted therapy (active or passive strategies). They are able to differentiate between healthy and cancerous cells thus

achieving a significant improvement of drug therapeutic index with reduced adverse effects [48]. Moreover, Nano carrier-based strategies encapsulate the molecules within a complex of natural or synthetic polymer matrix allowing to control the pharmacokinetic profile of the cargo to sustain their release for a long time and only in a specific environment [49, 50].

For this purpose, the understanding of the tumor biology has opened the way to design rationally a platform suitable for the preferential accumulation within tumor tissues. The first findings on tumor biology reveled important features such as leaky blood vessel and poor lymphatic drainage. Therefore, several nano-sized delivery systems have been designed according to the peculiar anatomical organization of tumors neo-vasculature [49, 51]. The vessels surrounding tumor mass are leaky and present bigger fenestrations, and consequently they are more permeable than the normal ones[52]. The increased permeability of tumor vasculature is also due to the inflammation that is present in tumor microenvironment [53]. This scenario is even more complicated by the less efficient recovery of molecules due to the inadequate development of the lymphatic system in the tumor area. The particular anatomical organization, gives rise to the Enhanced Permeation and Retention (EPR) effect through which drug delivery systems in the nanometer scale could target passively tumors considering also that the molecular cut-off for the extravasation in tumor tissues range from 50 to 400 nm [54, 55].

Conventional drug delivery platforms mainly developed for tumor targeting up to now present a spherical shape and a size smaller than 200 nm suitable for extravasation upon systemic injection[56]. Liposome containing Doxorubicin (Doxil) was the first nanomedicine approved for clinical treatment, as reported in the time line in *Figure 2.1* and nanotechnology-based therapeutics along with other polymeric delivery system still represents a large portion of clinically approved therapies [57].

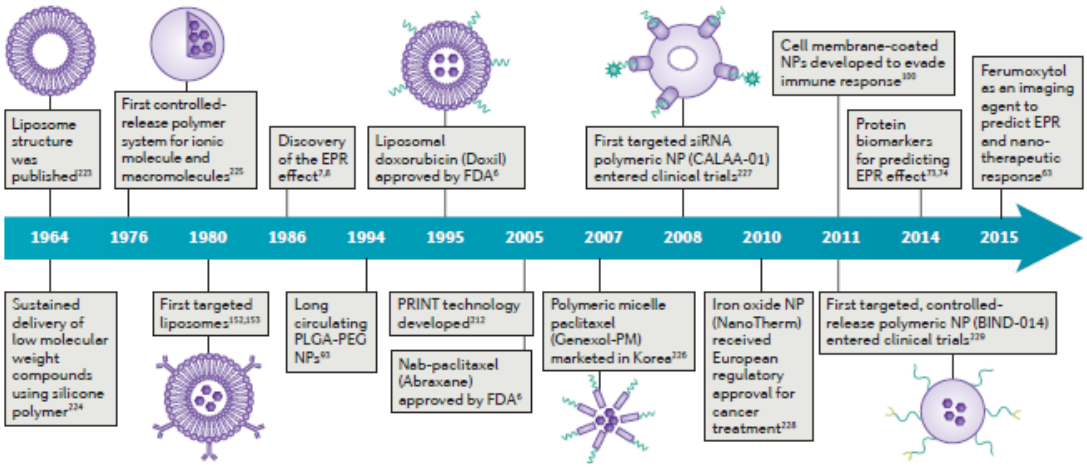

***Figure 2.1**: Historical timeline of major developments in the field of cancer nanomedicine [47]*

Nanoparticles can be made out of different materials and they have various physiochemical proprieties such as size, geometry, surface features, stiffness, among others, and all of them play an important role in regulating the processes involved in the actual delivery of the payload at the tumor tissue [58-60]. The family of Nano carriers includes polymer conjugate, polymeric nanoparticles, lipid-based carriers such as liposome and micelles, dendrimers, carbon nanotube and gold nanoparticles. They have been used for a variety of application such as drug delivery, imaging, phototermal ablation of tumors, radiation sensitizers and detection of apoptosis. Notably, the use of biodegradable and biocompatible materials has allowed mitigating the limitations ascribed to the use of excipients to solubilize hydrophobic drug in water as in the case of Paclitaxel [61]. Indeed, the use Albumin-bound paclitaxel has been the second class of Nano formulation that reached the market (nab-paclitaxel; abraxane). Albumin-paclitaxel complex have showed a better performance in terms of response rate and time to progression evaluated in patients with breast cancer compared with paclitaxel administered using the conventional chromophore EL

excipient[62]. A panel summarizing the main formulations approved by FDA or already in clinical trial for cancer therapy is reported in *Table 2* [63].

Therapy modality	Generic name and/or proprietary name	Nanotechnology platform	Active pharmaceutical ingredients	Cancer type	Status	Refs
Chemotherapy: non-targeted delivery	Liposomal doxorubicin (Doxil)	Pegylated liposome	Doxorubicin	HIV-related Kaposi sarcoma, ovarian cancer, and multiple myeloma	Approved by FDA	6
	Liposomal daunorubicin (DaunoXome)	Liposome	Daunorubicin	HIV-related Kaposi sarcoma	Approved by FDA	6
	Liposomal vincristine (Marqibo)	Liposome	Vincristine sulfate	Acute lymphoblastic leukaemia	Approved by FDA	6
	Liposomal irinotecan (Onivyde or MM-398)	Pegylated liposome	Irinotecan	Post-gemcitabine metastatic pancreatic cancer	Approved by FDA	230
	Liposomal doxorubicin (Myocet)	Liposome	Doxorubicin	Metastatic breast cancer	Approved in Europe and Canada	6
	Mifamurtide (Mepact)	Liposome	Muramyl tripeptide phosphatidyl-ethanolamine	Nonmetastatic, resectable osteosarcoma	Approved in Europe	6
	Nab-paclitaxel (Abraxane)	Albumin NP	Paclitaxel	Breast, lung and pancreatic cancer	Approved by FDA	6
	SMANCS	Polymer conjugate	Neocarzinostatin	Liver and renal cancer	Approved in Japan	6
	Polymeric micelle paclitaxel (Genexol-PM)	Polymeric micelle	Paclitaxel	Breast cancer and NSCLC	Approved in Korea	6
	Liposomal cisplatin (Lipoplatin)	Pegylated liposome	Cisplatin	NSCLC	Phase III	231
	NK-105	Polymeric micelle	Paclitaxel	Metastatic or recurrent breast cancer	Phase III	232
	Liposomal paclitaxel (EndoTAG-1)	Liposome	Paclitaxel	Pancreatic cancer, liver metastases and HER2-negative and triple-negative breast cancer	Phase II	233–236
	Nab-rapamycin (ABI-009)	Albumin NP	Rapamycin	Advanced malignant PEComa and advanced cancer with mTOR mutations	Phase II	237,238
	CRLX-101	Polymeric NP	Camptothecin	NSCLC, metastatic renal cell carcinoma and recurrent ovarian, tubal or peritoneal cancer	Phase II	239–241
Chemotherapy: targeted delivery	MM-302	HER2-targeting liposome	Doxorubicin	HER2-positive breast cancer	Phase II/III	242
	BIND-014	PSMA-targeting polymeric NP	Docetaxel	NSCLC and mCRPC	Phase II	243–245
	MBP-426	TfR-targeting liposome	Oxaliplatin	Gastric, oesophageal and gastro-oesophageal adenocarcinoma	Phase I/II	246
	Anti-EGFR immunoliposomes loaded with doxorubicin	EGFR-targeting liposome	Doxorubicin	Solid tumours	Phase I	247
Chemotherapy: stimuli-responsive delivery	ThermoDox	Liposome	Doxorubicin	Hepatocellular carcinoma	Phase III	248
Chemotherapy: combinatorial delivery	Liposomal cytarabine–daunorubicin (CPX-351 or Vyxeos)	Liposome	Cytarabine and daunorubicin (5:1)	High-risk acute myeloid leukaemia	Phase III	249
	CPX-1	Liposome	Irinotecan and floxuridine (1:1)	Advanced colorectal cancer	Phase II	250

Table 2: *Formulations approved by FDA ; others are currently in clinical trials.*

2.2 NANO CARRIER ASPECTS FOR TUMOR TARGETING

Since the 1986, the definition of the enhanced permeability of the tumor vessel has supported the statement that nanoparticles with sufficient size cut-off and long circulation times are able to accumulate passively within malignant tissue thanks to a physiological condition of the malignant neo-vascularization. However, a recent meta-analysis conducted on a large body of work published over the past years show that in many cases, less than 1% of the administered dose reach the malignant tissue [60]. To note, the use of nanoparticles to deliver chemotherapeutics increase the stability of the drug, improve the Pharmacokinetics and therefore the residence time of the drug after administration [64]. That justifies the decreased toxicity in clinical trial and the commercialization of few formulations as reported above (*Table 2*). However, the design of Nano-carrier for tumor targeting require the evaluation of the physiological aspects that may limit their bioavailability after systemic administration [60]. The size, shape and mechanical stiffness of nanoparticles are critical for vascular transport, Mononuclear phagocyte system (MPS) sequestration, blood longevity and tumor deposition [65-67].

While in the bloodstream, Nanoparticles encounter numerous biological barriers that limit their *in vivo* performance and favor their clearance in a short time. The principals circulating factors such as body elimination, blood flow and recognition by phagocytic cells can reduce Nanoparticles stability and hence lead to accumulation in tumor environment after administration. The specific effect of these biological factors are dependent on the physiochemical properties of the particles such as size, shape and surface properties leading to define general principles aimed to manipulate the above characteristics to achieve favorable outcomes[68]. In the context of size, particles with

a small diameter around 10 nm have demonstrated rapid elimination by kidney, whereas particles larger than 200 nm provoked the activation of the complement system if not modified.[69]

In this regard, hydrophilic polymer like Polyethylene- glycol (PEG) has helped to improve the circulation time shielding the particles surface from enzyme and antibody that may induce degradation and clearance conferring them stealth properties. In contrast, studies demonstrated that exposure to PEG caused the production of anti- PEG antibodies that can induce the rapid clearance of PEGylated NPs [70]. Another method tested included the use of platelet membrane cloaking which deceive the complement system but not the uptake from other cell population[71]. However, the plate-based cell interaction help to target the injury site owing to the ligands present on the surface such as mediators adhesion, Von Will brand factors and collagen pushing the wrapped nanoparticles around activated platelets [72]. In addition, proper modifications to hide the circulating NP helps from the sequestration by mononuclear phagocytic cells and RES which are responsible in overseeing the blood circulation from pathologists and undesired agents hence for the clearance of NP. They includes macrophages, monocytes and dendritic cells that quickly phagocytize particles and accumulate in spleen and liver. The sequestration by immune cells happen more rapidly for cationic and stiffer particles, whereas neutral or weakly negative particles have longer circulation half- life. Besides the clearance, the interaction between NP and MPS may cause toxicity due to the initiation of immune response, which involves the activation of tumor necrosis factors, interleukin and interferon that causes inflammation and tissue damage. Despite the success of FDA-approved nanodrugs in reducing the toxicity associated with the active pharmaceutical ingredients (API), the clinical application of them has thus far showed a limited improvement in overall survival of patients. Several hypothesis have been suggested by scientists over the past years to clarify the failure in clinical translation of Nano medicine supported by

evidences that reveled a complicated fate for nanoparticles injected systemically. For example, it is commonly know that the major obstacles for an increased efficacy of anticancer treatments relies on a feeble tumor penetration. An approach to boost tumor permeability is the application of tumor penetrating peptide on the surface of nano-drugs. The peptide is able to bind to a surface receptor specific for the blood vessels, tumor cells and stroma. Then the proteolytic cleavage shift the affinity for neutrophilin-1 receptor causing activation of the endocytic/exocytose trans-tissue transport pathway and therefor to an increased tumor penetration of small nanoparticles [73]. However, this approach has showed low effects due to low picomolar concentration of the target. Therefore, other efforts were presented focusing on the tumor microenvironment through radio frequency or high intensity focused ultrasound (HIFU) that effectively caused a remodeling of the tumor microenvironment and therefor enhanced nondrug accumulation leading to improved therapeutic efficacy [74]. Finally, a significant improvement in delivering payload in tumor targeting was achieved using the natural tropism of cell-delivered vehicles to tumors such as ghost of stem cells (naoghost) associated with tumor cells thought cellular uptake (endocytosis pathway) and via cellular binding (absorption, lipid exchange, fusion).

2.3 THE EPR EFFECT IN NANO MEDICINE DEVELOPMENT

The EPR effect clearly explain the enhanced accumulation and prolonged retention of NP in solid tumor compared with normal tissue. The majority of approved anticancer Nano medicines have been designed to exploit the concept of the EPR effect with a small subset of Nano medicine seeking to alter nanomedicine behavior further with ligand mediated targeting. In general, the use of EPR based therapeutics aimed to improve efficacy and tolerability by enhancing the pharmacokinetic and biodistribution of the drug. Indeed, by minimizing the peak free drug

concentration (Cmax) and increasing the area under the curve in plasma and tumor, the Nano delivery system provides a prolonged exposure to therapeutic and enhanced drug concentration at the target. Notably by reaching the right site and the right exposure, several Nano medicine have conferred a significantly enhanced therapeutic index to an existing therapy as for cerulean, a Nanoparticle formulation marketed by AstraZeneca as AZD2811.

However, new nanomedicine platforms suffer from poor clinical translation as was for the early antibodies therapeutics causing a slow market progression and the greater failure could be ascribed to our poor understanding of the disease heterogeneity in the patient population [75].

As highlighted above, traditionally, the research in nanomedicine field have been focused to adapt the physico-chemical parameters of a delivery system therefore loading, chemistry, size, charge and surface modification to control its *in vivo* behavior. Nevertheless, the heterogeneity of tumor patient has been overlooked and the correlation with nanomedicine behavior that causes their major limitation for optimal performance in clinic. Indeed, The practical evaluation of EPR effect in human tumor are relatively costly and time consuming , moreover the currently available methodologies still faces challenge in sufficient resolution. Although several studies has been performed using sophisticated techniques, they require expensive equipment not accessible for many laboratories. For example, a gamma-scintigraphy/SPECT imaging was used in a study involving few patients to follow indium/ technetium labeled liposome upon systemic injection[76]. Data revealed that the tumor accumulation varied between tumor type ranging from 3-5% of the injected dose in the case of breast cancer to the 33-16% in head and neck cancer. Thus disclosing that the access and/or accumulation of the nanomedicine may be disease dependent and differ from one tumor to the other [55-56]. Furthermore, a confirmation of the inter-tumor variability came out by a recent analysis of the EPR effect in spontaneous canine carcinomas and sarcomas that

showed substantial heterogeneity in the level of liposome uptake, as measured by CT/PET scanning [60].

Therefore, if tumor EPR is the driving principle in the design characteristics of a nanomedicine, then it is essential to treat tumors which present an EPR effect, as obviously variability in the level of EPR effect, or even a complete lack of an EPR effect, would significantly impact the clinical outcome.

2.4 TARGETING THE VASCULATURE USING DISCOIDAL NANOCONSTRUCTS

The nanoparticles relying mostly on EPR effect to reach target site represent the main category described over the last decades in literature. However, the presence of fenestrations is not the only peculiarity of tumor vasculature. For instance, tumor mass present also a tortuous vascular network, low mean blood velocity, impaired lymphatic system and high interstitial fluid pressure.

This environment prevents the penetration of nanosized drugs deep within the tumor and, therefore, contributes to tumor progression, metastasis and drug resistance. On the contrary, all these peculiarities can be used for the preferential accumulation of particles without relying on EPR effect. Interestingly, red blood cells (RBc) represent the majority of corpuscles in the circulation and accumulate within the vessel core creating a “cell free layer” next to the wall. This behavior is responsible of the migration, wall adhesion and extravasation of leukocytes and platelets and it is relevant in the case of inflammation [77].

Therefore, a second class of platform developed during these years represented by discoidal nanoconstruct targeting mostly the malignant vasculature. This category was designed to specifically recognize the altered tumor vasculature and adhere firmly to endothelial cells, without

penetrating the endothelial fenestration. Their size and shape determine its possibility to be pushed laterally in the “cell-free” layer and they consequently accost closely to the vessel walls and possibly create stable interaction within regions of low blood velocity[52;53;54].

3 CHAPTER 1: VASCULAR-CONFINED MULTI-PASSAGE DISCOIDAL NANOCONSTRUCTS FOR THE LOW-DOSE DOCETAXEL INHIBITION OF TRIPLE-NEGATIVE BREAST CANCER GROWTH

3.1 ABSTRACT

Insufficient tumor accumulation and severe off-target effects limit Taxol efficacy in Triple Negative Breast Cancer (TNBC). Nanomedicines offer the unique opportunity to enhance the potency of taxanes against such aggressive molecular subtype of breast cancer which are unresponsive to typical endocrine therapies. Here, 1,000x400 nm Discoidal Polymeric Nanoconstructs (DPNs) were engineered to encapsulate docetaxel (DTXL) and the near infra-red compound lipid-Cy5. DPNs were obtained by filling cylindrical wells in a poly(vinyl alcohol) template with a polymer mixture comprising poly(lactic-co-glycolic acid) (PLGA), poly(ethylene glycol)-diacrylate (PEG-DA), and the therapeutic and imaging agents. A 'multi-passage' loading strategy was proposed to improve DTXL encapsulation and release while ensuring lipid-Cy5 stability. Confocal microscopy confirmed that DTXL-DPNs were not taken up by MDA-MB-231 cells but would rather sit next to the plasma membrane and slowly release DTXL thereof. In orthotopic murine models, Cy5-DPNs efficiently accumulated in TNBC masses with a tumor-to-abdomen ratio of 1.3. With only 2 mg/kg of DTXL, intravenously administered every other day for 13 times, DTXL-DPNs induced tumor regression returning an 80% survival rate at 120 days as compared to 30% with free DTXL. Collectively, this data demonstrates that effective, low-dose tumor treatments can be achieved with vascular confined nanoconstructs by-passing the enhanced permeability and retention effect.

3.2 INTRODUCTION

Breast cancer is the most common malignancy in females and the second leading cause of cancer related deaths [5]. About 20% of breast cancers are negative for both hormones – estrogen and progesterone, and HER2 receptors. This phenotype characterizes the breast malignancy with the most dismal prognosis, known as the triple negative breast cancer (TNBC) [78], showing a faster growth rate and higher likelihood of relapse at secondary sites as compared to hormone positive breast cancers [17]. As hormones and HER2 are not fueling cancer growth, TNBC are unresponsive to typical endocrine therapies. Consequently, the poor outcome of TNBC patients is also attributed to the limited availability of effective therapeutic strategies [79, 80]. In addition, the significant tumor heterogeneity in TNBC has hindered the success of targeted medicines, such as tamoxifen and Herceptin [81]. Therefore, TNBC treatment still remains a challenge and, to date, the combination of surgery, radiation therapy and chemotherapy is the sole option for primary mases [82-84], whereas systemic chemotherapy is used for attacking metastatic niches [85]. Among the plethora of clinically approved chemotherapeutic molecules, docetaxel (DTXL) is one of the most potent but is also responsible for severe adverse reactions due to its non-specific accumulation in healthy tissues [86] and the need of toxic solubilizing agents [87, 88]. For this, the administered doses are often limited, thus significantly impairing the DTXL cytotoxic activity within the tumor tissue [89, 90].

In this scenario, Nanomedicine could play a fundamental role to increase the therapeutic efficacy of small anti-cancer molecules optimizing their bioavailability, tissue deposition, and cellular uptake while limiting off-site targeting [62, 75, 91, 92]. Traditionally, spherical nanoparticles with a sufficiently small size (< 200 nm) have been designed to cross the hyperpermeable tumor vasculature, thus relying on the well-known Enhanced Permeability and Retention (EPR) effect

[93, 94]. By passing through the ‘fenestrated’ endothelium, spherical nanoparticles can reach the tumor parenchyma and progressively accumulate therein, given the lack of a functional lymphatic drainage. A variety of EPR-dependent delivery systems for taxanes have been designed in the context of TNBC therapy, including macromolecular conjugations [95], liposomes [96], polymeric nanoparticles [97-99], micelles [100] and prodrugs [101]. Some of these platforms are already approved for clinical use or under clinical investigation [92, 102]. For instance, the albumin-bound (nab)-paclitaxel (Abraxane) was approved by FDA in 2005 as a second-line treatment of metastatic breast cancer [62]. Interestingly, the clinical use of Abraxane is associated with lower systemic toxicity and only a modest improvement in the therapeutic index [62, 103]. Other taxane-loaded polymeric micelles and nanoparticles, at different stages of clinical development, presented similar outcomes for both primary and metastatic TNBC [100, 104-106]. Recently, Rafael Contreras-Cáceres et al. [107] developed a pH-sensitive nano-carrier encapsulating Paclitaxel within the hollow structure of oxidized poly(4-vinyl pyridine) and demonstrated an improved antitumor activity on A-549 and MCF-7 multicellular tumor spheroids (MTS), as compared to the free drug. In other nanoparticle formulations, a targeting moiety was included on the nanoparticle surface to enhance tumor accumulation and deep penetration into the malignant mass [91, 108-110]. The cell receptor CD44 has been extensively investigated as a targeting molecule in TNBC. For instance, Huang et al. demonstrated that CD44-targeted docetaxel-loaded nanoparticles have enhanced antitumor activity over the untargeted nanoparticles [108]. De-Sheng Liang and colleagues implemented a dual targeting approach including on the same nanoparticle moieties to recognize CD44 molecules, expressed on the cancer cells and neuropilin receptors, exposed on the tumor neovasculature. This approach succeeded in suppressing tumor cell invasiveness and metastatic potential [109]. Also, EGFR-targeted immunoliposomes labeled with Technetium-99m were

shown to highly accumulate in MDA-MB-231 xenografts and in the metastatic lymph nodes of nude rats by SPECT/CT imaging [110].

For all the above listed nanoparticles and many more proposed in the open literature, tumor accumulation via the EPR effect has been always been sufficient to modulate disease progression or even induce regression. However, these encouraging preclinical results often have not been translated in clinical settings for a number of reasons. First, the permeability of the tumor neovasculature to nanoparticles is highly heterogeneous, both at the intra- and inter-patient levels [60, 94, 111, 112]. Second, targeting may improve nanoparticle retention in tumors, but could also favor sequestration by cells of the immune system [113]. Furthermore, bio-conjugation may not be intrinsically that specific because targeting receptors could also be expressed on healthy cells or the orientation of the moieties over the particle surface could be sub-optimal thus impairing the proper biological recognition. Along this line, a recent meta-analysis revealed that active targeting agents yield only modest improvements in intratumor nanoparticle accumulation [60]. In this scenario, designing particles to target and accumulate within the tumor vasculature without relying on the EPR effect could be a valuable, complementary strategy [114-117]. The tumor vasculature is tortuous and characterized by lower flow rates as compared to healthy vascular beds. This specific hemodynamic conditions and vascular architecture would favor the deposition of non-spherical micrometric particles over more conventional spherical nanoparticles [117-120]. These micrometric particles would mimic the behavior of circulating platelets, thus confirming the importance of bioinspiration and biomimicry in the development of novel drug delivery systems [121]. Indeed, the authors have previously demonstrated that discoidal particles can lodge within the tortuous and low perfused tumor microvasculature, up to 20% of the injected dose [117].

In this work, we presented a novel class of Discoidal Polymeric Nanoconstructs (DPNs) to boost drug loading and release at the targeted site without relying on the EPR effect. Specifically, 1,000×400 nm DPNs were directly loaded with the potent anti-cancer drug docetaxel (DTXL) and realized using a 'multi-passage' loading strategy. A comparison between the 'multi-passage' and 'single-passage' DPNs was first presented in terms of morphological, physico-chemical, and in vitro pharmacological characterizations. Then, the therapeutic efficacy and imaging efficiency of DTXL and Cy5-loaded DPN was tested preclinically in mice bearing an orthotopic model of triple negative breast cancer.

3.3 EXPERIMENTAL

3.3.1 Chemicals.

Polydimethylsiloxane (PDMS) (Sylgard 184) were purchased from Dow Coming Corp (Midland, USA). Poly(vinylalcohol) (PVA, Mw 31,000 - 50,000), Poly(DL-lactide-coglycolide) acid (PLGA, lactide:glycolide 50:50, Mw 38,000-54,000), Poly(ethylene glycol) diacrylate (Mn 750) (PEG diacrylate), 2-Hydroxy-40-(2-hydroxyethoxy)-2-methylpropiophenone (Photo-initiator) were purchased from Sigma-Aldrich (Missouri, USA), Rhodamin-B (lipid-RhodB) was purchased from Avanti Polar Lipids (Alabama, USA). Docetaxel was purchased from Alfa Easer (Massachusetts, USA)

3.3.2 Methods

3.3.2.1 Fabrication of Discoidal Polymeric Nanoconstructs.

Discoidal polymeric nanoconstructs (DPNs) were synthetized using a top-down fabrication strategy described in details in previous works by the authors [122, 123]. Briefly, the process started with the fabrication of the silicon master template via Laser Writer Lithography. This technique was used to imprint on a silicon wafer a specific pattern of wells with the geometry of the final DPN. Then, a solution composed by polydimethylsiloxane (PDMS – Sylgard 184) (10-parts base elastomer and 1-part curing agent) was cast over the Silicon wafer to reproduce a negative replica of it. Finally, a sacrificial template was realized by pouring a 5% w/v poly(vinyl alcohol) (PVA) solution on the PDMS template and letting the solution dry at 60° C for about 3 h. Once polymerized, the hydrophilic PVA template reproduced the same cylindrical holes of the original silicon master. DPN were synthetized using a mixture of poly(lactic acid-co-glycolic acid) (PLGA) and poly(ethylene glycol) diacrylate (PEG DA) polymers. 50 mg of PLGA was dissolved in 1 mL of Acetonitrile and mixed with 6 mg of PEG-DA and 10 mg of docetaxel (DTXL). Then, 0.6 mg of a photo-initiator (2-Hydroxy-4'-(2- hydroxyethoxy)-2-methylpropiophenone) was added into the polymeric solution to allow the crosslinking of PEG diacrylate chains after exposure to UV-light (366 nm). A fixed volume of polymeric mixture, including docetaxel (5 µL), was then spread with a blade over the PVA template to accurately fill each well. This step was performed one time for the 'single-passage' DPN and about 4-5 times till complete solvent evaporation for the 'multi-passage' DPN. Finally, the DPNs were released from the hydrophilic PVA templates upon dissolution in deionized water for 3h under gentle stirring, were collected through centrifugation (3,900 rpm for 20 min) and purified from residual debris and scum layer through 2 µm filtration (Sterlitech).

3.3.2.2 **Physio-chemical characterization.**

The DPN geometry and synthesis yielding was assessed through Multisizer 4E Coulter Particle Counter (Beckman Coulter, USA), that calculated particle concentration in a defined volume of 20 mL of isotone solution. The hydrodynamic diameter and surface electrostatic charge (ζ – potential) of DPN was measured using a Zetasizer Nano (Malvern, UK). The characteristic discoidal shape of DPN was confirmed using Electron Microscopy. DPN morphology was observed using a Jem-1011 Transmission Electron Microscope (Jeol, Japan) coated with sputtered carbon and Scanning Electron Microscopy (Helios Nanolab 650) after 10 nm aureum coating. Fluorescent DPN were synthesized by adding 30 µg of Rhodamin-B (DSPE-RhB) to the polymeric mix made of PLGA and PEGDA and were observed using an A1 confocal fluorescent microscope (Nikon).

3.3.2.3 **Loading and Release studies.**

The 'direct loading' method was used to uniformly disperse imaging and therapeutic agents within the DPN matrix [123, 124]. Specifically, a 5 µl homogenous drug/polymer solution was uniformly spread using a blade over the surface of a 3×3 cm PVA template, containing about 10^8 wells. This step was performed only once for the 'single-passage' DPN and several times till complete solvent evaporation for the 'multi-passage' DPN. This loading strategy was different from the 'absorbance loading' previously described by the authors [123]. The amount of drug loaded within DPN was calculated using a HPLC and by reading the characteristic docetaxel UV absorbance at 230 nm (Agilent 1260 Infinity, Germany). Samples for HPLC analysis were prepared by spinning down DPN at 12,700 RPM for 20 min, drying the pellet overnight and dissolving the particles upon incubation with acetonitrile (ACN). The encapsulation efficiency was calculated considering the percentage weight ratio between the drug amount loaded within the DPN matrix at the end of the

synthesis process and the initial drug input. Release studies were performed in a volume of 4L of buffer at controlled pH 7.4 and 37° C to reproduce typical physiological conditions. At each time point, 200 µL of DPN solution was poured into Slide-A-Lyzer MINI dialysis cups with a molecular cut off of 10 kDa (Thermo Scientific) and dialyzed. At each time point, DPN were collected and dissolved in ACN to read the amount of DTXL still entrapped in the matrix overtime.

3.3.2.4 **In vitro cell viability tests.**

For cytotoxicity tests in vitro, the human Triple Negative Breast Cancer cell line MDA-MB231 was obtained from the American Type Culture Collection (ATCC). Cells were cultured in Eagle's minimal essential medium (EMEM) (ATCC, USA) completed with 10% FBS (Gibco, Thermo Fisher Scientific, USA), 1% penicillin/streptomycin (Sigma-Aldrich, USA), under a humid atmosphere (37°C, 5% CO2, 95% air). Cell viability was determined by MTT assay, which detects the reduction of MTT (3-(4,5-dimethylthiazolyl)-2,5- diphenyltetrazolium bromide) (Sigma-Aldrich, USA) by mitochondrial dehydrogenase to blue formazan product. This reflects the normal function of mitochondria and, hence, cell viability. Briefly, different number of cells were seeded in 96-well plates for each time point, specifically 10^4 cells/well for the 24h, $7.5x10^3$ for 48h, and $5\ x10^3$ for 72h were seeded in 96-well plates and incubated at 37°C, 5% CO_2, for 24 h. The day after, cells were treated with EMEM containing the selected doses of DTXL and DTXL- DPN (0.1 – 1,000 nM). After 24, 48 and 72 h, the treatment solution was removed and replaced by MTT solutions, according to the manufacturer's instructions. The resulting formazan crystals were then dissolved in ethanol (200 µL/well) and the absorbance was read at 570 nm using a microplate reader (Tecan, CH). Six replicates were considered for each DTXL concentration. Data were

collected when the absorbance ranged between 0.8 and 1.2. Cell viability was normalized to that of untreated cells.

3.3.2.5 **Cell Uptake experiments.**

To assess DPN internalization, 4×10^4 MDA-MB-231 were seeded into 8 well cover slides and treated with the DPN at a concentration of 10 DPN/cell. After 2h, 4h, 8h and 24h incubation, cells were fixed using 4% paraformaldehyde and DPN uptake was studied via Z-stacks analysis performed on a Nikon confocal fluorescent microscope. For these studies, RhB-DPN were used.

3.3.2.6 **Optical imaging of orthotopic breast cancer.**

0.9 million of MDA-MB-231 luciferin positive cells were injected in the 3rd mammary fat pad of female CD1 immunodeficient nude mice to allow the development of orthotopic breast cancer. The growth of the tumor mass was followed by whole animal optical imaging (IVIS Spectrum system, Perkin-Elmer) until 4 weeks post cells inoculation. Once tumors reached an average radiance in the order of 10^8 [p/s/cm²/sr], mice were intravenously injected with Cy5-DPN.

3.3.2.7 **Tumor model and therapeutic experiments.**

All animal experiments were performed according to the guidelines established by the European Communities Council Directive (Directive 2010/63/EU of 22 September 2010) and approved by the National Council on Animal Care of the Italian Ministry of Health. All efforts were made to minimize animal suffering and use the lowest possible number of animals required to produce statistical relevant results, according to the "3Rs concept". For the orthotopic breast tumor model, 6-weeks old female CD1 immunodeficient nude mice (Charles River, Calco, Italy) were used.

Animals were grouped in ventilated cages and able to freely access food and water. They were maintained under controlled conditions: temperature (21 ± 2 °C), humidity (50 ± 10%) and light (12 and 12 h of light and dark, respectively). Before injection of cells, animals were anaesthetized with a mixture of ketamine (10%) and xylazine (5%), which was administered via a single intraperitoneal injection. For the injection, trypsinized 0.9×10^7 MDA-MB-231 luciferase positive cells were resuspended in cold matrigel solution. A total of 100 µl of matrigel was subcutaneously injected into the third mammary fat gland. Animals were carefully monitored until recovered from anesthesia. Tumor growth was followed by IVIS Spectrum system every 2 day, upon intraperitoneal injection of D-luciferin, Potassium salt (GoldBio) at a dose of 150 mg/Kg and by caliper measurement. Tumor growth was calculated by tumor volume (V) with the formula V = W 2 × L /2 (W = width; L = length). When tumors reached an overall volume of about 0.15 cm^3, mice were randomized into three groups (six mice per group). The groups were dosed for 30 day by retro-orbital injection every 2 day with saline, Free-DTXL and DTXL-DPNs. Each injected dose contained 40 µg of docetaxel into DPN or as commercial clinical formulation. The therapeutic efficacy of the different treatments was evaluated by whole animal optical imaging (IVIS Spectrum system) and caliper measurement every two days. All mice were euthanized when they became moribund or tumor volume passed a volume of 1 cm^3. Survival was monitored and plotted using the Kaplan-Meier method.

3.3.2.8 **Statistical Analysis.**

All data were processed using Excel 2010 software (Microsoft) and GraphPad PRISM. Results were expressed as mean + standard deviation. Statistical analyses on *in-vivo* experiments were performed using t-test. Log-rank test was used to test the significance of different survival curves.

The p values of <0.05 (*), <0.01 (**), and <0.001 (***) were considered to be statistically significant.

3.4 RESULTS AND DISCUSSIONS

3.4.1 'Multi-passage' loaded Discoidal Polymeric Nanoconstructs.

The particle fabrication comprises of a number of sequential steps (*Figure 3.1 A*) through which the *4S parameters* of DPN – size, shape, surface properties and mechanical stiffness – were precisely tailored in order to optimize their *in vitro* and *in vivo* performance. Briefly, the initial manufacturing step involved the use of a direct laser writing system to realize a silicon master template with billions of wells per wafer presenting a well-defined geometry. In the present study, the wells in the silicon wafer were cylinders with a ~1,000 nm diameter and a ~400 nm depth (*Figure 3.1 B*). Then, a soft lithographic technique was used to generate multiple negative replicas of the original master template in polydimethylsiloxane (PDMS) (*Figure 3.1 C*). The wells in the master template were turned into cylindrical posts, comparable in diameter and height to the wells. Finally, the PDMS template was replicated into multiple polyvinyl alcohol (PVA), sacrificial templates presenting wells with the same geometry as in the master silicon template *(Figure 3.1 D).* After drying the PVA template, its wells were accurately filled by uniformly spreading a polymeric paste. This comprised of an homogeneous mixture of the hydrophobic poly(D,L-lactide-co-glycolide)-acid carboxylic terminated (PLGA-COOH) and hydrophilic poly(ethylene glycol) diacrylate (PEG-DA) including the therapeutic and imaging agents of interest. The PLGA-COOH

and PEG-DA mixture formed the actual polymeric matrix of DPN, which was characterized by hydrophobic and hydrophilic pockets entrapping the loaded agents. In the current configuration, the chemotherapeutic molecule docetaxel (DTXL) and the red fluorescent molecule RhB-DSPE or the near-infra red molecule Cy5-DSPE were dispersed within the polymer matrix. To release and collect the DPN loaded with DTXL and Cy5-DSPE, the PVA templates were dissolved in water for 3 hours at room temperature and under gentle stirring (*Figure 3.1 A*). Differently the previous authors' practice [123], in this work, the spreading of the polymeric paste on the PVA template was performed multiple times till complete solvent evaporation (4-5 times).

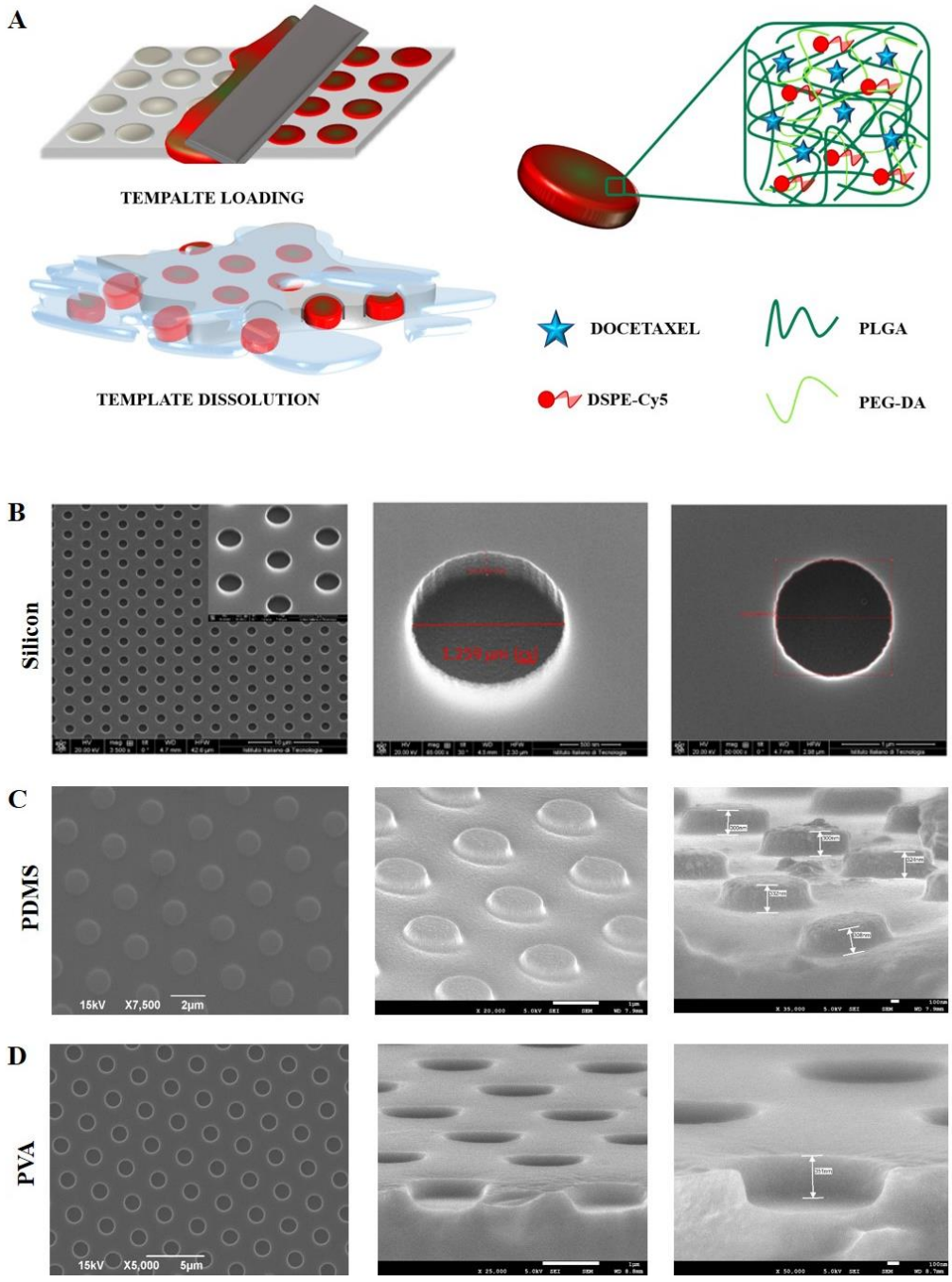

***Figure 3.1**: **DPNs morphological characterization.** **A.** Schematic representation of the DPN fabrication and purification process (**left**). Structure and molecular constituents of DPNs (**right**). **Scanning Electron Microscopy images of the templates. B**. Silicon master template; **C.** PDMS intermediate template; **D.** PVA sacrificial template.*

This modification in the fabrication protocol, named ‘multi-passage’ loading, allowed the authors to increase the amounts of loaded agents per particle and thus, improve the DPN pharmacological and imaging properties as compared to the previous configuration (‘single-passage’ loading).

The morphological properties of the ‘multi-passage’ loaded DPN were investigated using scanning electron microscopy (SEM) *(Figure 3.2 A),* transmission electron microscopy (TEM) *(Figure 3.2 B)* and confocal fluorescent microscopy *(Figure 3.2 C).* As compared to the ‘single-passage’ method, the electron and optical density of the ‘multi-passage’ DPN were higher suggesting a larger mass of polymers and fluorescent imaging probes trapped within the matrix, as can be inferred by looking at *Figure 3.2 B-C.* The DPN morphological and physico-chemical properties were also characterized by using a Multisizer Particle Counter and a Zetasizer Nano *(Figure 3.2 D-F).* The Multisizer Particle Counter spectrum for the ‘multi-passage’ DPN showed a sharp peak around 700 ± 150 nm that is slightly, but not significantly ($p = 0.1$), larger than for the ‘single-passage’ DPN (670 ± 100 nm) (*Figure 3.2 D* – ‘single-passage’: purple; ‘multi-passage’: blue). This again would imply that the ‘multi-passage’ strategy allows for a more accurate filling of the PVA wells with the polymer and functional agents without changing DPN geometrical proprieties. The Dynamic Light Scattering (DLS) analysis *(Figure3.2 E,F)* showed a uniform and monodispersed size distribution for the ‘multi-passage’ DPN around 880 ± 200 nm and a negative surface charge ζ of – 32 ± 0.15 mV, ensuring the colloidal stability of the suspension. Even the DLS analysis confirmed a small difference in size between the ‘single-passage’ and ‘multi-passage’ DPN design ($p=0.5$). (*Figure 3.2 E,F* – ‘single-passage’: purple; ‘multi-passage’: blue). Therefore, the ‘multi-passage’ does not alter significantly the morphological and physico-chemical

properties of DPNs. Overall, the data of *Figure 3.2* confirm that the DPN size, shape and surface properties are well preserved.

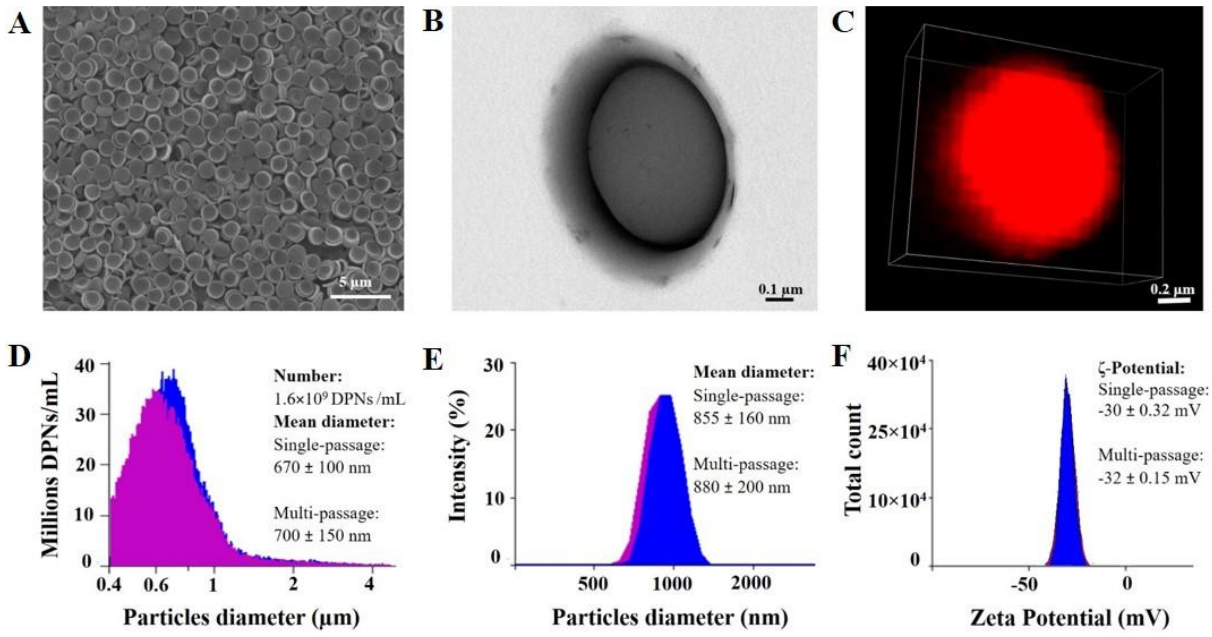

***Figure 3.2**: **DPNs morphological characterization.** **A.** Scanning Electron Microscopy of DPNs. **B.** Transmission Electron Microscopy of a single DPNs. **C.** Confocal Fluorescent Microscopy of a DPN loaded with Rhodamine B – DSPE. **D.** Size distribution and number of DPNs measured via a Multisizer Coulter Counter system. **E.** DPN size distribution measured via Dynamic Light Scattering. **F.** Surface electrostatic ζ-potential of DPNs (purple curve: 'single-passage' vs blue curve: 'multi-passage').*

3.4.2 Controlled drug release and *in vitro* cytotoxicity.

So far, RhB-DSPE was consistently loaded into DPN to highlight the particle morphological features via fluorescent microscopy. Following the same strategy, any other imaging agent and therapeutic molecule could be directly loaded into the polymeric matrix of DPN. Thus, the

chemotherapeutic drug docetaxel (DTXL) was dispersed directly within the polymer paste and loaded into DPN. The encapsulation efficiency (EE%) and release profile of DTXL over time are presented in *Figure 3.3 A-B,* as derived by high performance liquid chromatography (HPLC). A direct comparison between the 'single-passage' and 'multi-passage' strategies documented a two-fold increase in drug loading retuning a 10 versus 20 μg of DTXL per 10^9 DPN, respectively. Interestingly, by introducing a simple variation in the fabrication protocol, a two-fold increase in drug loading was achieved. Therefore, the additional passages of the polymeric paste over the PVA template mainly helped to fill more homogenously the discoidal wells and, thus, increase the amount of polymer and drug molecules encapsulated per particle.

Then, release studies were performed by incubating DTXL- DPN into PBS (infinite sink condition: 4 liters) up to 72h at pH 7.4 and 6.5, representing the mildly acidic environmental conditions of the tumor microenvironment. Figure 3B shows the release curves for the 'multi-passage' DTXL-DPN. Under physiological conditions (pH 7.4), despite a moderate burst within the first few hours (30% in 1h), which is most likely related to DTXL molecules adsorbed on the DPN surface, drug release appeared to be sustained overtime up to 72h. At 24h, almost 80% of the loaded DTXL was released, and this percentage grew to 85% and 90% at 48 and 72h, respectively. As expected, drug release was accelerated under acidic conditions for the partial degradation of the DPN matrix [125]. Specifically, at pH 6.5, 90% of the drug was released within 24h while it took 72h to completely release all loaded DTXL. The 'multi-passage', direct loading strategy here demonstrated allowed the authors to improve the pharmacological properties of DPNs reaching drug loading conditions that are compatible with tumor treatment. However, the 'multi-passage' DPN were characterized by higher loading and a slower release rate as compared to the 'single-passage' configuration.

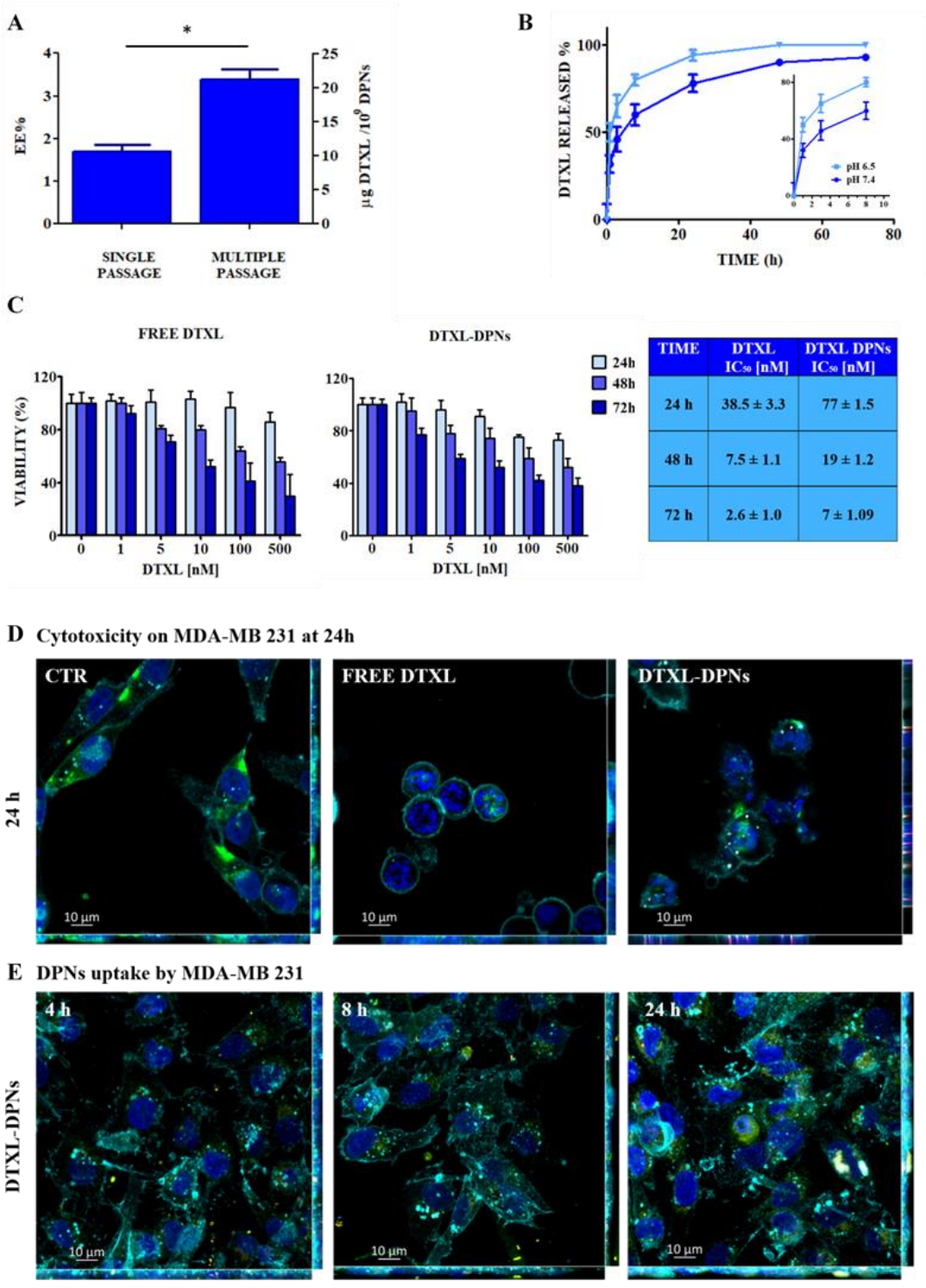

***Figure 3.3**:**Pharmacological characterization and in vitro therapeutic properties of DPNs. A.** Docetaxel (DTXL) amounts and encapsulation efficiencies (EE) for DPNs loaded using the 'single-passage' vs the 'multi-passage' strategy. **B**. Docetaxel release out of 'multi-passage' DPNs*

over time under physiological (pH 7.4) and acidic (pH 6.5) conditions. ***C****. Cytotoxic potential on triple negative breast cancer MDA-MB 231 cells treated with Free DTXL and DTXL-DPNs up to 72 hrs incubation time (**left**). Table listing the* IC_{50} *values for each treatment condition and time point (**right**).* ***D****. Confocal fluorescent microscopy images of untreated (**left**); Free DTXL treated (**center**); DTXL-DPNs treated MDA-MB 231 cells (20 nM DTXL, at 24h).* ***E****. Confocal fluorescent microscopy images of MDA-MB 231 cells incubated with DPNs labeled with RhB-DSPE (red) and loaded with curcumin (green) at different time point (respectively 4, 8, 24h).*

Finally, the *in vitro* cell-killing efficacy of 'multi-passage' DPN was tested against a triple negative breast cancer cell line, namely the MDA-MB 231 cells. These were incubated with different concentrations of DTXL-DPN to estimate the IC_{50} values at 24, 48 and 72h. Figure 3C shows the percentage of viable cells as a function of free and DPN-loaded DTXL concentrations. As expected, DTXL-DPN were less cytotoxic on tumor cells as compared to free DTXL molecules for a given time, documenting an IC_{50} value of 77 ± 1.5 nM against 38.50 ± 3.3 nM at 24h. Similarly, at longer time points (72h), the particle formulation confirmed a slightly lower toxicity than the free drug with an IC_{50} value of 7 ± 1.09 nM against 2.6 ± 1.0 nM. Data are presented in Figure 3C in graphical and tabular forms. The controlled release of DTXL from the DPN was indeed responsible for the lower efficacy of the DTXL-DPN for any given time point. However, the cytotoxic potential of free DTXL was essentially preserved upon encapsulation into DPNs. Furthermore, the pharmacological activity on cytoskeletal microtubules was assessed by confocal microscopy as showed in *Figure 3.3 D*. The untreated MDA-MB 231 displayed a well-organized microtubule cytoskeleton (green) and a typical, elongated shape. On the contrary, cells treated with free DTXL and DTXL-DPNs (20 nM) presented microtubule bundles and aberrant mitotic multinucleated morphologies already at 24h post incubation. Moreover, confocal microscopy was

used to assess further DPN interaction with MDA-MB 231 at 2, 4, 8, 24h for the concentration of 10 DPN/cell. Representative images in Figure 3E proved that just a few particles were internalized while most DPN sat on or next to the cell membrane releasing thereof the therapeutic cargo.

3.4.3 Preclinical imaging and therapeutic performance of DTXL-DPN.

To evaluate the *in vivo* imaging (Cy5-DPN) and therapeutic (DTXL-DPN) performance of the discoidal polymeric nanoconstructs, an orthotopic murine model of triple negative breast cancer (TBNC) was considered. *Figure 3.4 A* reports schematically the timeline of the preclinical experiment. Initially, MDA-MB-231 luciferin positive cells were injected into the 3rd mammary fat pad of 7-weeks old immunodeficient mice and left to proliferate for 45 days to establish a palpable tumor mass. Tumor growth was monitored by whole animal optical bioluminescence imaging (IVIS) and manually with a caliper. Upon reaching an average tumor size of 0.15 cm^3, mice were randomly divided in three experimental groups: the 'saline' group, including mice injected with PBS; the 'free-DTXL' group, including mice injected with a DTXL solution (2 mg/kg); and the 'DTXL-DPN' group, including mice treated with 2 mg/kg of DTXL-loaded within the DPN. In all the cases, the administration was performed intravenously every 2 days for up to 30 days, returning a total number of injections equals to 13. Note that the DTXL administered dose of 2 mg/kg was significantly lower than that conventionally used in pre-clinical experiments, which typically ranges between 10 and 20 mg/kg.

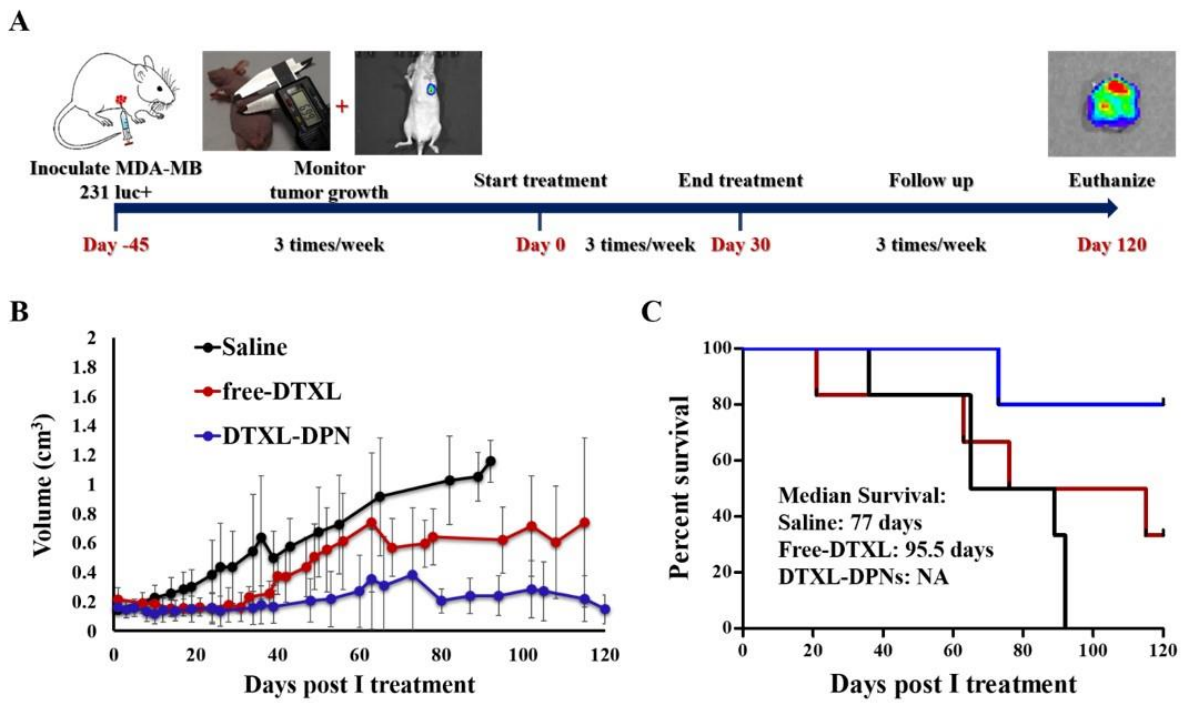

Figure 3.4: In vivo therapeutic and imaging studies on orthotopic breast cancer murine models. ***A****. Timeline of the preclinical experiments performed on mice bearing orthotopic breast cancer and including bioluminescence/fluorescent imaging and tumor growth analysis.* ***B.*** *Average tumor growth curves comparing the efficacy of three different intervention. Data are presented as the average tumor volumes ± SD. (black line: saline; red line: Free DTXL; blue line: DTXL-DPN). (At 120 days: $p < 0.05$ for free DTXL vs saline and DTXL-DPNs vs saline; and $p = 0.05$ for DTXL-DPNs vs DTXL. At 92 days: $p < 0.05$ for DTXL-DPNs vs DTXL – $n \geq 5$).* ***C.*** *Kaplan–Meier curves for survival. (black line: saline; red line: free DTXL; blue line: DTXL-DPN).*

Figure 3.4 B summarizes the tumor growth curves for the three different treatment groups over a period of 120 days. Malignant masses in the 'saline' group (black line) continuously grew over time reaching an average size of 1.16 ± 0.14 cm^3 at about 90 days, at which time the surviving mice

(only 2) were sacrificed. Mice treated with systemically administered free-DTXL (red line) showed an initial positive response to therapy with a stabilization of the tumor mass within the first 3 weeks of treatment, then followed by a progressive growth demonstrating relapsing of the disease. The mice that survived at 120 days (n = 2) showed an average malignant mass of 0.74 ± 0.57 cm^3. The 'DTXL-DPN' group (blue line) showed an overall positive response to the treatment with a significant tumor stabilization during the whole observation period. As documented in *Figure 3.4 B*, a moderate increase in tumors size was observed during the first 70 days up to an average volume of 0.48 ± 0.4 cm^3 that was then followed by a steady decrease for the remaining observation period below the original tumor size. It was noted that even in the initial phase, the tumor growth rate was lower for the mice treated with DTXL-DPN rather than with Free-DTXL. Mice survival was plotted in *Figure 3.4 C.* The three curves demonstrate that 80% of the DTXL-DPN mice survived at 120 days against the 30% for the case of Free-DTXL. The control mice were sacrificed within 90 days because of excessive tumor burden. The difference between average tumor volumes for DTXL-DPN and Free-DTXL was statistically significant at day 92 ($p = 0.02$), representing the end point for the saline group, and at day 120 ($p = 0.05$), indicating the end of the study. The average radiance associated with the tumors of the surviving animals at the end of the treatment are reported in *Figure 3.5*, documenting once again the smaller size of the DTXL-DPN treated tumors over the Free-DTXL group. Furthermore, to assess any severe toxicity associated with the treatment, the mouse weight was monitored for the whole duration of the experiment *(Figure 3.6).* Free-DTXL and DTXL-DPN treatments caused a negligible reduction (10%) in mouse weight over the first 20 days. As the treatment was completed, all mice progressively regained the lost weight and, at 120 days, no difference was observed as compared to the initial

point. Overall, the treatment with DPN was well tolerated by the mice and the moderate loss of weight should be mostly attributed to the drug inherent toxicity.

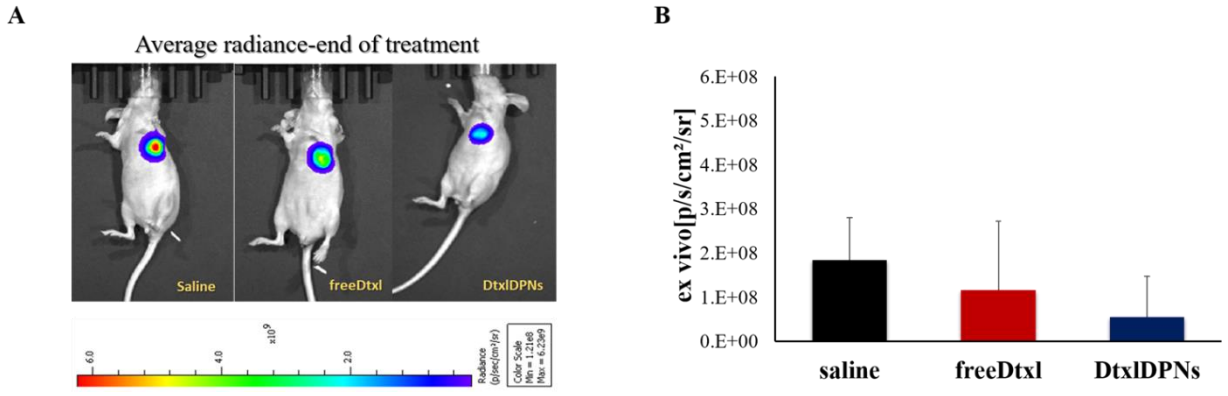

Figure 3.5: Tumor size at the end of the treatment. A. *Representative images of average radiance at the end of the treatments for the three different experimental groups.* ***B.*** *Average radiance of the explanted tumors. (Data are plotted as mean radiance ± SD).*

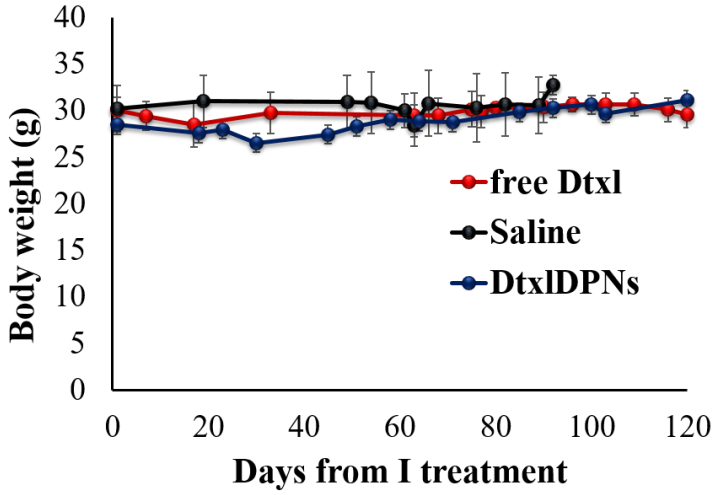

Figure 3.6: Body weight curves of the three different experimental groups. *(Data are presented as the mean weights ± SD).*

By loading the near infra-red molecule Cy5 into DPN, the polymeric nanoconstructs were turned into theranostic agents, whose accumulation in different organs upon intravenous injection could be assessed via whole animal optical imaging (IVIS) [126, 127]. Mice bearing orthotopic breast cancers were systemically administered with 10^9 fluorescent DPN and monitored longitudinally by acquiring images at 30 min, 1, 3, 6 and 24h post injection. In the first few hours, fluorescence was mostly detected in the abdominal cavity, where almost the totality of the blood is processed through the liver. However, the radiance associated with this portion of the animal body was observed to continuously reduce over time in favor of a stable tumor accumulation. This was documented in *Figure 3.7 A* where the average normalized radiance in the abdomen and tumor was plotted over time, while in the right side the tumor to abdominal cavity ratio was plotted.

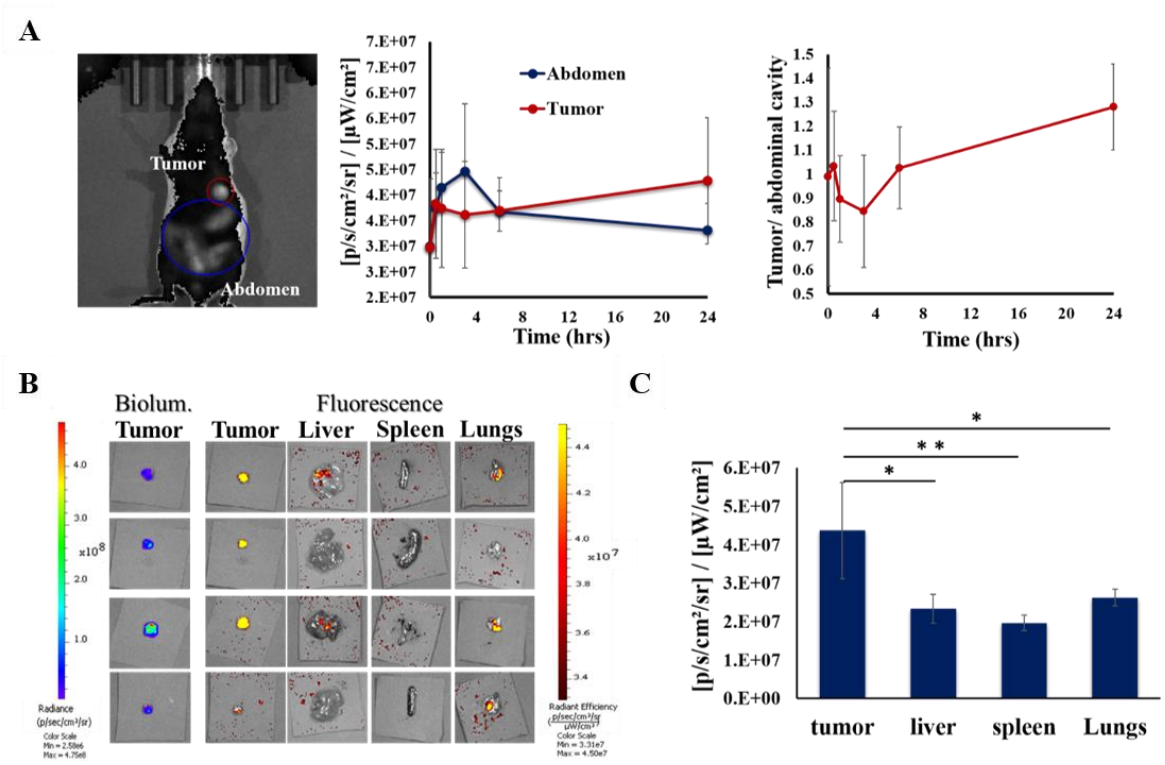

Figure 3.7: In vivo therapeutic and imaging studies on orthotopic breast cancer murine models. ***A.*** *Quantification of the average radiance in the tumor tissue and abdominal cavity: identification of the Regions of Interest (**left**); average radiance variation over time within the ROIs (**center**); ratios between the average radiance estimated in the two ROIs over time (**right**). (Time zero: background fluorescence before Cy5-DPNs injections. Data are plotted as mean average radiance ± SD).* ***B.*** *ex-vivo bioluminescence and fluorescence analysis for main organs (Liver, Spleen, Kidneys, Tumor, Lungs) harvested at 24 hrs post Cy5-DPN injection.* ***C****. Quantification of the average radiance associated with the main harvested organs at 24hrs post Cy5-DPN injection (p = 0.02 for Tumor vs Liver; p = 0.009 for Tumor vs Spleen; p = 0.033 for Tumor vs Lungs).*

This data showed that at time zero the ratio was equal to 1, demonstrating an equal background signal in both ROIs (abdomen and tumor) before particle injection. The ratio became lower than one in the first few hours, as a consequence of continuous blood processing through the liver and other major organs in the abdominal cavity. After the first three hours, the ratio started to steadily increase reaching a value of about 1.3 in favor of the tumor at 24 hrs. These observations continued to suggest that, at longer time points, DPN would tend to accumulate in the tortuous tumor vasculature escaping non-specific sequestration in organs of the Reticulo Endothelial System (RES) [128]. Characteristic ex-vivo fluorescent images of different organs, including the tumor (112.325 ± 70.5 mg), liver (2292.7 ± 271.5 mg), spleen (145.7 ± 73 mg) and lungs (259.25 ± 99.4 mg), are assembled in *Figure 3.7 B.* These confirmed a significant particle accumulation in the tumors as opposed to the liver, spleen and lungs, as quantified in the bar chart of *Figure 3.7 C.* The surface-normalized radiance associated to the tumor was significantly larger than for other RES organs.

The presented results suggested that the combination of a micrometric size with the discoidal shape and the overall deformable hydrogel structure allowed DPNs to stay longer in the blood stream. Thereby avoided a rapid and massive accumulation in typical RES organs, such as the liver and the spleen, and thus increasing the likelihood to deposit with the tortuous vasculature of malignant masses [114]. Specifically, the DPN deformability has been shown to play a major role in limiting the uptake by phagocytic cells residing in the liver and the spleen (see also *Figure 3.3 E*), while DPN geometry was instrumental in favoring vascular deposition and firm adhesion in tortuous and low perfused malignant vessels [118, 122, 129]. Indeed, *Figure 3.7* documents a significant accumulation of Cy5-DPNs within the tumor tissue. Also, the tumor-to-abdominal cavity accumulation appeared to grow monotonously over time to reach a value of 1.3 at 24h post Cy5-DPN administration *(Figure 3.7 A).*

Overall, the high tumor accumulation, low liver sequestration and sustained drug release would contribute to explain the efficacy demonstrated by DTXL-DPNs in treating triple negative breast cancer. It is important to highlight that animals were injected every 2 days for 13 consecutive times with only 2 mg/kg of DTXL. This was sufficient to modulate the growth of orthotopic TNBC during the first 70 days and, eventually, induce tumor regression for the following 50 days. This resulted in an 80% survival as compared to 30% for the Free-DTXL treatment. Conventionally, in these preclinical studies, DTXL doses ranging between 10 and 50 mg/ kg of animal masses were considered [106, 109, 130].

Finally, it should be also noted that given the characteristic size of 1,000×400 nm, DPNs were not expected to cross the fenestrated endothelium and migrate into a perivascular position as most nanomedicine do. In this sense, DPNs do not rely on the EPR effect to deposit within malignant masses but would rather mimic the vascular behavior of platelets. In this sense, DPN would

continue to confirm the importance of bioinspiration and biomimicry in the development of novel drug delivery systems [121].

3.5 CONCLUSIONS

In conclusions, it has been demonstrated that Discoidal Polymeric Nanoconstructs could be loaded with therapeutic and imaging agents to realize a theranostic particle for the treatment of triple negative breast cancer. A potent chemotherapeutic agent – docetaxel – and a fluorescent compound – Cy5 conjugated to a lipid chain – were efficiently entrapped into the hydrogel matrix of DPNs using a 'multi-passage' direct loading strategy. Independent of the enhanced permeability and retention effect, the geometrical and mechanical attributes of DPNs favored high tumor accumulation and supported tumor regression with modest drug doses. These results continued to support the notion that effective tumor treatment could be achieved even without relying on the EPR effect and, as such, DPNs could be used together with conventional nanomedicines and small anti-cancer molecules against a variety of malignancies.

4 CHAPTER 2: MODULATING THE CHEMICAL PROPRIETIES OF DOCETAXEL FOR IMPROVING THE RETENTION WITHIN A SOFT PLGA MATRIX

4.1 ABSTRACT

High loading and specific release of therapeutic agents within the tumor microenvironment are key factors in the development of novel nano-based therapeutic systems against cancer. Although drug availability and preferential tumor accumulation improved with advanced drug delivery system for cancer therapy, they still faces challenge in drug encapsulation and retention. Here, Discoidal Polymeric Nanoconstructs (DPNs) were employed to load and systemically deliver both hydrophilic and hydrophobic therapeutic molecules. DPNs appear as disks, with a diameter of about 1 μm and a height of 400 nm, designed for vascular adhesion in a tortuous and low perfused vasculature as in the case of tumor. Moreover, soft DPNs presenting a stiffness of about few kPa, were shown to circulate longer, more effectively avoid the sequestration by hepatic and splenic immune cells and accumulate at higher doses in the tumor vasculature as compared to rigid DPNs. DPNs were synthetized by mixing together hydrophobic – poly(lactic-co-glycolic acid) (PLGA) and hydrophilic – polyethylene glycol diacrylate (PEG-diacrylate) using a top-down, template-based fabrication process. Therapeutic molecules were incorporated within the polymer matrix of soft DPNs following two different loading approaches: *direct loading*, where the molecules of interest were directly mixed together with the constituting polymers while forming the actual DPN matrix; *absorption loading*, where the molecules of interest was introduced within an already formed DPN polymer matrix via capillary suction. In the latter case, DPNs were first lyophilized and then re-hydrated in a highly concentrated solution of the molecules of interest. Indeed, only

therapeutic molecules that could be dispersed in organic solvents could be incorporated via direct loading; whereas, only therapeutic molecules that can be dispersed in water could be incorporated via absorption loading.

Following this notion, two different prodrugs were realized, namely oleic-Docetaxel (O-DTXL) and PEG-Docetaxel (PEG-DTXL). O-DTXL was incorporated via both direct and absorption loading within the polymeric matrix. Conversely, the more hydrophilic PEG derivatives were loaded via absorption. The size and stability of the resulting DPNs were characterized using dynamic light scattering. Moreover, electron microscopy (SEM and TEM) were used to reconstruct the actual morphology of the particles .The prodrug encapsulation efficiency and release kinetics were examined using HPLC. With the absorption loading, it was observed that O-DTXL formed small micelle-like particles, returning encapsulation efficiencies as high as 13%. Differently, free DTXL and O-DTXL loaded directly within the DPN matrix returned low encapsulation efficiencies of about 1 and 2%, respectively. The more hydrophilic PEG-DTXL were associated with a 15% of encapsulation efficiency. The cytotoxicity of the prodrug-loaded DPNs was performed via a conventional MTT assay on MDA-MB-231. *In vitro* cytotoxicity tests confirmed that hydrophilic prodrugs were more efficient than O-DTXL mostly for their faster rate of release.

4.2 INTRODUCTION

Nanostructured polymer particles can be designed and engineered with a wide range of properties and can provide new ways to diagnose and treat diseases[131]. In a biological setting, some important parameters like surface chemistry, size, shape and stiffness (4S parameters) of

nanostructures play an important role in controlling the *in vivo* performance and the ability to overcome biological barriers to reach the desired site[132, 133]. In this context, human red blood cells (RBCs) have largely inspired the nanostructure design and has been even investigated as drug delivery tool[134]. For example, Anselmo et al. used the flexibility, circulation and vascular mobility of red blood cells (RBCs) to deliver nanoparticles and simultaneously overcome biological barriers and coining the term "cellular hitchhiking". A noncovalent attachment of nanoparticles to RBCs simultaneously increases their level in blood over a 24 h period and allows transient accumulation in the lungs, while reducing their uptake by liver and spleen. The flexibility is one of the key properties that enables long circulation of RBCs, and the reduced deformability is a characteristic of several pathological states[135]. Moreover, as previously demonstrated, discoidal nanostructures with micrometric size exhibit deformable proprieties and are able to circulate in the bloodstream for a long time[136]. In the last few years, several important steps have been made toward engineering soft particles with stealth properties inspired by red blood cells [125]. Using mixtures of PEG di-acrylate with poly(lactic-co-glycolic acid) PLGA in presence of a photo initiator, a template-based photo polymerization have been used to prepare hydrogel particles with tunable elasticity, controlled size and morphology[137]. Such properties were achieved by modulating the ratio of PEG di-acrylate and PLGA used for polymeric mixtures and have been evaluated atomic force microscopy (AFM)[122]. Although these studies represent important advances in bioengineering of the 4S proprieties, the drug loading and retention capability of deformable Nano constructs still faces challenges when used to encapsulate small or hydrophilic drug entities for therapeutic investigation. In the previous chapter, it was demonstrated that a multiple passage approach improved the loading efficiency, retention and stability of the drug showing a significant tumor suppression in the context of triple negative breast cancer.

Contemporary attempts were focused on optimizing the compatibility between the drug and polymers in order to achieve higher encapsulation of the drug. The prodrug strategy has been largely used to overcome multiple barrier such as low solubility, poor stability, lack of cite specificity and inefficient cell uptake improving the efficacy of existing anticancer agents.(ref) Recently, several prodrug Nano system based on polymer –drug conjugate has been developed using block polymers, polyaminoacids, polypeptides or polysaccharides. For example, polyprodrug amphiphiles self-assembled from PEG-b-PCPTM was developed for captothecin delivery where PCPTM was polymerized with CPT prodrug monomer to achieve a reduction responsive drug release. Interestingly, these block polymer can self-assemble in four different nanostructures with extremely high CPT loading content of 50%. Furthermore, NKO12, a prodrug based nano micelles, with SN-38 conjugated with a PEG-poly(glutamic acid)copolymer, has been evaluated in clinical trial. Different from polymer prodrug, self-assembling small weight prodrugs refer to conjugates usually synthetized by coupling one drug molecules to another small molecules such as lipid chains, low molecular weight oligo or amphiphilic peptidic prodrug. Among all, the squalene based prodrugs have drawn widespread attention in recent years for displaying high drug loading efficiency. Drug molecules with poor water solubility such as Docetaxel or Paclitaxel, would certainly benefit from the lipid prodrug strategy for improved lipid solubility and enhanced miscibility within the polymer matrix. Ansell et al. reported improved antitumor activity of paclitaxel prodrug encapsulated in Nano carriers by manipulating the hydrophobicity of paclitaxel-lipid alcohol conjugate.(ref) However, the lipid-derivate suffer from short blood circulation due to the lack of a dense shielding layer. Therefore, usually they were stabilized with PEG chain to obtain both long circulation time and high structural stability. Cho et al. pointed out that , since the tumor appeared as a complex reality, hybrid nano system, integrating multiple nanoparticulate

drug delivery approach, could become a prominent trend in both parenteral and non-parenteral administration [138].

Herein, we engineered a novel class of Discoidal PLGA-PEG-DA Nanoconstructs (DPNs) to boost drug loading and release at the targeted site without relying on the EPR effect. Specifically, the hydrophobic derivate oleic-docetaxel and the hydrophilic derivative PEG-Docetaxel were loaded within the matrix of 1,000×400 nm DPNs directly or by absorption of aqueous solution of the drug. While the PEG-DTXL was associated with a higher encapsulation efficiency it also exhibiter faster release from the particles. The cytotoxicity of the Nanoconstructs was evaluated using MTT assay on two cell lines and the tests confirmed that the hydrophilic prodrugs were more potent than the hydrophobic counterpart due to their faster rate of release.

4.3 EXPERIMENTAL

4.3.1 Chemicals

Polydimethylsiloxane (PDMS) (Sylgard 184) were purchased from Dow Coming Corp (Midland, USA). Poly(vinylalcohol) (PVA, Mw 31,000 - 50,000), Poly(DL-lactide-coglycolide) acid (PLGA, lactide:glycolide 50:50, Mw 38,000-54,000), Poly(ethylene glycol) diacrylate (Mn 750) (PEG diacrylate), 2-Hydroxy-40-(2-hydroxyethoxy)-2-methylpropiophenone (Photo-initiator) were purchased from Sigma-Aldrich (Missouri, USA). Docetaxel was purchased from Alfa Easer (Massachusetts, USA). 4-(dimethylamino) pyridine (DMAP) (99%), Oleoyl Chloride was procured from Sigma Aldrich; Dichloromethane anhydrous ≥99.8%, contains 40-150 ppm amylene as stabilizer, Sigma Aldrich; ammine-PEG (1 kDa, 550 Da, 350 Da) creative PEG works.

4.3.2 Methods

4.3.2.1 Synthesis of Discoidal polymeric nanoconstructs

Discoidal polymeric nanoconstructs (DPNs) were synthetized using a top-down fabrication strategy described in details in previous works [122, 123]. Briefly, the process involved the use of polyvinyl-alcohol template as a hydrophilic molds presenting an ordinate pattern of cylindrical wells 1000 x 400 nm that were filled with the polymeric paste. DPNs were synthetized using a mixture of poly(lactic acid-co-glycolic acid) (PLGA) and poly(ethylene glycol) diacrylate (PEG DA) polymers. 50 mg of PLGA are dissolved in 1 mL of Dichloromethane and mixed with 6 mg of PEG-DA and drug. Then, 0.6 mg of a photo-initiator (2-Hydroxy-4'-(2- hydroxyethoxy)-2-methylpropiophenone) was added into the polymeric solution to allow the crosslinking of PEG diacrylate chains after exposure to UV-light (366 nm). A fixed volume of polymeric mixture, including docetaxel (5 µL), was then spread through a blade over the PVA template to accurately fill each well. Finally, the DPNs were purified by filtration and centrifugation.

4.3.2.2 Loading of Discoidal polymeric nanoconstructs with Drug

Here two different loading approaches were adopted, namely "direct loading" and "absorption loading." In "direct loading," the Docetaxel prodrugs were dispersed within the original polymeric paste and directly distributed into the wells of the PVA template. In "absorption loading," the collected DPNs were lyophilized to form a powder. This was eventually dispersed in an aqueous solution in the case of PEG-docetaxel and methanol solution in the case of oleic-docetaxel . Re-hydration led to the rapid absorption of the molecules within the hydrogel structure of the DPNs.

4.3.2.3 **Synthesis of oleic-docetaxel prodrug**

DTXL (50 mg, 6.19 × 10^{-5} mol) and DMAP (12.38× 10^{-5} mol) were dissolved in 15 ml of anhydrous dichloromethane in a 50 ml round-bottom flask. The regents was stirred for a few minutes in nitrogen atmosphere at 0° C. Then oleoyl chloride (14.7 µL) was added dropwise to the mixture followed by stirring for 4 h under nitrogen atmosphere and the temperature was maintained at 0° C to produce the mono-substituted (2′- oleic-docetaxel). The conjugation of oleic-docetaxel was monitored by thin layer chromatography (TLC) using dichloromethane: methanol (97:3) as solvent. The formation of DTXL conjugate was verified using ^{1}H nuclear magnetic resonance (NMR). The reaction mixture was diluted with diethyl ether and washed first with 5% HCL and then using brine. The solution of 2′- oleoil-docetaxel was collected and filtered to remove the impurities. The product was finally dried with Rotavapor and stored at 0° C. The collected solution was dissolved in a minimal amount of dichloromethane and purified using a silica gel column with dichloromethane: ethanol (97:3) as mobile phase to obtain the pure conjugate product.

4.3.2.4 **Synthesis of Succinic-docetaxel**

DTXL (50 mg, 6.19 × 10^{-5} mol) and DMAP (12.38× 10^{-5} mol) were dried under vacuum for two hours before to start the reaction to completely remove trace of humidity. Then, the dried compounds were dissolved in 2 ml of anhydrous Pyridine in a 50 ml round-bottom flask. The regents was stirred for a few minutes in nitrogen atmosphere at room temperature. Then, succinic anhydride dissolved in pyridine (1 eq) was added dropwise and left to react for 4 h under nitrogen atmosphere at room temperature to produce the mono-substituted 2′-succinic-docetaxel (2-S-DTXL). The formation of S-DTXL conjugate was verified using ^{1}H nuclear magnetic resonance (NMR) The reaction mixture was washed three times with Toluene and dried with Rotavapor to

remove the pyridine and obtain a crystalline powder. The crude compound was dissolved in a minimal amount of dichloromethane and purified with automatic silica chromatography using a gradient of DCM and DCM: Methanol (9:1) to obtain only the mono-substituted derivate. The purity of the intermediate was investigated using a mass spectrum.

4.3.2.5 **Synthesis of PEG 1k-Docetaxel**

Purified Succinic- DTXL (50 mg) was dissolved in anhydrous dichloromethane in a 50 ml round-bottom flask and was activated using EDC (1.2 eq) and NHS (1.2 eq) and TEA for two hours under nitrogen atmosphere and room temperature. Then 1 equivalent of amine-PEG 1k was added to the reaction mixture and left overnight. The reaction mixture was washed with DCM and dried with Rotavapor to remove the residual TEA. The crude compound was dissolved in a minimal amount of dichloromethane and purified with automatic silica chromatography using a gradient of DCM and DCM: Methanol (9:1) to obtain only the mono-substituted derivate. The purity of the products was monitored by NMR and UPLC-MS.

4.3.2.6 **Particles size and shape characterization.**

The DPN geometry and yielding of the synthesis was assessed using the Multisizer 4E Coulter Particle Counter (Beckman Coulter, USA), that calculated particle concentration in a defined volume of 20 mL of isotone solution. The hydrodynamic diameter and surface electrostatic charge (ζ – potential) of DPN was measured using a Zetasizer Nano (Malvern, UK). The characteristic discoidal shape of DPN was confirmed using Electron Microscopy. DPN morphology was observed using a Jem-1011 Transmission Electron Microscope (Jeol, Japan) coated with sputtered carbon and Scanning Electron Microscopy (Helios Nanolab 650) after 10 nm gold coating.

Fluorescent DPN were synthesized by adding 30 µg of Rhodamin-B (DSPE-RhB) to the polymeric mix made of PLGA and PEGDA and were observed using an A1 confocal fluorescent microscope (Nikon).

4.3.2.7 **Chemical characterization**

Nuclear magnetic resonance (NMR) spectroscopy. NMR experiment were run on a Burker Avance III 400 Systhem (400.13 MHz for ^{1}H) spectra were acquired using deuterated chloroform (CDCl3) as solvent. UPLC –MS analysis were run on waters ACQUITY UPLC-MS system consisting of a SQD (single quadrupole detection) mass spectrometer equipped with an electron spray ionization interface and a photodiode array detector. The PDA range was 210-400 nm.

4.3.2.8 **Loading and Release studies.**

The ‘direct loading’ method was used to uniformly distribute and load the drug within the DPN matrix [123, 124]. Specifically, a 5 µl homogenous drug/polymer solution was uniformly spread using a blade over the surface of a 3×3 cm PVA template, containing about 108 wells. On the contrary, “absorption loading” has been adopted to concentrate the drugs over the surface of DPN that closely interact with the tumor vasculature. In this case, the particles have been synthesized using the same procedures of the direct loading but without include the drug in the polymeric mixture. Actually, DPN without drugs has been purified and suspended in a small volume of water (200 µl), freeze in liquid nitrogen for a few seconds, and readily lyophilized overnight obtaining powder of particles. The powder was suspended in a concentrated solution containing the drug of

interest. In the case of the hydrophobic Oleic-Docetaxel, the absorption process is divided in two consecutive steps. First, 10 µl of the drug solubilized in methanol (5mg/ml) was poured slowly on the particles powder then, the resulting solution has been washed with an excess of water (1ml) multiples time. In the case of hydrophilic compounds, concentrate water solutions containing the drug were used to directly suspend dried particles. Also in this case multiple washes has been performed to remove the unloaded drugs. The amount of drug loaded within DPN was calculated using a HPLC and by reading the characteristic docetaxel UV absorbance at 230 nm (Agilent 1260 Infinity, Germany). Samples for HPLC analysis were prepared by spinning down DPNs at 12,700 RPM for 20 min, drying the pellet overnight and dissolving the particles upon incubation with acetonitrile (ACN). The encapsulation efficiency was calculated considering the percentage weight ratio between the drug amount loaded within the DPN matrix at the end of the synthesis process and the initial drug input. Release studies were performed in a volume of 4L of buffer at controlled pH 7.4 and 37° C to reproduce typical physiological conditions. At each time point, 200 µL of DPN solution was poured into Slide-A-Lyzer MINI dialysis cups with a molecular cut off of 10 kDa (Thermo Scientific) and dialyzed. At each time point, DPNs were collected and dissolved in ACN to read the amount of DTXL entrapped in the matrix overtime.

4.3.2.9 **In vitro cell viability tests.**

For cytotoxicity tests *in vitro*, the human Triple Negative Breast Cancer cell line MDA-MB231 was obtained from the American Type Culture Collection (ATCC). Cells were cultured in Eagle's minimal essential medium (EMEM) (ATCC, USA) completed with 10% FBS (Gibco, Thermo Fisher Scientific, USA), 1% penicillin/streptomycin (Sigma-Aldrich, USA), under a humid atmosphere (37°C, 5% CO2, 95% air). Cell viability was determined by MTT assay, which detects

the reduction of MTT (3-(4,5-dimethylthiazolyl)-2,5- diphenyltetrazolium bromide) (Sigma-Aldrich, USA) by mitochondrial dehydrogenase to blue formazan product. This reflects the normal function of mitochondria and, hence cell viability. Briefly, different number of cells were seeded in 96-well plates for each time point, in the specific 10^4 cells/well for the 24h, $7.5x10^3$ for 48h, and 5 $x10^3$ for 72h were seeded in 96-well plates and incubated at 37°C, 5% CO_2, for 24 h. The day after, cells were treated with EMEM containing the selected doses of DTXL, O-DTXL and PEG-DTXL (0.1 – 1,000 nM). After 24, 48 and 72 h, the treatment solution was removed and replaced by MTT solutions, according to the manufacturer's instructions. The resulting formazan crystals were then dissolved in ethanol (200 μL/well) and the absorbance was recorded at 570 nm using a microplate reader (Tecan, CH). Six replicates were considered for each DTXL concentration. Data were collected when the absorbance ranged between 0.8 and 1.2. Cell viability was normalized to that of untreated cells.

4.4 RESULTS AND DISCUSSION

4.4.1 Synthesis of Discoidal polymeric nanoconstructs

The synthesis of discoidal particles comprises of a number of sequential steps as previously described in chapter 1. In this way, the morphological and mechanical proprieties were precisely controlled in order to optimize their *in vitro* and *in vivo* performance.

After drying the PVA template, its wells were accurately filled by uniformly spreading a polymeric paste. This comprised of an homogeneous mixture of the hydrophobic poly(D,L-lactide-co-glycolide)-acid carboxylic terminated (PLGA-COOH) and hydrophilic poly(ethylene glycol) diacrylate (PEG-DA) including the therapeutic and imaging agents of interest. The PLGA-COOH

and PEG-DA mixture formed the actual polymeric matrix of DPN, which was characterized by hydrophobic and hydrophilic pockets entrapping the loaded agents. In the current configuration, highly hydrophobic drug oleic docetaxel (O-DTXL) was dispersed within the polymer matrix. Following the absorption loading method, empty particles were lyophilized and re-dispersed in a water solution containing the hydrophilic derivate (Figure 4.1). To release and collect the DPNs empty or loaded with the drug, the PVA templates were dissolved in water for 3 hours at room temperature under gentle stirring.

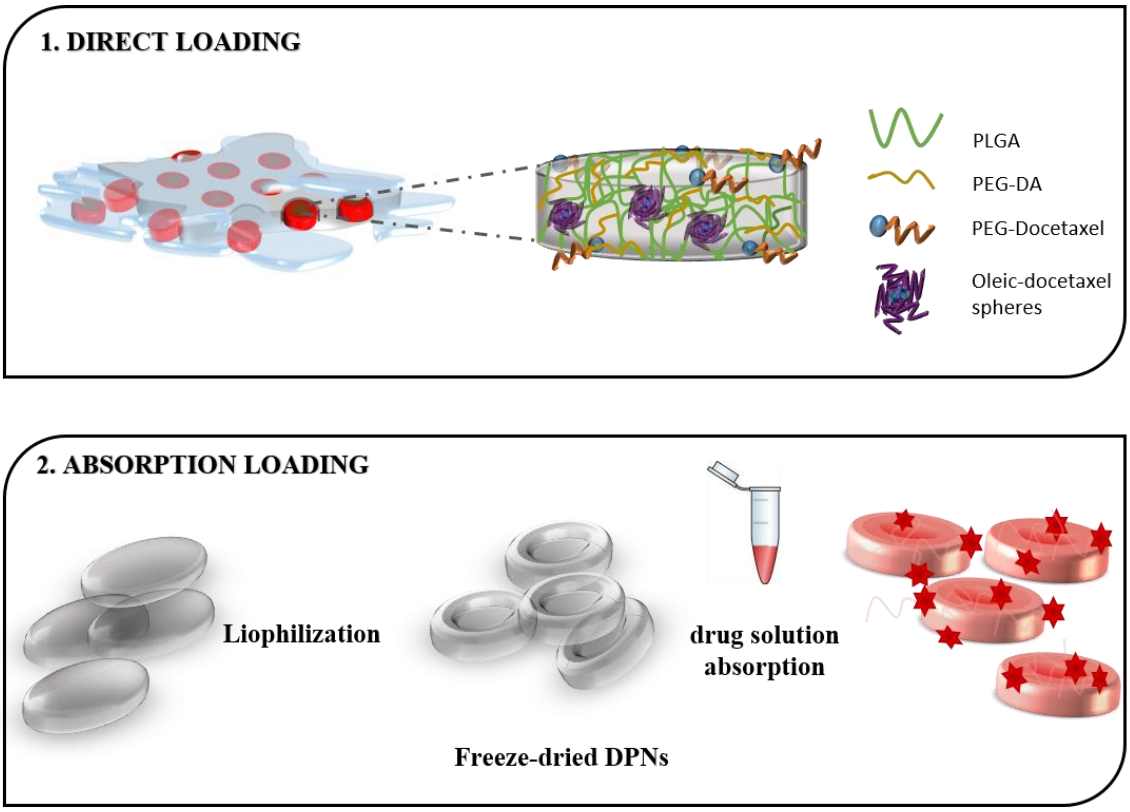

***Figure 4.1**: Description of two different approach of loading either hydrophilic or hydrophobic drug within DPNs matrix*

4.4.2 Characterization of Docetaxel conjugates

The ability to synthesize and evaluate polymer-drug conjugate libraries in which molecular mass, architecture and linker chemistry are varied is crucial step to develop promising therapeutic candidates. It was challenging to understand specific physicochemical properties of the final NPs to one singular element in the design of the conjugate. Here, has been applied the structure-activity relationship (SAR) approach that has been routinely practiced for small molecule drugs to develop optimal polymer-drug conjugate. In this pilot study, we investigated how the PEG molecular weight could affect the physicochemical properties *in vitro* and *in vivo* efficacy and toxicity of the resulting conjugates.

In this study, Docetaxel was mono substituted with oleic moieties using an efficient method that produced the docetaxel conjugate in high yield. The oleoyl acid-chloride group of was directly conjugated to the hydroxyl group (OH) group of docetaxel in a single step. Site- specific conjugation of the fatty acid moieties to the OH group of DTXL was achieved by variation of the temperature during the reaction procedure. The conjugation of the fatty acid moieties was confirmed by 1H-NMR as reported in *Figure 4.2*. The chemical shifts for the hydroxyl hydrogens at the C2' (OH-C2') position 3.35 ppm disappear following conjugation. Furthermore, the 1H chemical shift for the hydrogens connected to C2' (HC-2') 4.62 ppm resonated at lower field strengths due to the conjugation showing a shift in the peak to 5.45 ppm. As previously reported, following this protocol the mono-substitution of Docetaxel was favored in the more reactive C2' position *(Figure 4.2).*

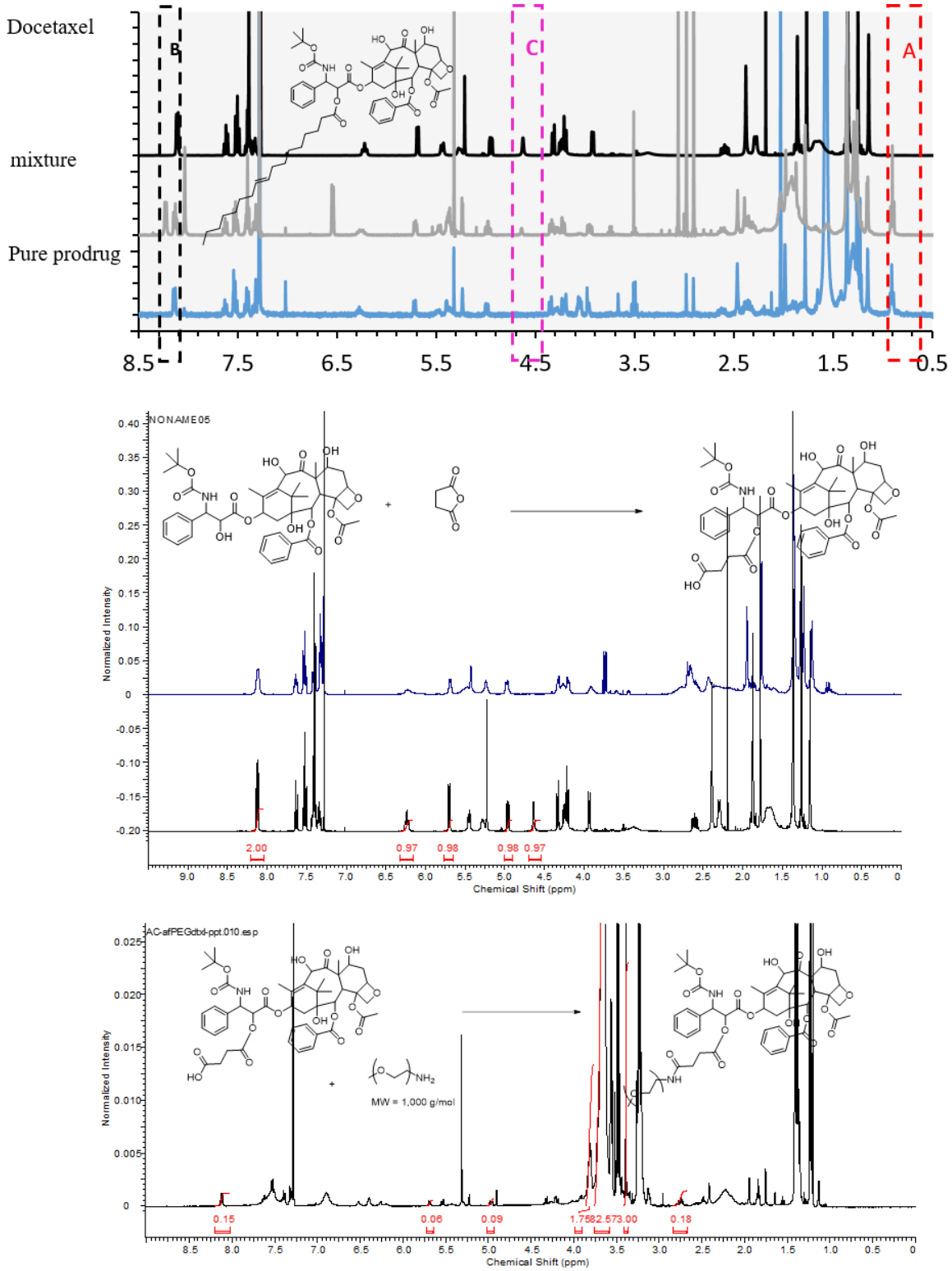

Figure 4.2: Chemical characterization of modified Docetaxel. *^{1}H NMR spectra of oleic docetaxel (A), Succinic-Docetaxel (B) and PEG1k-DTXL (C)*

4.4.3 Loading of Docetaxel prodrug into Discoidal polymeric nanoconstructs

The dispersion of therapeutic molecules within the polymeric structure of DPNs was achieved following two different strategies: a "direct method," where the agent was dissolved in the organic solvent and directly mixed with the PLGA, PEG and PI paste prior to deposition over the PVA template. Instead in the "absorption method," the agent was dispersed in a high concentration in water, which was then exposed to the lyophilized powder of DPNs. In direct loading, the agent had to be soluble and stable in an organic solvent whereas, for the absorption method, the agent had to be soluble in water at high concentrations without forming micellar structures. The direct loading was used for the highly hydrophobic derivate oleic docetaxel (*Figure 4.1*).

In general, "direct loading" is the most straightforward procedure. The main requirement for the agent to be "directly loaded" is its solubility and stability in organic solvents, like dichloromethane (DCM), chloroform ($CHCl_3$) or acetonitrile (ACN). The compound was directly mixed with the original polymeric paste forming the DPNs and applied over the PVA template. A drawback of this loading procedure was the low encapsulation efficiency (EE), which was related to the yielding in the preparation of the DPNs, the characteristic soft polymeric matrix of DPNs and the chemical proprieties of the loaded agent. As per the yielding, it was noted that a portion of the loaded agent and polymeric paste are wasted during the deposition onto the PVA wells. Moreover, using a small volume of polymeric solution in organic solvent (5ul in DCM) to save the chemotherapic agent and materials, this procedure favored the faster evaporation of the solvent making the spreading of the solution over the wells difficult. As per the chemical proprieties, hydrophilic compounds (lower LogP) possessed a tendency to rapidly escape the DPN polymeric matrix during the purification and collection steps that occur in water.

Therefore, the hydrophobic compound oleic-docetaxel was selected to be tested after direct loading in DPNs. Oleic acid has been extensively used to modify the chemical proprieties of docetaxel and increase the compatibility of the drug with delivery system[139]. The conjugation of oleic acid with Docetaxel should have increased the Hydrophobicity and consequently the affinity for the DPN polymeric matrix. However, a morphological analysis of the particles performed by electron transmission microscopy (TEM) after O-DTXL direct loading showed that the hydrophobic prodrug was poorly compatible with the polymeric interior and even less with the water exterior causing aggregation events within the particles (*Figure4.3*). In the same fashion, as shown in *Figure 3*, when O-DTXL was adsorbed on DPNs, it formed self-assembled nano-spheres around 100nm that fused with the DPNs.

"Absorption loading" consisted of exposing a concentrated solution of the agent to lyophilized DPNs. For O-DTXL, the first step of the absorption included the exposition of freeze-dried particles to a concentrated methanol solution of the prodrug followed by several wash of the particles suspension in water to remove unloaded drugs. After the first interaction between the prodrug and the particles in methanol solution, the re-hydration phase caused a self-assembling of the prodrug, resulting in fusion of the spheres on the surface of DPNs. Interestingly, lipid prodrugs with higher lipophilic character and decreased water solubility easily precipitated in water in form of spheres. This was due to the shift of crystallinity in favor of amorphous state as compared with free Docetaxel. For derivate PEG1k-DTXL, given the hydrophilicity, only the absorption loading was performed using a water solution of the prodrug. In this case, dried DPNs avidly absorbed water into their polymeric structure, which was enriched with the molecules of the agent to be loaded. To be noted that a fine balance between compound hydrophilicity and hydrophobicity was required for this loading strategy.

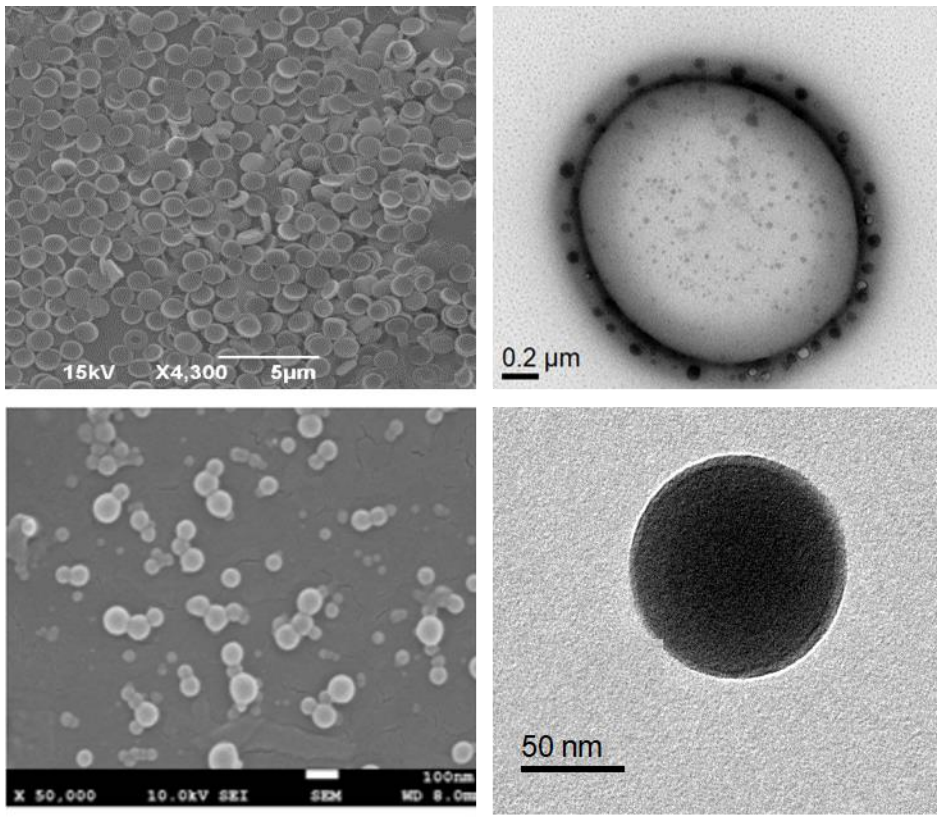

***Figure 4.3**: **Morphological characterization DPN direct loaded with oleic-Docetaxel.** Images by Scanning electron microscopy (left) and transmission electron microscopy (right) of DPNs with oleic docetaxel direct loaded (top panel) and self-assembling structures of oleic docetaxel by water precipitation.*

4.4.4 Encapsulation and release profile of prodrug loaded in DPNs

Based on the above reasoning, the encapsulation efficiency (EE) into the DPNs would vary for each considered prodrug and loading strategy. By direct loading the hydrophobic derivate showed improved encapsulation efficiency up to 2% compared with only 1 % of the free drug. The comparison between the TEM images in *Figure 4.3* with the results in *Figure 4.4 C*, clearly showed that the higher amount of drug prodrug encapsulated in DPNs both by direct or absorption loading

was mostly related to the prodrug aggregates rather than the increased affinity for the polymer. Indeed the aggregate formation suggested that the oleic docetaxel was not properly soluble in PLGA but preferred to self-aggregate.

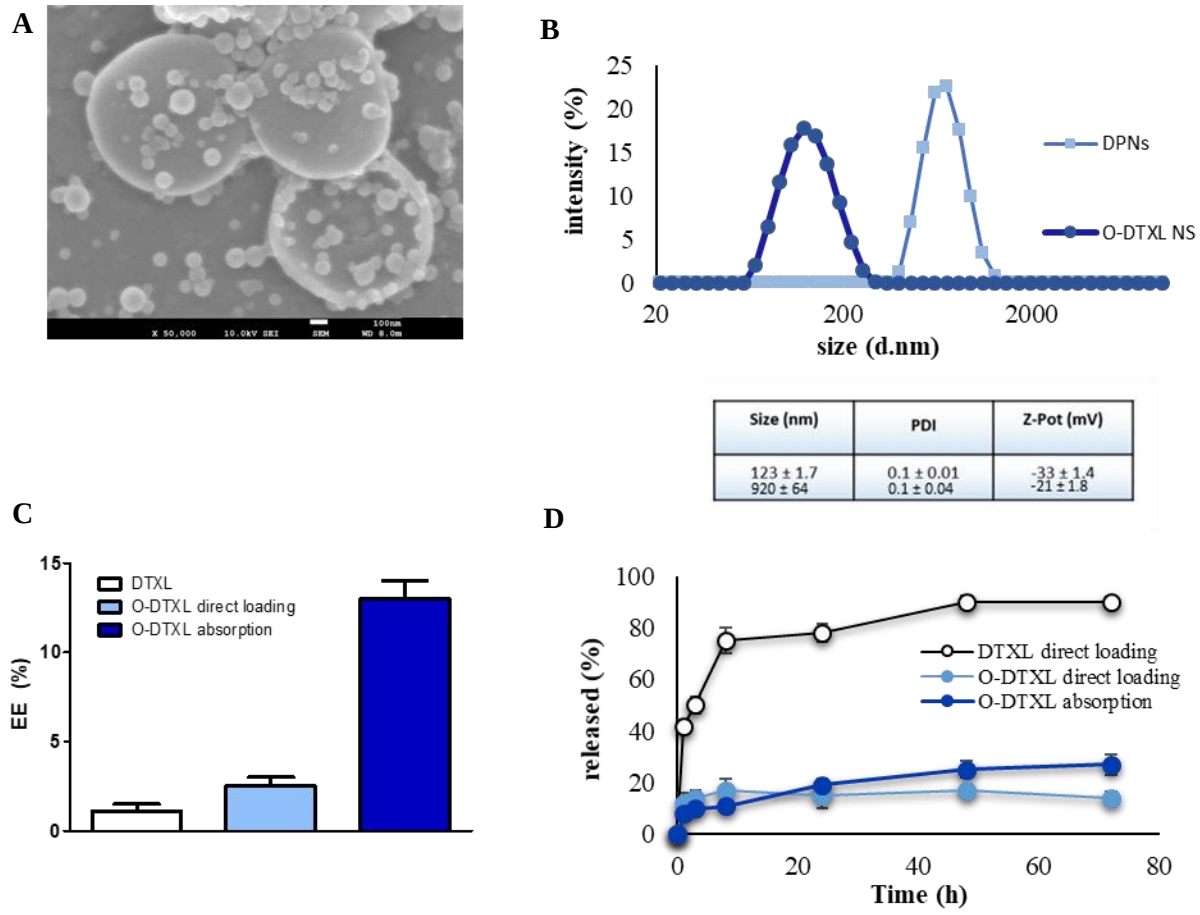

***Figure 4.4**: **Morphological and pharmaceutical characterization of DPNs loaded with oleic-docetaxel. A)** SEM images after O-DTXL absorption; **B)** Dynamic light scattering of purified DPNs (light blue) and O-DTXL Nano spheres; **C)** Encapsulation efficiency (EE%)**; D)** release profile.*

By "absorption loading", the particles were dissolved in methanol solution and then they were treated with extra wash of water. Notably, after absorption, the particles actually maintained the

characteristic morphology evaluated by SEM (*Figure 4.4 A*) and size evaluated by DLS (*Figure 4.4 B*). Moreover, extra wash was essential to remove the unloaded drugs as observed from the DLS analysis of the supernatant after centrifugation of the DPNs (*Figure 4.4 B*). Following this approach the encapsulation increased to even more up to 13%. Interestingly, the lipid prodrugs with higher lipophilic character and decreased water solubility could easily precipitate in water in the form of spheres due to the drop of crystallinity in favor of amorphous state as compared with free Docetaxel [96]. Despite these promising results, in terms of drug loading, the release of O-DTXL after absorption was too slow with a profile very similar to the O-DTXL loaded by direct method both not optimal for tumor treatment (*Figure 4.4 D*). These results suggested that O-DTXL is too hydrophobic to be released efficiently.

Consequently, to modulate the release profile, the synthesis of a water soluble derivate using PEG with amine termination was investigated. PEG-Docetaxel prodrug was synthesized starting from succinic-docetaxel intermediate. In fact its carboxylic termination was easily reacted with PEG functionalized with amine group in presence of coupling reagent such as EDC/NHS and TEA, to form the expected product. Given the high hydrophilicity, PEG-Docetaxel was loaded, at the beginning, only by using the above-mentioned absorption method, specifically by suspending dried particles on a PEG-DTXL solution. Data reported in *Figure 4.5* showed an encapsulation efficiency comparable with O-DTXL. This confirmed that DPNs were able to capture both hydrophilic and hydrophobic derivate after absorption. These results were very promising showing the possibility to produce docetaxel derivatives to enhance the loading efficiency of DPNs. However, since most of the PEG-Docetaxel was absorbed on the surface and given its high solubility in water, the release data in *Figure 4.5* showed a fast release profile but comparable with

directly loaded DTXL. Therefore, there is need of fine tuning the affinity of the prodrug for the polymeric matrix to control more precisely the release rate *in vitro*.

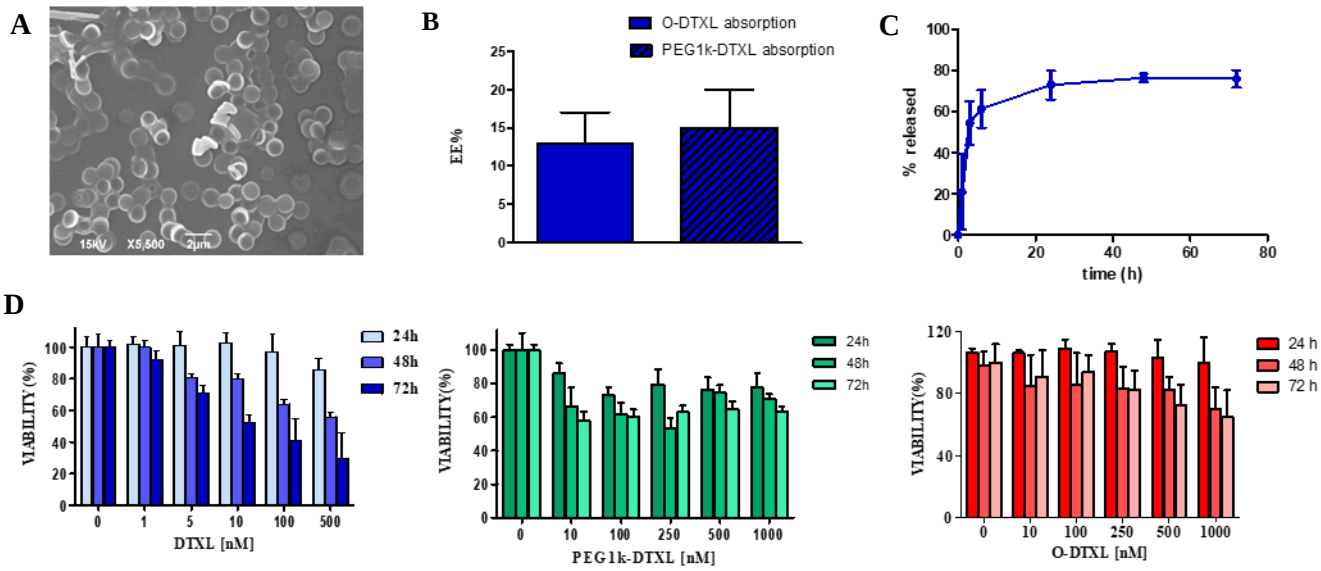

Figure 4.5: Morphological and pharmaceutical characterization of DPNs loaded with PEG1k-docetaxel. ***A)*** *SEM images after PEG1k-DTXL absorption;* ***B)*** *Encapsulation efficiency (EE%);* ***C)*** *release profile at 37° C and pH 7.4* ***D)*** *Cytotoxicity in vitro on MDA-MB 231 cell line*

4.4.5 Cell Viability Studies for the Prodrugs

MTT tests were performed to assess the therapeutic efficacy of prodrugs as compared to the free compound. Specifically, MDA-MB231 breast cancer cells were incubated with increasing concentration of free DTXL, O-DTXL and PEG1k-DTXL. Results depicted in Figure 4.5 clearly showed the cytotoxic properties of free DTXL where the IC_{50} was evaluated to be equal to 25 nM after 72hrs. On the other hand, cell viability upon O-DTXL treatment was not significantly affected even at the higher doses. These result may be ascribed to the ester bond connecting DTXL to the

lipid chain. Since O-DTXL was released very slowly, the therapeutic efficacy of the prodrug would be reached only at much longer incubation time.

On the contrary, the therapeutic efficacy of the hydrophilic prodrug PEG1k-DTXL reported in green bar chart, deftly showed that the conjugation of docetaxel with hydrophilic chain to be slightly more effective on MDA-MB 231. When compared with hydrophobic derivate the therapeutic effect was dependent on the hydrolysis of the parental drug and not on the concentration of the drug in the treatment. Finally, PEG modification slightly improved the pharmacological proprieties of Docetaxel conjugate but future studies were needed to find the right balance of hydrophilicity with the aim to maintain pharmacological activity of docetaxel.

4.5 CONCLUSION

Two different loading strategies were documented to encapsulate hydrophobic and hydrophilic therapeutic compounds within the polymeric matrix of Discoidal Polymeric Nanoconstructs (DPNs). The hydrophobicity/hydrophilicity ratio of Docetaxel were modulated by conjugating it directly with lipid (oleic acid) and polymeric chains (PEG 1 kDa). In the “direct loading” method, the compounds were first dissolved in the polymeric paste forming the DPNs and then applied to the PVA template. This approach suffered from the current sub-optimal fabrication yielding of DPNs returning encapsulation efficiencies roughly of 1% for Docetaxel. When the highly hydrophobic prodrug oleic-docetaxel were loaded directly within the DPNs, the percentage of encapsulation increased up to 2% due to phenomena of aggregation. In the “absorption method,” the compounds were suspended in methanol (for hydrophobic prodrug) or in water (for hydrophilic prodrug) using high concentrations and dragged inside the polymeric matrix of DPNs upon rehydration. This approach required a fine-tuning between the compound hydrophobicity and

hydrophilicity and returned encapsulation efficiencies roughly of 13% and 15 % respectively. These two features were also shown to affect the release profiles of the loaded compounds. In general, direct loading was associated with lower release rates as compared to absorption loading for a given compound. This was ascribed to the fact that the compounds in the absorption loading were mostly confined in the vicinity of the DPN surface and were therefore more rapidly released into the surrounding aqueous environment. Differently, in direct loading, the compounds were uniformly distributed within the polymeric matrix. As expected, a delay was documented in the cytotoxic activity *in vitro* mostly due to the esterification of the parental drug and the therapeutic effect strongly depended on the hydrolysis rate that clearly was more favored for the hydrophilic derivate such as PEG1k-DTXL. Collectively, these results demonstrated that the properties of DPNs could be finely tuned during the fabrication process by changing the loading strategies (direct vs. absorption) and compound properties (hydrophobicity and molecular weight). Future studies will focus more on further optimizing the loading and release conditions and pre-clinically demonstrate the therapeutic performance of this nanostructured platform in appropriate tumor model.

5 Chapter 3: Soft Discoidal polymeric Nanoconstructs delivering PEG-Docetaxel prodrug for the treatment of Glioblastoma multiforme

5.1 ABSTRACT

Glioma is recognized as the most aggressive and fatal form of brain cancer. Current therapeutic approaches for glioma consist of surgery and chemotherapy, but they have a poor rate of success. They are associated with major drawbacks such as invasiveness of the intracranial surgical procedure and poor brain tumor accumulation of the anticancer drugs. Conventional nanoparticles have been explored for their potential of increasing the distribution of chemotherapeutic agents in systemic tumors. In the present work, soft Discoidal Polymeric Nanocontructs without further modifications, have been prepared and tested as nanocarriers for the delivery of PEG-Docetaxel Prodrug to human glioblastoma cells (U87). For achieving a better loading efficiency and drug stability within the soft DPN matrix, the Hydrophobic Docetaxel was covalently linked to an hydrophilic portion of Poly-(ethylene)glycol and was included in the formulation to form a prodrug-encapsulated complex within the hydrophilic pockets of DPN. In particular, PEG550 was used for the reaction with Docetaxel activated with a succinic linker. In the current configuration, DPNs loaded with DTXL-PEG_{550} exhibited better pharmaceutical behavior in terms of encapsulation, release rate and therapeutic efficacy *in vitro* as reported in previous chapter. The advantage of using the DPNs as a delivery tool for hydrophilic prodrug was primarily to protect the prodrug from Esterase hydrolysis, confirmed by the higher IC_{50} reported for the MTT test followed up to 96h . Moreover, these results confirmed that DPNs were not internalized by tumor

cells but localized very close to cells where they released the drug overtime and the delayed efficacy *in vitro* was ascribed to the higher stabilization of the drug within DPNs. Although the lower efficacy of PEG_{550}-Docetaxel DPN *in vitro* compared with Docetaxel and PEG_{550}-Docetaxel, the systemic treatment of DPNs loaded with PEG_{550}-DTXL have showed an increased therapeutic efficacy in glioblastoma *in vivo* model using a very low doses of 1 mg/kg. Thus, the present work demonstrated the feasibility of using soft DPN as a tool to control the relapse of GBM after tumor resection.

.

5.2 INTRODUCTION

Glioblastoma multiforme (GBM) is considered as the most aggressive form of gliomas tumor and encompass the 80% of all primary brain tumor in adults [140, 141]. The current WHO classification of gliomas includes GBM in the grade IV subtype for the high rate of proliferation and infiltration in the neighboring tissue causing the worst clinical outcome. After diagnosis the patients show a mean survival of 15 months and only 5% survive more than 5 years despite the use of aggressive therapies [142, 143]. Although the limitation associated with the location of the disease and its complex biology, current treatment includes surgical resection followed by radiation and chemotherapy using cytotoxic agents. For the surgery, the major complication observed is the difficulties related the complete removal of the malignant mass due to the absence of sharpened confinement and an amenable site reveling in all cases a high probability of recurrence [144].

In addition to the multiple obstacles ascribed with systemic delivery of cytotoxic agents into the brain, the strict control of the blood brain barrier for penetration of molecules have showed the

major obstacle. Upon systemic administration, very low concentration of drugs were actually delivered in tissue surrounding the tumor even in the case of active agents for glioma therapy [145, 146]. GBM is typically characterized by a damaged tumor neovasculature (TBB) due to the high grade of proliferation, other factor such as the size of the molecules, the lipophilicity and the presence of active efflux pumps influenced the drug entry into the central nervous system [147].

Temozolomide (TMZ) is the first agent in 20 years approved by the FDA to treat glioblastoma and has been one of the most commonly used anti-glioma agents with limited adverse effects due to its ability to penetrating the blood brain barrier (BBB)[148]. Despite the multi modal invasive treatment, just few patients survive beyond 5 years and it is mostly related to drug resistance developed by the tumor cells [149]. However, other potent drugs acting on cell cycle disruption as Docetaxel (DTXL) has been tested in various tumors. Docetaxel is currently used as first-line therapy for patients with breast cancer and non-small cell lung carcinoma. Furthermore, it was reported that DTXL presented a good apoptosis-inducing effect even for glioblastoma cells *in vitro*. However it's *in vivo* efficacy was highly compromised due to extensive efflux by p-gp present in the brain endothelial cells, hydrophobicity and dose-limiting toxicity [150]. To overcome these physicochemical limitations and to increase the site-specific activity, several efforts has been focused on the chemical modification, for example, the conjugation of chemotherapeutic drugs with polyethylene glycol (PEG), known as PEGylation [151]. Beyond the advantage of increasing circulation kinetics by extending residence time in the blood and human safety, administrating PEGylated cytotoxic drugs instead of the free drugs could lead to the possibility of by-passing drug efflux, mediated by P-glycoproteins (P-gps)[91, 152].

Here we tested the Discoidal Polymeric Nanoconstructs (DPNs) that intrinsically target the vasculature owing to their size, shape and mechanical proprieties that was directly loaded with the

PEG_{550}-DTXL prodrug. The presence of PEG-prodrug with a sufficiently short length favored the longer circulation of the drug and increased the *in vivo* efficacy.

5.3 EXPERIMENTAL

5.3.1 Chemicals

Polydimethylsiloxane (PDMS) (Sylgard 184) were purchased from Dow Coming Corp (Midland, USA). Poly(vinylalcohol) (PVA, Mw 31,000 - 50,000), Poly(DL-lactide-coglycolide) acid (PLGA, lactide:glycolide 50:50, Mw 38,000-54,000), Poly(ethylene glycol) diacrylate (Mn 750) (PEG diacrylate), 2-Hydroxy-40-(2-hydroxyethoxy)-2-methylpropiophenone (Photo-initiator) were purchased from Sigma-Aldrich (Missouri, USA). Docetaxel was purchased from Alfa Easer (Massachusetts, USA). 4-(dimethylamino) pyridine (DMAP) (99%) Sigma Aldrich; Dichloromethane anhydrous ≥99.8%, contains 40-150 ppm amylene as stabilizer, Sigma Aldrich; ammine-PEG 550 Da creative PEGworks.

5.3.2 Methods

5.3.2.1 Synthesis of Discoidal polymeric nanoconstructs

Discoidal polymeric nanoconstructs (DPNs) were synthetized using a top-down fabrication strategy described in details in previous works [122, 123]. Briefly, the process involved the use of polyvinyl-alcohol template as a hydrophilic molds presenting an ordinate pattern of cylindrical wells 1000 x 400 nm that were filled with the polymeric paste. DPN were synthetized using a mixture of poly(lactic acid-co-glycolic acid) (PLGA) and poly(ethylene glycol) diacrylate (PEG DA) polymers. 50 mg of PLGA was dissolved in 1 mL of Dichloromethane and mixed with 6 mg of PEG-DA and drug. Then, 0.6 mg of a photo-initiator (2-Hydroxy-4’-(2- hydroxyethoxy)-2-

methylpropiophenone) was added into the polymeric solution to allow the crosslinking of PEG diacrylate chains after exposure to UV-light (366 nm). A fixed volume of polymeric mixture, including PEG_{550}-DTXL (5 µL), was then spread through a blade over the PVA template to accurately fill each well. Finally, the DPNs were purified by filtration and centrifugation.

5.3.2.2 **Synthesis of PEG 550-Docetaxel**

Succinic- DTX was synthesized and purified as described in the previous chapter. Pure succinic-docetaxel (50 mg) was dissolved in anhydrous dichloromethane in a 50 ml round-bottom flask and was activated using EDC (1.2 eq) and NHS (1.2 eq) and TEA for two hours under nitrogen atmosphere at room temperature. Then 1 equivalent of amine-PEG 550 Da was added into the reaction mixture and the reaction was left overnight. The reaction mixture was washed with DCM and dried with Rotavapor to remove residual TEA. The crude compound was dissolved in a minimal amount of dichloromethane and purified with automatic silica chromatography using a gradient of DCM and DCM: Methanol (9:1) to obtain only the mono-substituted derivate. The purity of the product was monitored by NMR and UPLC-MS.

5.3.2.1 **Particles size and shape characterization.**

The DPN geometry and yielding of the synthesis was assessed through Multisizer 4E Coulter Particle Counter (Beckman Coulter, USA), that calculated particle concentration in a defined volume of 20 mL of isotone solution. The hydrodynamic diameter and surface electrostatic charge (ζ – potential) of DPN was measured using a Zetasizer Nano (Malvern, UK). The characteristic

discoidal shape of DPN was confirmed using Electron Microscopy. DPN morphology was observed using Scanning Electron Microscopy (Helios Nanolab 650) after 10 nm aureum coating.

5.3.2.2 **Chemical characterization**

Nuclear magnetic resonance (NMR) spectroscopy. NMR experiment were run on a Burker Avance III 400 Systhem (400.13 MHz for 1 H). Spectra were acquired using deuterated chloroform (CDCl3) as solvent. UPLC –MS analysis were run on waters ACQUITY UPLC-MS system consisting of a SQD (single quadrupole detenction) mass spectrometer equipped with an electron spray ionization interface and a photodiode array detector. The PDA range was 210-400 nm.

5.3.2.1 **Loading and Release studies.**

The direct loading method was used to uniformly incorporate PEG_{550}-DTXL derivate within the DPN matrix [123, 124]. Specifically, a 5µl homogenous drug/polymer solution was uniformly spread using a blade over the surface of a 3×3 cm PVA template, containing about 10^8 wells. The amount of drug loaded within the DPN was calculated using a HPLC and by reading the characteristic docetaxel UV absorbance at 230 nm (Agilent 1260 Infinity, Germany). Samples for HPLC analysis were prepared by spinning down DPN at 12,700 RPM for 20 min, drying the pellet overnight and dissolving the particles upon incubation with acetonitrile (ACN). The encapsulation efficiency was calculated considering the percentage weight ratio between the drug amount loaded within the DPN matrix at the end of the synthesis process and the initial drug input. Release studies were performed in a volume of 4L of buffer at controlled pH 7.4 and 37° C to reproduce typical physiological conditions. At each time point, 200 µL of DPN solution was poured into Slide-A-

Lyzer MINI dialysis cups with a molecular cut off of 10 kDa (Thermo Scientific) and dialyzed. At each time point, DPN were collected and dissolved in ACN to read the amount of DTXL entrapped in the matrix overtime.

5.3.2.2 **In vitro cell viability tests.**

For cytotoxicity tests *in vitro*, the human glioblastoma cell line U87-MG was obtained from the American Type Culture Collection (ATCC). Cells were cultured in Eagle's minimal essential medium (EMEM) (ATCC, USA) completed with 10% FBS (Gibco, Thermo Fisher Scientific, USA), 1% penicillin/streptomycin (Sigma-Aldrich, USA), under a humid atmosphere (37°C, 5% CO_2, 95% air). Cell viability was determined by MTT assay, which detected the reduction of MTT (3-(4,5-dimethylthiazolyl)-2,5- diphenyltetrazolium bromide) (Sigma-Aldrich, USA) by mitochondrial dehydrogenase to blue formazan product. This reflected the normal function of mitochondria and, hence cell viability. Briefly, different number of cells were seeded in 96-well plates for each time point, in the specific 10^4 cells/well for the 24h, $7.5x10^3$ for 48h, and $5\ x10^3$ for 72h were seeded in 96-well plates and incubated at 37°C, 5% CO_2, for 24 h. The day after, cells were treated with EMEM containing the selected doses of PEG_{550}-DTXL (1 – 1,000 nM). After 24, 48, 72, and 96h the treatment solution was removed and replaced by MTT solutions, according to the manufacturer's instructions. The resulting formazan crystals were then dissolved in ethanol (200 µL/well) and the absorbance was read at 570 nm using a microplate reader (Tecan, CH). Six replicates were considered for each drug concentration. Data were collected when the absorbance ranged between 0.8 and 1.2. Cell viability was normalized to that of untreated cells.

.

5.3.2.1 **Tumor model and therapeutic experiments.**

All animal experiments were performed according to the guidelines established by the European Communities Council Directive (Directive 2010/63/EU of 22 September 2010) and approved by the National Council on Animal Care of the Italian Ministry of Health. All efforts were made to minimize animal suffering and use the lowest possible number of animals required to produce statistical relevant results, according to the "3Rs concept". For the orthotopic intracranial GBM tumor model, 5-6 week old female athymic nude mice were stereotactically inoculated with U87MG luciferin positive cells (Charles River, Calco, Italy). Animals were grouped in ventilated cages and able to freely access food and water. They were maintained under controlled conditions: temperature (21 ± 2 °C), humidity (50 ± 10%) and light (12 and 12 h of light and dark, respectively). Before cells injection, animals were anaesthetized with a mixture of ketamine (10%) and xylazine (5%), which was administered via a single intraperitoneal injection. For the injection, trypsinized $5x10^5$ U-87MG luciferase positive cells were resuspended in cold phosphate-buffered saline. A total of 3 ul of PBS was injected into the right hemisphere of the mouse brain (1.5 mm posterior to the bregma, 1.4 mm lateral to the midline, and 1 mm depth from skull, at a speed of 0.3 μL/min using a 10 μL sterile Hamilton syringe fitted with a 26-gauge needle attached to a stereotaxic frame. Wounds were closed with sterile wound clips and animals were carefully monitored until recovered from anesthesia. Tumor growth was followed by IVIS every 2 day, upon intraperitoneal injection of D-luciferin, Potassium salt (GoldBio) at a dose of 150mg/Kg. At day 15, before starting the treatments, a bigger hole of about 3 mm was created in the same stereotactic coordinates by using a Trephine - 2.7mm Diameter. The more superficial part of the tumor was resected by using a scalpel. The skull was then sealed by a drop of silicon elastomer. IVIS was performed the day after the surgery to assess tumor resection. Mice were then randomly divided

in three experimental groups: saline, free TMZ and PEGDtxlDPNs, were intravenously injected at a dose of 1mg/Kg every other day. The effectiveness of the different treatments was valued by optical imaging (IVIS) every two days. All mice were euthanized when they became moribund. Survival was monitored and plotted using the Kaplan-Meier method. Log-rank test was used to test the significance of different survival curves.

5.4 RESULTS AND DISCUSSION

5.4.1 Synthesis and Characterization of Docetaxel conjugates

As a large number of novel polymeric-drug vehicles are being developed, the ability to robustly synthesize and evaluate polymer-drug conjugate libraries in which molecular mass, architecture and linker chemistry are varied is increasingly valuable to develop promising therapeutic candidates. Here, we have employed the SAR approach that has been routinely practiced for small molecule drugs to develop optimal polymer-drug conjugate delivery systems. In this pilot study, we investigated how the PEG molecular weight could affect the physicochemical properties and *in vitro* and *in vivo* efficacy of the resulting conjugates. Based on the previous study, here we evaluated the effect of a short molecular weight PEG and tested the hypothesis that SAR must be performed to develop the optimal conjugates. To effectively generate only the mono-substituted conjugates and simultaneously limit other variables, we employed two-step reaction to functionalize short-chain mPEG-NH_2 with Docetaxel. Firstly, to prepare the suggested PEG_{550}-DTXL conjugates, the intermediate Succinic-docetaxel (S-DTXL) was synthesized according to *Figure 5.1 A.* The exact mass of Docetaxel mono-functionalization with succinic acid was confirmed by mass spectra as showed in *Figure 5.1 B.* Automatic silica-chromatography (combiflash) was employed to isolate the mono-substituted docetaxel compound as confirmed by

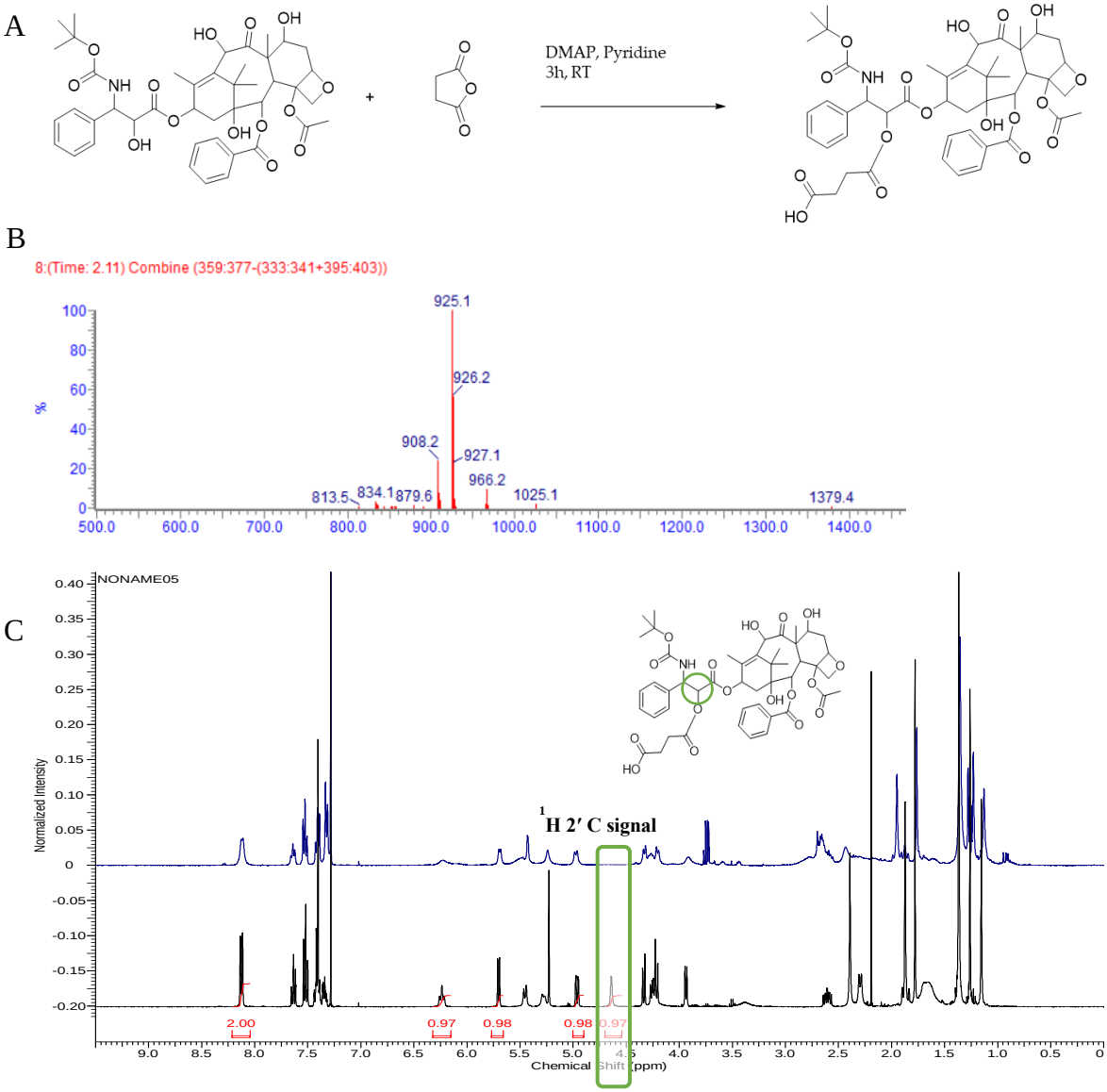

Figure 5.1: Chemical characterization of Succinic-Docetaxel. A) *Scheme of reaction for succinic-Docetaxel;* ***B)*** *reaction control by TLC (right) and UPLC-MS;* ***C)*** *Nuclear magnetic resonance characterization of succinic-Docetaxel products.*

^{1}H-NMR, reporting the characteristic shift of the ^{1}H signal at 4.6 ppm (*Figure 5.1 C*). To link the PEG-amine with S-DTXL, the coupling reagents EDC and NHS were used to activate the carboxyl group of S-DTXL and accelerate the reaction (*Figure 5.2 A*). Mass spectra was employed to monitor the reaction end point and purification of m-PEG-Docetaxel conjugate reported in *Figure 5.2 B.* Furthermore confirmation of the reaction were achieve by 2D-HSCQ spectra confirming the formation of amidic bond with the signal of -CH_2NHCO- (3.40, 39.8 ppm) *(Figure5.2 C).*

and accelerate the reaction (*Figure 5.2 A*). Mass spectra was employed to monitor the reaction end and purification of m-PEG-Docetaxel conjugate as reported in *Figure 5.2 B.* furthermore confirmation of the reaction were achieve by 2D-HSCQ spectra confirming the formation of amidic bond with the signal of -CH2NHCO- (3.40, 39.8 ppm) *(Figure5.2 C).*

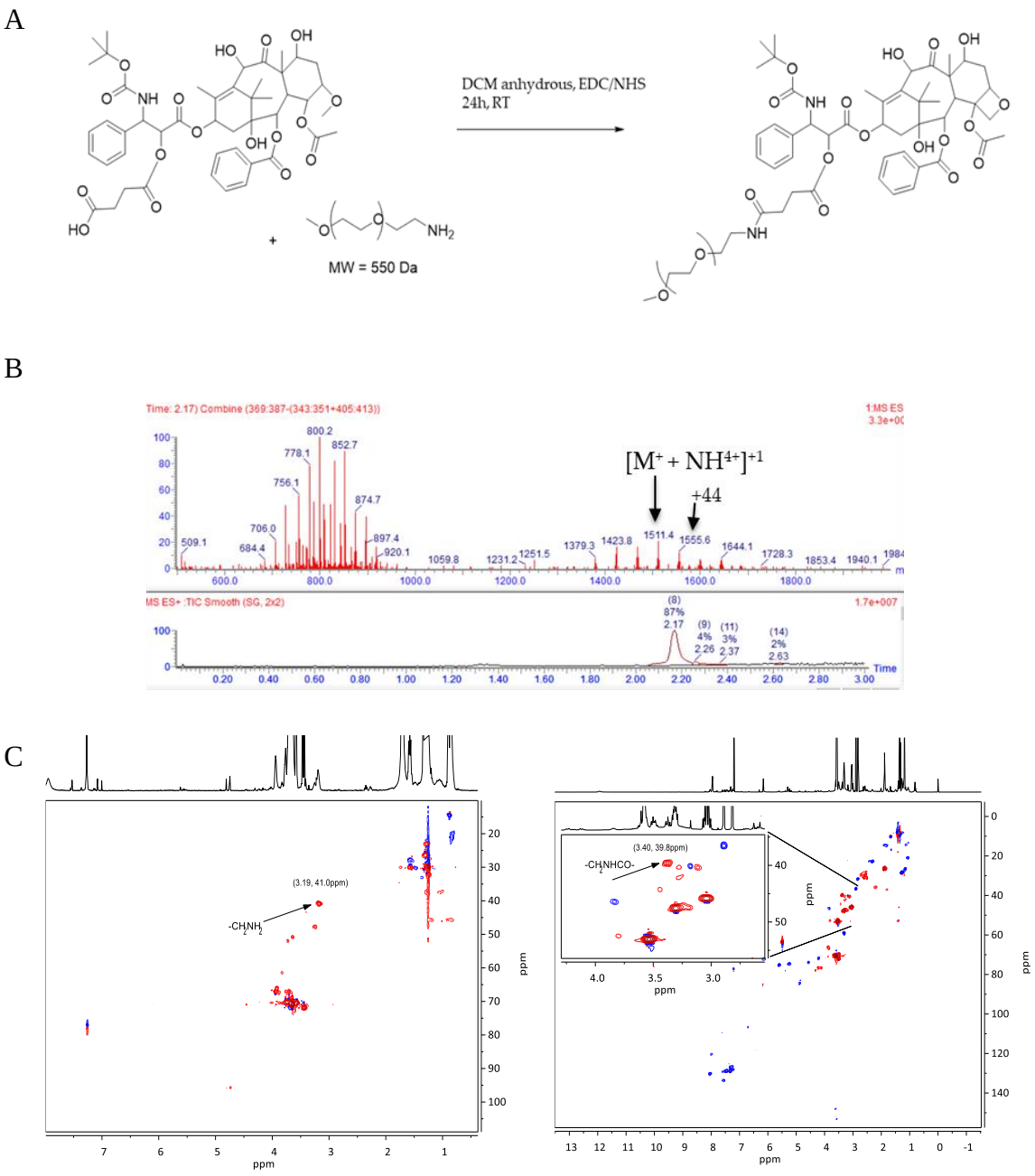

***Figure 5.2**: **Chemical characterization of PEG$_{550}$-Docetaxel. A)** Scheme of reaction for PEG$_{550}$-Docetaxel; **B)** mass spectra obtained by UPLC-MS; **C)** Nuclear magnetic resonance characterization (HSQC) of the product after purification.*

5.4.2 Loading of Docetaxel prodrug into Discoidal polymeric nanoconstructs

We hypothesized that the functionalization of Docetaxel with short m-PEG chain like PEG_{550} Da stabilized the drug within the hydrophilic pocket of the soft matrix of DPNs owing to non-covalent chemical interactions between similar polymers and waters (i.e. hydrogen bond). Instead, as reported in previous work, self-aggregations events were recorded by using longer PEG lengths[153]. So far, modified drug was consistently loaded into DPNs to improve the encapsulation efficiency following two loading strategies [123]. Direct loading was preferred to uniformly disperse and slowly release the hydrophobic drug. Whereas, absorption was preferred for hydrophilic drug displaying a faster release in comparison within the first hours upon systemic injection. Therefore, the two strategies were selected based on the drug and the application of interest. Here, PEG_{550}-DTXL was directly loaded into the DPNs and characterized.

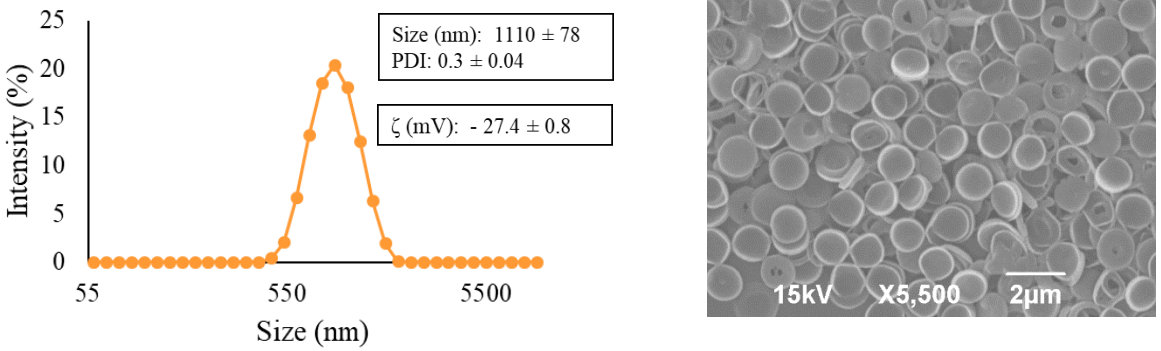

Figure 5.3: DPNs morphological characterization. A) *size distribution of DPNs loaded with PEG550-DTXL and zeta-potential* ***(B)*** *measured by Dynamic Light Scattering (DLS).* ***C)*** *Morphological characterization of the particles after loading using Scanning Electron Microscopy.*

Given the solubility of the PEG derivate in DCM, the prodrug was loaded directly to achieve a slow and controlled release that, together with the prolonged circulation of DPNs, allowed to display a longer availability of the treatment over time. DPNs after loading with PEG_{550}-DTXL maintained the characteristic size distribution around 1100 nm as reported in *Figure 5.3 A.* This data confirmed the versatility of the synthesis process that allowed direct encapsulation of hydrophilic compounds without affecting the physiochemical proprieties. Moreover, the negative zeta potential around -27 mV was preserved although the direct loading of the drug, ensuring the stability of the suspension. Effectively, the presence of the PEGylated prodrug could be appreciated in *Figure 5.3 B* acquired with electron scanning microscopy. After drug loading by top-down approach, most of the drug should be displayed on the surface or at the interface with the water. Indeed, it was possible to appreciate from the image that the particles presented a sort of PEGylated coating favoring stealth proprieties and escape from macrophages sequestration.

5.4.3 Pharmacological proprieties of PEG_{550}-DTXL prodrug loaded in DPNs

The amount of drug encapsulated and release profile over time were presented in *Figure 5.4 A* as derived by high performance liquid chromatography (HPLC). A direct comparison between the Docetaxel and PEG550-Docetaxel strategies documented a two-fold increase in drug loading retuning a 10 versus 20 μg of DTXL per 10^9 DPN, respectively. Interestingly, the introduction of a short PEG chain favor the retention of the drug within the matrix.

Then, release studies were performed by incubating PEG_{550}-DTXL DPN and DTXL DPN into PBS (infinite sink condition: 4 liters) up to 72h at pH 7.4 and both profile are showed in *Figure 5.4 B.* Under physiological conditions, the characteristic burst release within the first hour, which was most likely related to molecules at the interface of polymer-water, reach 40% for Docetaxel and near 20% for PEG_{550}-DTXL. At 24h, almost 70% of the loaded DTXL was released against the 60% for the conjugate and this percentage increased in the following hours arriving up to 80% and 70% respectively. Together these results, confirmed our hypothesis that the conjugation with PEG stabilized the drug within the polymeric nanostructures by chemical interactions.

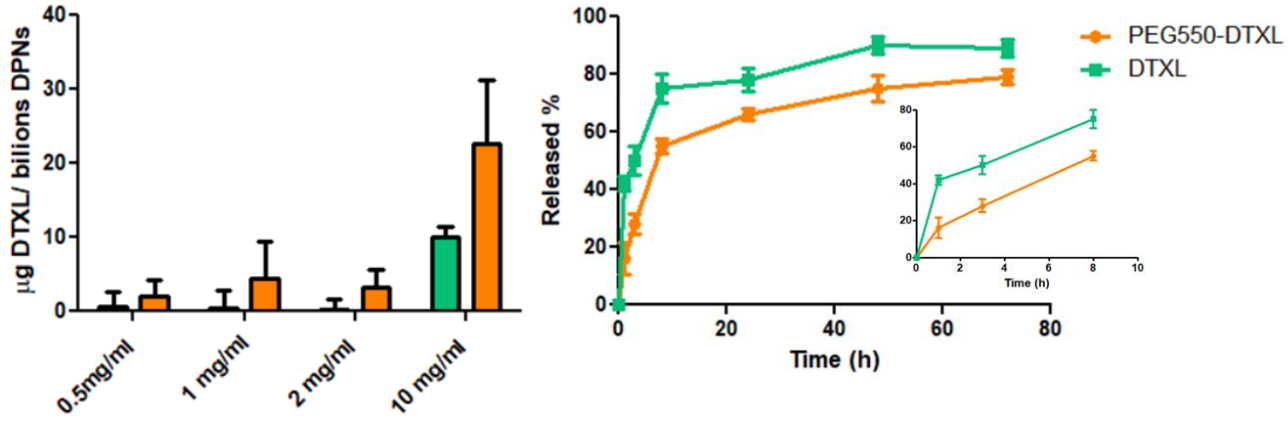

Figure 5.4: Pharmacological characterization. ***A.*** *Docetaxel (DTXL) amounts for DPNs loaded using the 'Docetaxel' vs the 'PEG$_{550}$-Docetaxel' strategy.* ***B****. Docetaxel (green) and PEG550-DTXL (orange) release out of DPNs over time under physiological condition (pH 7.4- 37° C).*

5.4.4 Cell Viability Studies for PEG_{550}-DTXL and preliminary in vivo study

Finally, the pharmacological activity of the prodrug was tested against glioblastoma cell line (U87-MG) that were incubated with increasing concentration of DTXL, S-DTXL and PEG_{550}-DTXL.

In general, the treatment with PEG_{550}-DTXL was associated with delayed response as compared with free drug. Specifically, at 24 h IC_{50} increased from 52 nM for DTXL to 75 n M for prodrug. However, this difference became negligible at 96h showing a comparable value of 6 nM and 8 nM respectively. As documented in the previous study the conjugation with polymeric or lipid chains had a considerable effect on the pharmacological activity of the drug that should be ascribed to the rate of hydrolysis of the new bond. As showed in the table in *Figure 5.5,* in the case of S-DTXL treatment the IC_{50} value was much higher compared to the other treatment, reporting a value of 52 nM at 96h. These results suggested that the esterification of Docetaxel with short PEG could be the right hydrophobicity-hydrophilicity balance to maintaining the pharmacological proprieties of the drug.

Preliminary studies *in vivo* were conducted on glioblastoma tumor model. In the present study, the treatment with DPNs was evaluated after surgical removal of tumor mass after 15 days from U87-MG injection into the brain. In the preliminary pilot study, the treatment was conducted with a very low dose of 1 mg/kg every other day. As reported in *Figures 5.6* the treatment with PEG_{550}DTXL-DPNs was more effective compared to TMZ administrated intravenously at doses of 3 mg/kg. Overall, this data are still insufficient to demonstrate the preferential accumulation of the soft particles into the brain. Therefore, currently studies are ongoing to increase the group size in the treatment studies and perform bio distribution experiments with a contrast agent.

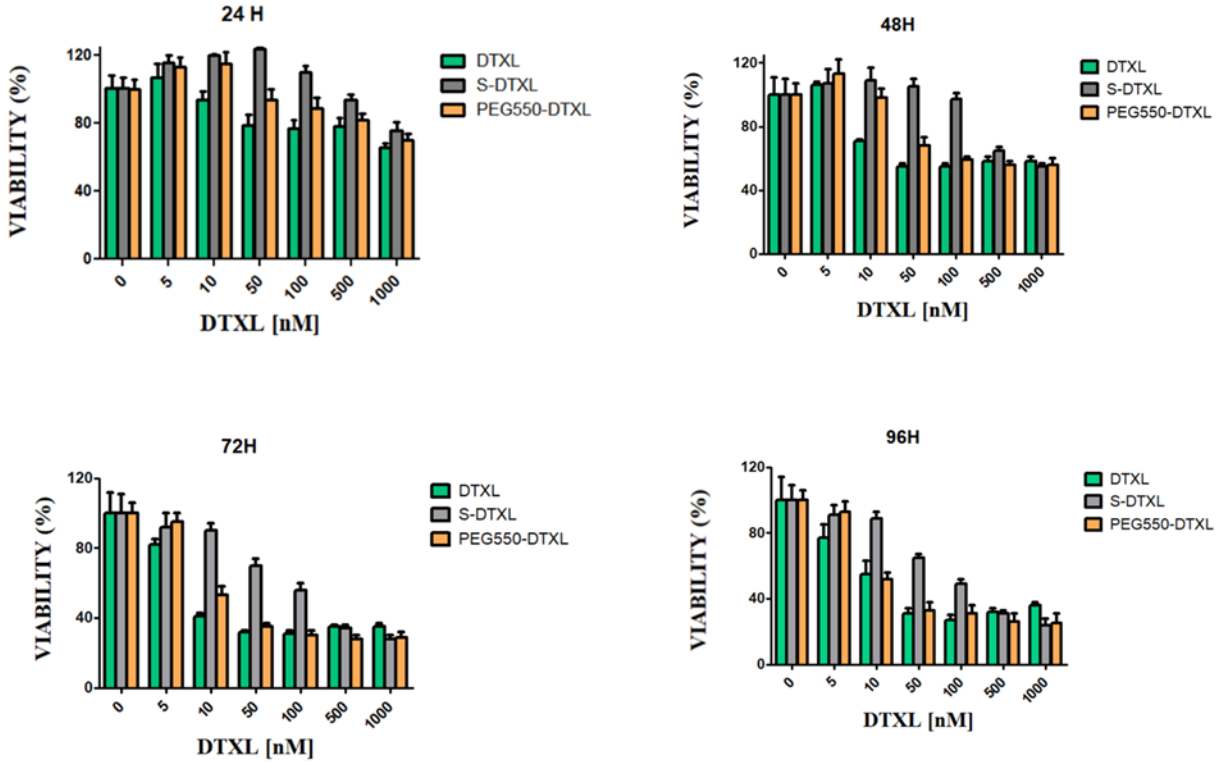

Time	Free DTXL	Succinic-DTXL	PEG_{550}DTXL
24h	52.35 ±1.28	520.9	75.52 ± 1.13
48h	9.6 ± 1.05	340.5 ± 1.06	21.59 ± 1.10
72h	6.1 ± 1.03	63.38 ± 1.03	8.75 ± 1.03
96h	6.6 ± 1.09	52.40 ± 1.02	8.67 ± 1.04

Figure 5.5: In vitro therapeutic properties of PEG550-DTXL. Cytotoxic potential on Glioblastoma multiform cancer U87-MB cells treated with Free DTXL (green), SUCCINIC-DTXL (grey) and PEG550-DTXL (orange) up to 96 hrs incubation time (bar chart) . Table listing the IC_{50} values for each treatment condition and time point.

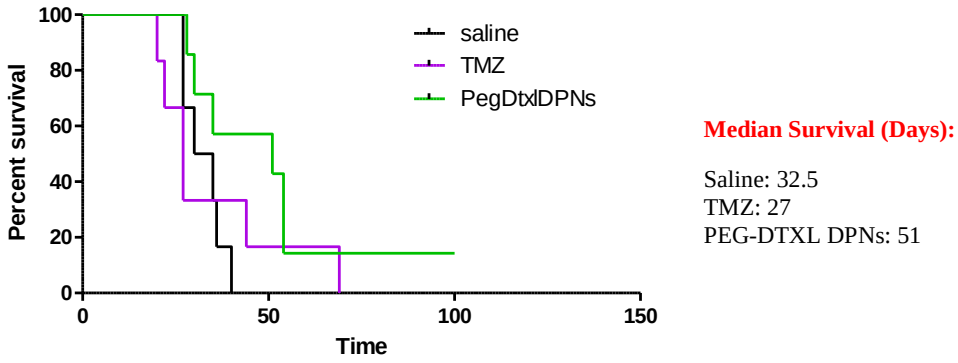

Figure 5.6: *In vivo therapeutic studies on Glioblastoma multiform cancer murine models.*

5.5 CONCLUSION

In this work it was demonstrated that the conjugation of docetaxel with hydrophilic polymer chains of PEG improved the favorable interaction with the polymer backbone of the nanostructures obtained by mold-fabrication and the encapsulation efficiency increased. This resulted controlled release of the drug with a decreased burst of the 20% in the first hour. Furthermore, the manipulation of Docetaxel with short PEG resulted in a similar pharmacological efficacy *in vitro* in comparison with unmodified Taxol. Significant improvement was observed when the prodrug loaded DPNs were tested in preclinical model of glioblastoma *in vivo* compared with the currently approved treatment with TMZ.

6 REFERENCES

1. Parkin, D.M., *Global cancer statistics in the year 2000.* The lancet oncology, 2001. **2**(9): p. 533-543.
2. Nowell, P.C., *The clonal evolution of tumor cell populations.* Science, 1976. **194**(4260): p. 23-28.
3. Hanahan, D. and R.A. Weinberg, *The hallmarks of cancer.* cell, 2000. **100**(1): p. 57-70.
4. Coleman, W.B. and G.J. Tsongalis, *Multiple mechanisms account for genomic instability and molecular mutation in neoplastic transformation.* Clinical chemistry, 1995. **41**(5): p. 644-657.
5. Perue, C., et al., *Molecular portraits of human breast tumors.* Nature, 2000. **406**(6797): p. 747-52.
6. Reis-Filho, J. and S.R. Lakhani, *Breast cancer special types: why bother?* The Journal of Pathology: A Journal of the Pathological Society of Great Britain and Ireland, 2008. **216**(4): p. 394-398.
7. Makki, J., *Diversity of breast carcinoma: histological subtypes and clinical relevance.* Clinical Medicine Insights: Pathology, 2015. **8**: p. CPath. S31563.
8. Weigelt, B., et al., *Refinement of breast cancer classification by molecular characterization of histological special types.* The Journal of Pathology: A Journal of the Pathological Society of Great Britain and Ireland, 2008. **216**(2): p. 141-150.
9. Tavassoli, F.A., *Pathology and genetics of tumours of the breast and female genital organs.* World Hhealth Organization Classification of Tumours, 2003.
10. Schnitt, S.J., *Will molecular classification replace traditional breast pathology?* International journal of surgical pathology, 2010. **18**(3_suppl): p. 162-166.
11. Elston, C.W. and I.O. Ellis, *Pathological prognostic factors in breast cancer. I. The value of histological grade in breast cancer: experience from a large study with long-term follow-up.* Histopathology, 1991. **19**(5): p. 403-410.
12. Ellis, I., et al., *Pathological prognostic factors in breast cancer. II. Histological type. Relationship with survival in a large study with long-term follow-up.* Histopathology, 1992. **20**(6): p. 479-489.
13. Hu, Z., et al., *The molecular portraits of breast tumors are conserved across microarray platforms.* BMC genomics, 2006. **7**(1): p. 1-12.
14. Azzopardi, J., et al., *The World Health Organization histological typing of breast tumors—Second edition.* American Journal of Clinical Pathology, 1982. **78**(6): p. 806-816.
15. Perou, C.M., et al., *Molecular portraits of human breast tumours.* nature, 2000. **406**(6797): p. 747-752.
16. Rivenbark, A.G., S.M. O'Connor, and W.B. Coleman, *Molecular and cellular heterogeneity in breast cancer: challenges for personalized medicine.* The American journal of pathology, 2013. **183**(4): p. 1113-1124.
17. Sørlie, T., et al., *Gene expression patterns of breast carcinomas distinguish tumor subclasses with clinical implications.* Proceedings of the National Academy of Sciences, 2001. **98**(19): p. 10869-10874.
18. Senkus, E., et al., *Primary breast cancer: ESMO Clinical Practice Guidelines for diagnosis, treatment and follow-up.* Annals of oncology, 2013. **24**: p. vi7-vi23.
19. Wolff, A.C., et al., *American Society of Clinical Oncology/College of American Pathologists guideline recommendations for human epidermal growth factor receptor 2 testing in breast cancer.* Archives of pathology & laboratory medicine, 2007. **131**(1): p. 18-43.

20. Rakha, E.A., et al., *The prognostic significance of lymphovascular invasion in invasive breast carcinoma.* Cancer, 2012. **118**(15): p. 3670-3680.
21. Krop, I., et al., *Use of biomarkers to guide decisions on adjuvant systemic therapy for women with early-stage invasive breast cancer: American Society of Clinical Oncology clinical practice guideline focused update.* Journal of clinical oncology: official journal of the American Society of Clinical Oncology, 2017. **35**(24): p. 2838.
22. Lester, J. *Local treatment of breast cancer*. in *Seminars in oncology nursing*. 2015. Elsevier.
23. Xie, Y., et al., *Surgery of the primary tumor improves survival in women with stage IV breast cancer in Southwest China: a retrospective analysis.* Medicine, 2017. **96**(22).
24. Vila, J., S. Gandini, and O. Gentilini, *Overall survival according to type of surgery in young (≤ 40 years) early breast cancer patients: a systematic meta-analysis comparing breast-conserving surgery versus mastectomy.* The Breast, 2015. **24**(3): p. 175-181.
25. Krug, D., et al., *Individualization of post-mastectomy radiotherapy and regional nodal irradiation based on treatment response after neoadjuvant chemotherapy for breast cancer.* Strahlentherapie und Onkologie, 2018. **194**(7): p. 607-618.
26. Group, E.B.C.T.C., *Relevance of breast cancer hormone receptors and other factors to the efficacy of adjuvant tamoxifen: patient-level meta-analysis of randomised trials.* The lancet, 2011. **378**(9793): p. 771-784.
27. Francis, P.A., et al., *Tailoring adjuvant endocrine therapy for premenopausal breast cancer.* New England Journal of Medicine, 2018. **379**(2): p. 122-137.
28. Group, E.B.C.T.C., *Aromatase inhibitors versus tamoxifen in early breast cancer: patient-level meta-analysis of the randomised trials.* The Lancet, 2015. **386**(10001): p. 1341-1352.
29. Taylor, C., et al., *Estimating the risks of breast cancer radiotherapy: evidence from modern radiation doses to the lungs and heart and from previous randomized trials.* Journal of Clinical Oncology, 2017. **35**(15): p. 1641.
30. Mackey, J., et al., *Long-term outcomes after adjuvant treatment of sequential versus combination docetaxel with doxorubicin and cyclophosphamide in node-positive breast cancer: BCIRG-005 randomized trial.* Annals of Oncology, 2016. **27**(6): p. 1041-1047.
31. Von Minckwitz, G., et al., *Trastuzumab emtansine for residual invasive HER2-positive breast cancer.* New England Journal of Medicine, 2019. **380**(7): p. 617-628.
32. Tolaney, S.M., et al., *Adjuvant paclitaxel and trastuzumab for node-negative, HER2-positive breast cancer.* New England Journal of Medicine, 2015. **372**(2): p. 134-141.
33. Earl, H.M., et al., *6 versus 12 months of adjuvant trastuzumab for HER2-positive early breast cancer (PERSEPHONE): 4-year disease-free survival results of a randomised phase 3 non-inferiority trial.* The Lancet, 2019. **393**(10191): p. 2599-2612.
34. Gnant, M., et al., *Adjuvant denosumab in postmenopausal patients with hormone receptor-positive breast cancer (ABCSG-18): disease-free survival results from a randomised, double-blind, placebo-controlled, phase 3 trial.* The lancet oncology, 2019. **20**(3): p. 339-351.
35. Coleman, R.E., et al., *Adjuvant denosumab in early breast cancer: First results from the international multicenter randomized phase III placebo controlled D-CARE study*. 2018, American Society of Clinical Oncology.
36. Ostrom, Q.T., et al., *CBTRUS statistical report: primary brain and central nervous system tumors diagnosed in the United States in 2008-2012.* Neuro-oncology, 2015. **17**(suppl_4): p. iv1-iv62.
37. Bailey, P. and H.W. Cushing, *A Classification of the Tumors of the Glioma Group on a Histo-genetic Basis, with a Correlated Study of Prognosis... With 108 Illustrations*. 1926: JB Lippincott Company.
38. Huse, J.T. and E.C. Holland, *Targeting brain cancer: advances in the molecular pathology of malignant glioma and medulloblastoma.* Nature reviews cancer, 2010. **10**(5): p. 319-331.

39. Louis, D.N., et al., *The 2016 World Health Organization classification of tumors of the central nervous system: a summary.* Acta neuropathologica, 2016. **131**(6): p. 803-820.
40. Collins, V., *Brain tumours: classification and genes.* Journal of Neurology, Neurosurgery & Psychiatry, 2004. **75**(suppl 2): p. ii2-ii11.
41. Brem, S. and J.G. Panattil, *An era of rapid advancement: diagnosis and treatment of metastatic brain cancer.* Neurosurgery, 2005. **57**(suppl_5): p. S4-5-S4-9.
42. Kearney, C.J. and D.J. Mooney, *Macroscale delivery systems for molecular and cellular payloads.* Nature materials, 2013. **12**(11): p. 1004-1017.
43. Misra, R., S. Acharya, and S.K. Sahoo, *Cancer nanotechnology: application of nanotechnology in cancer therapy.* Drug discovery today, 2010. **15**(19-20): p. 842-850.
44. Bourzac, K., *Nanotechnology: carrying drugs.* Nature, 2012. **491**(7425): p. S58-S60.
45. Yang, W., et al., *Gold nanoparticle based photothermal therapy: Development and application for effective cancer treatment.* Sustainable Materials and Technologies, 2019. **22**: p. e00109.
46. Arias, L.S., et al., *Iron oxide nanoparticles for biomedical applications: a perspective on synthesis, drugs, antimicrobial activity, and toxicity.* Antibiotics, 2018. **7**(2): p. 46.
47. Manshian, B.B., et al., *Personalized medicine and follow-up of therapeutic delivery through exploitation of quantum dot toxicity.* Biomaterials, 2017. **127**: p. 1-12.
48. Couvreur, P. and C. Vauthier, *Nanotechnology: intelligent design to treat complex disease.* Pharmaceutical research, 2006. **23**(7): p. 1417-1450.
49. Duncan, R., *The dawning era of polymer therapeutics.* Nature reviews Drug discovery, 2003. **2**(5): p. 347-360.
50. Peer, D., et al., *Nanocarriers as an emerging platform for cancer therapy.* Nature nanotechnology, 2007. **2**(12): p. 751.
51. Chauhan, V.P. and R.K. Jain, *Strategies for advancing cancer nanomedicine.* Nature materials, 2013. **12**(11): p. 958-962.
52. Gerlowski, L.E. and R.K. Jain, *Microvascular permeability of normal and neoplastic tissues.* Microvascular research, 1986. **31**(3): p. 288-305.
53. Alonso, M.J., *Nanomedicines for overcoming biological barriers.* Biomedicine & Pharmacotherapy, 2004. **58**(3): p. 168-172.
54. Prabhakar, U., et al., *Challenges and key considerations of the enhanced permeability and retention effect for nanomedicine drug delivery in oncology*. 2013, AACR.
55. Matsumura, Y. and H. Maeda, *A new concept for macromolecular therapeutics in cancer chemotherapy: mechanism of tumoritropic accumulation of proteins and the antitumor agent smancs.* Cancer research, 1986. **46**(12 Part 1): p. 6387-6392.
56. Cabral, H., et al., *Accumulation of sub-100 nm polymeric micelles in poorly permeable tumours depends on size.* Nature nanotechnology, 2011. **6**(12): p. 815-823.
57. Barenholz, Y.C., *Doxil®—the first FDA-approved nano-drug: lessons learned.* Journal of controlled release, 2012. **160**(2): p. 117-134.
58. Sheridan, C., *Proof of concept for next-generation nanoparticle drugs in humans*. 2012, Nature Publishing Group.
59. Blanco, E., H. Shen, and M. Ferrari, *Principles of nanoparticle design for overcoming biological barriers to drug delivery.* Nature biotechnology, 2015. **33**(9): p. 941.
60. Wilhelm, S., et al., *Analysis of nanoparticle delivery to tumours.* Nature reviews materials, 2016. **1**(5): p. 1-12.
61. Lavan, D.A., T. McGuire, and R. Langer, *Small-scale systems for in vivo drug delivery.* Nature biotechnology, 2003. **21**(10): p. 1184-1191.

62. Gradishar, W.J., et al., *Phase III trial of nanoparticle albumin-bound paclitaxel compared with polyethylated castor oil–based paclitaxel in women with breast cancer.* Journal of clinical oncology, 2005. **23**(31): p. 7794-7803.
63. Shi, J., et al., *Cancer nanomedicine: progress, challenges and opportunities.* Nature Reviews Cancer, 2017. **17**(1): p. 20.
64. Vizirianakis, I.S., *Nanomedicine and personalized medicine toward the application of pharmacotyping in clinical practice to improve drug-delivery outcomes.* Nanomedicine: Nanotechnology, Biology and Medicine, 2011. **7**(1): p. 11-17.
65. Gratton, S.E., et al., *The effect of particle design on cellular internalization pathways.* Proceedings of the National Academy of Sciences, 2008. **105**(33): p. 11613-11618.
66. Thorek, D.L. and A. Tsourkas, *Size, charge and concentration dependent uptake of iron oxide particles by non-phagocytic cells.* Biomaterials, 2008. **29**(26): p. 3583-3590.
67. Champion, J.A. and S. Mitragotri, *Role of target geometry in phagocytosis.* Proceedings of the National Academy of Sciences, 2006. **103**(13): p. 4930-4934.
68. Cooley, M., et al., *Influence of particle size and shape on their margination and wall-adhesion: implications in drug delivery vehicle design across nano-to-micro scale.* Nanoscale, 2018. **10**(32): p. 15350-15364.
69. Hoshyar, N., et al., *The effect of nanoparticle size on in vivo pharmacokinetics and cellular interaction.* Nanomedicine, 2016. **11**(6): p. 673-692.
70. Wang, X., T. Ishida, and H. Kiwada, *Anti-PEG IgM elicited by injection of liposomes is involved in the enhanced blood clearance of a subsequent dose of PEGylated liposomes.* Journal of Controlled Release, 2007. **119**(2): p. 236-244.
71. Hu, C.-M.J., et al., *Nanoparticle biointerfacing by platelet membrane cloaking.* Nature, 2015. **526**(7571): p. 118-121.
72. Anselmo, A.C., et al., *Platelet-like nanoparticles: mimicking shape, flexibility, and surface biology of platelets to target vascular injuries.* ACS nano, 2014. **8**(11): p. 11243-11253.
73. Sugahara, K.N., et al., *Tissue-penetrating delivery of compounds and nanoparticles into tumors.* Cancer cell, 2009. **16**(6): p. 510-520.
74. Li, H., L. Pordesimo, and J. Weiss, *High intensity ultrasound-assisted extraction of oil from soybeans.* Food research international, 2004. **37**(7): p. 731-738.
75. van der Meel, R., et al., *Smart cancer nanomedicine.* Nature Nanotechnology, 2019. **14**(11): p. 1007-1017.
76. Harrington, K.J., et al., *Effective targeting of solid tumors in patients with locally advanced cancers by radiolabeled pegylated liposomes.* Clinical Cancer Research, 2001. **7**(2): p. 243-254.
77. Pappu, V. and P. Bagchi, *Hydrodynamic interaction between erythrocytes and leukocytes affects rheology of blood in microvessels.* Biorheology, 2007. **44**(3): p. 191-215.
78. Foulkes, W.D., I.E. Smith, and J.S. Reis-Filho, *Triple-negative breast cancer.* New England journal of medicine, 2010. **363**(20): p. 1938-1948.
79. Kennecke, H., et al., *Metastatic behavior of breast cancer subtypes.* Journal of clinical oncology, 2010. **28**(20): p. 3271-3277.
80. Bianchini, G., et al., *Triple-negative breast cancer: challenges and opportunities of a heterogeneous disease.* Nature reviews Clinical oncology, 2016. **13**(11): p. 674.
81. Lee, A. and M.B. Djamgoz, *Triple negative breast cancer: emerging therapeutic modalities and novel combination therapies.* Cancer treatment reviews, 2018. **62**: p. 110-122.
82. Chavez, K.J., S.V. Garimella, and S. Lipkowitz, *Triple negative breast cancer cell lines: one tool in the search for better treatment of triple negative breast cancer.* Breast disease, 2010. **32**(1-2): p. 35.

83. Anders, C.K. and L.A. Carey, *Biology, metastatic patterns, and treatment of patients with triple-negative breast cancer.* Clinical breast cancer, 2009. **9**: p. S73-S81.
84. Bourgeois-Daigneault, M.-C., et al., *Neoadjuvant oncolytic virotherapy before surgery sensitizes triple-negative breast cancer to immune checkpoint therapy.* Science Translational Medicine, 2018. **10**(422): p. eaao1641.
85. Isakoff, S.J., *Triple negative breast cancer: role of specific chemotherapy agents.* Cancer journal (Sudbury, Mass.), 2010. **16**(1): p. 53.
86. Cleator, S., W. Heller, and R.C. Coombes, *Triple-negative breast cancer: therapeutic options.* The lancet oncology, 2007. **8**(3): p. 235-244.
87. Kloover, J., et al., *Fatal outcome of a hypersensitivity reaction to paclitaxel: a critical review of premedication regimens.* British journal of cancer, 2004. **90**(2): p. 304-305.
88. Gelderblom, H., et al., *Cremophor EL: the drawbacks and advantages of vehicle selection for drug formulation.* European journal of cancer, 2001. **37**(13): p. 1590-1598.
89. De Laurentiis, M., et al., *Taxane-based combinations as adjuvant chemotherapy of early breast cancer: a meta-analysis of randomized trials*, in *Database of Abstracts of Reviews of Effects (DARE): Quality-assessed Reviews [Internet]*. 2008, Centre for Reviews and Dissemination (UK).
90. Engels, F.K., R.A. Mathot, and J. Verweij, *Alternative drug formulations of docetaxel: a review.* Anti-cancer drugs, 2007. **18**(2): p. 95-103.
91. Yu, M.K., J. Park, and S. Jon, *Targeting strategies for multifunctional nanoparticles in cancer imaging and therapy.* Theranostics, 2012. **2**(1): p. 3-44.
92. Anselmo, A.C. and S. Mitragotri, *Nanoparticles in the clinic: An update.* Bioengineering & Translational Medicine, 2019. **4**(3): p. e10143.
93. Maeda, H., H. Nakamura, and J. Fang, *The EPR effect for macromolecular drug delivery to solid tumors: Improvement of tumor uptake, lowering of systemic toxicity, and distinct tumor imaging in vivo.* Advanced drug delivery reviews, 2013. **65**(1): p. 71-79.
94. Golombek, S.K., et al., *Tumor targeting via EPR: Strategies to enhance patient responses.* Advanced drug delivery reviews, 2018. **130**: p. 17-38.
95. Esmaeili, F., et al., *Docetaxel–albumin conjugates: preparation, in vitro evaluation and biodistribution studies.* Journal of pharmaceutical sciences, 2009. **98**(8): p. 2718-2730.
96. Immordino, M.L., et al., *Preparation, characterization, cytotoxicity and pharmacokinetics of liposomes containing docetaxel.* Journal of controlled release, 2003. **91**(3): p. 417-429.
97. Chan, J.M., et al., *PLGA–lecithin–PEG core–shell nanoparticles for controlled drug delivery.* Biomaterials, 2009. **30**(8): p. 1627-1634.
98. Hwang, H.-Y., et al., *Tumor targetability and antitumor effect of docetaxel-loaded hydrophobically modified glycol chitosan nanoparticles.* Journal of controlled release, 2008. **128**(1): p. 23-31.
99. Tan, L., et al., *A Novel MPEG-PDLLA-PLL Copolymer for Docetaxel Delivery in Breast Cancer Therapy.* Theranostics, 2017. **7**(10): p. 2652-2672.
100. Gaucher, G., R.H. Marchessault, and J.-C. Leroux, *Polyester-based micelles and nanoparticles for the parenteral delivery of taxanes.* Journal of controlled release, 2010. **143**(1): p. 2-12.
101. Huynh, L., J.-C. Leroux, and C. Allen, *Enhancement of docetaxel solubility via conjugation of formulation-compatible moieties.* Organic & biomolecular chemistry, 2009. **7**(17): p. 3437-3446.
102. Sun, B., R.M. Straubinger, and J.F. Lovell, *Current taxane formulations and emerging cabazitaxel delivery systems.* Nano Research, 2018. **11**(10): p. 5193-5218.
103. Pillai, G., *Nanomedicines for cancer therapy: an update of fda approved and those under various stages of development. SOJ Pharm Pharm Sci 1 (2): 13.* Nanomedicines for Cancer Therapy: An Update of FDA Approved and Those under Various Stages of Development, 2014.

104. Hawkins, M.J., P. Soon-Shiong, and N. Desai, *Protein nanoparticles as drug carriers in clinical medicine.* Advanced drug delivery reviews, 2008. **60**(8): p. 876-885.
105. Ernsting, M.J., et al., *A docetaxel-carboxymethylcellulose nanoparticle outperforms the approved taxane nanoformulation, Abraxane, in mouse tumor models with significant control of metastases.* Journal of controlled release, 2012. **162**(3): p. 575-581.
106. Bowerman, C.J., et al., *Docetaxel-loaded PLGA nanoparticles improve efficacy in taxane-resistant triple-negative breast cancer.* Nano letters, 2017. **17**(1): p. 242-248.
107. Contreras-Cáceres, R., et al., *Paclitaxel-loaded hollow-poly (4-vinylpyridine) nanoparticles enhance drug chemotherapeutic efficacy in lung and breast cancer cell lines.* Nano Research, 2017. **10**(3): p. 856-875.
108. Huang, J., et al., *Biodegradable self-assembled nanoparticles of poly (d, l-lactide-co-glycolide)/hyaluronic acid block copolymers for target delivery of docetaxel to breast cancer.* Biomaterials, 2014. **35**(1): p. 550-566.
109. Liang, D.-S., et al., *Treating metastatic triple negative breast cancer with CD44/neuropilin dual molecular targets of multifunctional nanoparticles.* Biomaterials, 2017. **137**: p. 23-36.
110. Li, S., et al., *Feasibility of eradication of breast cancer cells remaining in postlumpectomy cavity and draining lymph nodes following intracavitary injection of radioactive immunoliposomes.* Molecular pharmaceutics, 2012. **9**(9): p. 2513-2522.
111. Petersen, A.L., et al., *Liposome imaging agents in personalized medicine.* Advanced drug delivery reviews, 2012. **64**(13): p. 1417-1435.
112. Moss, J.I., et al., *High-resolution 3D visualization of nanomedicine distribution in tumors.* Theranostics, 2020. **10**(2): p. 880-897.
113. Hauert, S., et al., *A computational framework for identifying design guidelines to increase the penetration of targeted nanoparticles into tumors.* Nano today, 2013. **8**(6): p. 566-576.
114. Palange, A.L., et al., *Deformable discoidal polymeric nanoconstructs for the precise delivery of therapeutic and imaging agents.* Molecular Therapy, 2017. **25**(7): p. 1514-1521.
115. Kolhar, P., et al., *Using shape effects to target antibody-coated nanoparticles to lung and brain endothelium.* Proc Natl Acad Sci U S A, 2013. **110**(26): p. 10753-8.
116. Myerson, J.W., et al., *Non-affinity factors modulating vascular targeting of nano- and microcarriers.* Adv Drug Deliv Rev, 2016. **99**(Pt A): p. 97-112.
117. Key, J., et al., *Soft Discoidal Polymeric Nanoconstructs Resist Macrophage Uptake and Enhance Vascular Targeting in Tumors.* ACS Nano, 2015. **9**(12): p. 11628-41.
118. Decuzzi, P., et al., *Size and shape effects in the biodistribution of intravascularly injected particles.* Journal of Controlled Release, 2010. **141**(3): p. 320-327.
119. van de Ven, A.L., et al., *Rapid tumoritropic accumulation of systemically injected plateloid particles and their biodistribution.* J Control Release, 2012. **158**(1): p. 148-55.
120. Adriani, G., et al., *The preferential targeting of the diseased microvasculature by disk-like particles.* Biomaterials, 2012. **33**(22): p. 5504-13.
121. Valcourt, D.M., et al., *Advances in targeted nanotherapeutics: From bioconjugation to biomimicry.* Nano research, 2018. **11**(10): p. 4999-5016.
122. Palomba, R., et al., *Modulating phagocytic cell sequestration by tailoring nanoconstruct softness.* ACS nano, 2018. **12**(2): p. 1433-1444.
123. Ferreira, M., et al., *Optimizing the Pharmacological Properties of Discoidal Polymeric Nanoconstructs Against Triple-Negative Breast Cancer Cells.* Frontiers in Bioengineering and Biotechnology, 2020. **8**: p. 5.
124. Colasuonno, M., et al., *Erythrocyte-inspired discoidal polymeric nanoconstructs carrying tissue plasminogen activator for the enhanced lysis of blood clots.* ACS nano, 2018. **12**(12): p. 12224-12237.

125. Key, J., et al., *Engineering discoidal polymeric nanoconstructs with enhanced magneto-optical properties for tumor imaging.* Biomaterials, 2013. **34**(21): p. 5402-5410.
126. Liu, Y., J.-J. Yin, and Z. Nie, *Harnessing the collective properties of nanoparticle ensembles for cancer theranostics.* Nano Research, 2014. **7**(12): p. 1719-1730.
127. Ma, Z., et al., *A theranostic agent for cancer therapy and imaging in the second near-infrared window.* Nano research, 2019. **12**(2): p. 273-279.
128. Van De Ven, A.L., et al., *Rapid tumoritropic accumulation of systemically injected plateloid particles and their biodistribution.* Journal of Controlled Release, 2012. **158**(1): p. 148-155.
129. Decuzzi, P. and M. Ferrari, *Design maps for nanoparticles targeting the diseased microvasculature.* Biomaterials, 2008. **29**(3): p. 377-384.
130. Mosallaei, N., et al., *Docetaxel-loaded solid lipid nanoparticles: preparation, characterization, in vitro, and in vivo evaluations.* Journal of pharmaceutical sciences, 2013. **102**(6): p. 1994-2004.
131. Bao, G., S. Mitragotri, and S. Tong, *Multifunctional nanoparticles for drug delivery and molecular imaging.* Annual review of biomedical engineering, 2013. **15**: p. 253-282.
132. Sun, H., et al., *Structure governs the deformability of polymer particles in a microfluidic blood capillary model.* ACS Macro Letters, 2015. **4**(11): p. 1205-1209.
133. Albanese, A., P.S. Tang, and W.C. Chan, *The effect of nanoparticle size, shape, and surface chemistry on biological systems.* Annual review of biomedical engineering, 2012. **14**: p. 1-16.
134. Zhang, L., et al., *Softer zwitterionic nanogels for longer circulation and lower splenic accumulation.* ACS nano, 2012. **6**(8): p. 6681-6686.
135. Mokken, F.C., et al., *The clinical importance of erythrocyte deformability, a hemorrheological parameter.* Annals of hematology, 1992. **64**(3): p. 113-122.
136. Key, J., et al., *Soft discoidal polymeric nanoconstructs resist macrophage uptake and enhance vascular targeting in tumors.* ACS nano, 2015. **9**(12): p. 11628-11641.
137. Haghgooie, R., M. Toner, and P.S. Doyle, *Squishy non-spherical hydrogel microparticles.* Macromolecular rapid communications, 2010. **31**(2): p. 128-134.
138. Cho, Y.W., et al., *Complex adaptive therapeutic strategy (CATS) for cancer.* Journal of Controlled Release, 2014. **175**: p. 43-47.
139. Feng, L., et al., *Development and optimization of oil-filled lipid nanoparticles containing docetaxel conjugates designed to control the drug release rate in vitro and in vivo.* International journal of nanomedicine, 2011. **6**: p. 2545.
140. Wen, P.Y. and S. Kesari, *Malignant gliomas in adults.* New England Journal of Medicine, 2008. **359**(5): p. 492-507.
141. Schwartzbaum, J.A., et al., *Epidemiology and molecular pathology of glioma.* Nature clinical practice Neurology, 2006. **2**(9): p. 494-503.
142. Wesseling, P. and D. Capper, *WHO 2016 classification of gliomas.* Neuropathology and applied neurobiology, 2018. **44**(2): p. 139-150.
143. Dolecek, T.A., et al., *CBTRUS statistical report: primary brain and central nervous system tumors diagnosed in the United States in 2005–2009.* Neuro-oncology, 2012. **14**(suppl_5): p. v1-v49.
144. Wen, P.Y. and D.A. Reardon, *Progress in glioma diagnosis, classification and treatment.* Nature Reviews Neurology, 2016. **12**(2): p. 69-70.
145. Ostermann, S., et al., *Plasma and cerebrospinal fluid population pharmacokinetics of temozolomide in malignant glioma patients.* Clinical cancer research, 2004. **10**(11): p. 3728-3736.
146. Portnow, J., et al., *The neuropharmacokinetics of temozolomide in patients with resectable brain tumors: potential implications for the current approach to chemoradiation.* Clinical Cancer Research, 2009. **15**(22): p. 7092-7098.

147. Neuwelt, E.A., et al., *Engaging neuroscience to advance translational research in brain barrier biology.* Nature Reviews Neuroscience, 2011. **12**(3): p. 169-182.
148. Hau, P., et al., *Safety and feasibility of long-term temozolomide treatment in patients with high-grade glioma.* Neurology, 2007. **68**(9): p. 688-690.
149. Kitange, G.J., et al., *Induction of MGMT expression is associated with temozolomide resistance in glioblastoma xenografts.* Neuro-oncology, 2009. **11**(3): p. 281-291.
150. Fruehauf, J.P., et al., *In vitro drug response and molecular markers associated with drug resistance in malignant gliomas.* Clinical Cancer Research, 2006. **12**(15): p. 4523-4532.
151. Gaudin, A., et al., *PEGylated squalenoyl-gemcitabine nanoparticles for the treatment of glioblastoma.* Biomaterials, 2016. **105**: p. 136-144.
152. Swierczewska, M., K.C. Lee, and S. Lee, *What is the future of PEGylated therapies?* Expert opinion on emerging drugs, 2015. **20**(4): p. 531-536.
153. Liu, J., et al., *Nano-sized assemblies of a PEG-docetaxel conjugate as a formulation strategy for docetaxel.* Journal of pharmaceutical sciences, 2008. **97**(8): p. 3274-3290.